

Spinodal decomposition in thin films of binary polymer blends

Citation for published version (APA):

Velázquez Sánchez, M. E. (2002). *Spinodal decomposition in thin films of binary polymer blends*. [Phd Thesis 1 (Research TU/e / Graduation TU/e), Chemical Engineering and Chemistry]. Technische Universiteit Eindhoven. <https://doi.org/10.6100/IR560071>

DOI:

[10.6100/IR560071](https://doi.org/10.6100/IR560071)

Document status and date:

Published: 01/01/2002

Document Version:

Publisher's PDF, also known as Version of Record (includes final page, issue and volume numbers)

Please check the document version of this publication:

- A submitted manuscript is the version of the article upon submission and before peer-review. There can be important differences between the submitted version and the official published version of record. People interested in the research are advised to contact the author for the final version of the publication, or visit the DOI to the publisher's website.
- The final author version and the galley proof are versions of the publication after peer review.
- The final published version features the final layout of the paper including the volume, issue and page numbers.

[Link to publication](#)

General rights

Copyright and moral rights for the publications made accessible in the public portal are retained by the authors and/or other copyright owners and it is a condition of accessing publications that users recognise and abide by the legal requirements associated with these rights.

- Users may download and print one copy of any publication from the public portal for the purpose of private study or research.
- You may not further distribute the material or use it for any profit-making activity or commercial gain
- You may freely distribute the URL identifying the publication in the public portal.

If the publication is distributed under the terms of Article 25fa of the Dutch Copyright Act, indicated by the "Taverne" license above, please follow below link for the End User Agreement:

www.tue.nl/taverne

Take down policy

If you believe that this document breaches copyright please contact us at:

openaccess@tue.nl

providing details and we will investigate your claim.

Spinodal decomposition in thin films of binary polymer blends

PROEFSCHRIFT

ter verkrijging van de graad van doctor aan de
Technische Universiteit Eindhoven, op gezag van de
Rector Magnificus, prof.dr. R.A. van Santen, voor een
Commissie aangewezen door het College voor
Promoties in het openbaar te verdedigen
op maandag 16 december 2002 om 16.00 uur

door

María Eugenia Velázquez Sánchez

geboren te Mexico-stad, Mexico

Dit proefschrift is goedgekeurd door de promotoren:

prof.dr. G. de With
en
prof.dr.ir. H.E.H. Meijer

Copromotor:
dr.ir. P.D. Anderson

CIP-DATA LIBRARY TECHNISCHE UNIVERSITEIT EINDHOVEN

Velázquez Sánchez, M.E.

Spinodal decomposition in thin films of binary polymer blends / by M.E. Velázquez Sánchez. – Eindhoven : Technische Universiteit Eindhoven, 2002.

Proefschrift. – ISBN 90-386-2764-5
NUR 913

Trefwoorden: polymeren ; morfologie / polymeermengsels / fasescheiding ; spinodale decompositie / dunne lagen / fysisch-chemische simulatie en modellering

Subject headings: polymers ; morphology / polymer blends / phase separation ; spinodal decomposition / thin films / physicochemical simulation and modelling

© 2002 by M.E. Velázquez Sánchez

Printed by Universiteitsdrukkerij Technische Universiteit Eindhoven,
Eindhoven, the Netherlands

This research was financially supported by NWO (Nederlandse Organisatie voor Wetenschappelijk Onderzoek)

A mis padres

A la memoria de Víctor

CONTENTS

CHAPTER 1	1
INTRODUCTION	1
1.1 Structure in Nature	1
1.2 Morphology development in polymer systems	2
1.3 Aim and outline of this thesis	4
1.4 References	5
CHAPTER 2	7
REVIEW	7
2.1 Introduction	7
2.2 Polymer chains	7
2.3 Historical review on the development of mean field and self-consistent field theories	8
2.4 Self-consistent field versus square-gradient theories	10
2.5 Surface-directed spinodal decomposition	11
2.6 Conclusions	13
2.7 References	13
CHAPTER 3	15
SPINODAL DECOMPOSITION IN A THIN POLYMER FILM INTERACTING WITH A RIGID WALL	15
3.1 Introduction	15
3.2 Conservation equations	15
3.3 Energy functional	19
3.3.1 Homogeneous contribution to the energy functional	20
3.3.2 Equilibrium, spinodal and critical conditions	21
3.3.3 Gradient contribution	24
3.3.4 Concentration profile and interfacial thickness	25
3.3.5 Interaction potential of a polymer blend with a rigid wall	30
3.4 Conclusions	35
3.5 References	36
CHAPTER 4	37
MODEL IMPLEMENTATION	37
4.1 Introduction	37
4.2 System definition	37
4.3 Scaling chemical potential, mass balance and momentum equations	39
4.4 Spatial and temporal discretization of the conservation equations	40
4.5 Temporal and spatial validation of the model	43
4.6 Conclusions	45
4.7 References	45

CHAPTER 5	47
NUMERICAL RESULTS	47
5.1 Introduction	47
5.2 Morphology development in bulk	47
5.3 Morphology development in the presence of a rigid wall	52
5.3.1 Quantification of the morphology	58
5.4 Conclusions	62
5.5 References	62
CHAPTER 6	63
PHASE BEHAVIOR OF THE BINARY SYSTEM POLY [METHYL METHACRYLATE-CO-1H,1H- PERFLUOROHEPTYLMETHYL METHACRYLATE] / BISPHENOL-A-DIGLYCIDYLEETHER	63
6.1 Introduction	63
6.2 Phase behavior	63
6.2.1 Materials	64
6.2.2 Methods	64
6.2.3 Results	65
6.3 Morphology development	67
6.4 Conclusions	72
6.5 References	72
CHAPTER 7	73
EPILOGUE	73
7.1 Facts	73
7.2 Constraints of the model used	74
7.3 Suggestions	75
7.4 References	75
APPENDIX I	77
I.1 Helfand's self-consistent field model	77
I.2 Derivation of the pre-factor of the square-gradient term	78
I.3 Common tangent construction	80
I.4 Conservation law	82
I.4.1 Conserved quantities in the one-dimensional case	82
I.4.2 Calculation of k_0 for an asymmetric system	84
I.4.3 Maximum slope method	85
I.5 Interaction parameter of a binary polymer blend in contact with a rigid wall	86
I.5.1 Calculation of $\Delta\gamma_i$ for $\theta \neq 0$	87
I.6 References	88

APPENDIX II	89
SOLUBILITY REGION OF THE BINARY SYSTEM BISPHENOL-A-DIGLYCIDYLETHER / COPOLYMER POLY [CF₃(CF₂)₆SO₂NCH₂CH₃BA-CO-MMA]	89
II.1 Introduction	89
II.2 Theory	89
II.3 Experimental	91
II.4 Results	91
II.5 A possible application	95
II.5.1 Coating preparation	95
II.5.2 Results	95
II.6 Conclusions	98
II.7 References	98
SUMMARY	99
SAMENVATTING	101
RESUMEN	103
ACKNOWLEDGMENTS	105
CURRICULUM VITAE	107

CHAPTER 1

INTRODUCTION

1.1 Structure in Nature

Mother Nature gave to humankind a precious present: a complex brain that allowed it to be rational; but, as she is so wise, she gave together with the present a perpetual series of tasks: to observe, to explore, to understand and to create. So men and women started observing and the most straightforward feature that came into their eyes was the beauty of Nature represented by the huge amount of forms, structures and patterns present in it.

The forms present in Nature can be as simple as a honeycomb (figure 1.1) or as diverse as the structures of a snowflake (figure 1.2) that inspired Kepler to write a short treatise about it.¹ Structure development for amorphous materials will be illustrated in this thesis. Whatever is the shape we observe there is always a physical reason behind it. For instance, in the case of a honeycomb, the hexagonal packing is the structure that contains the greatest amount of honey with the least amount of beeswax and therefore it requires the least energy for the bees to construct it.²



Figure 1.1 Honeycombs.³

Snowflakes on the other hand, present diverse crystalline structures that are formed depending of the temperature and the amount of water vapor present in the air⁴ (supersaturation), as illustrated in figure 1.2. The most common and simple shape of a snowflake is the hexagonal plate that forms at temperatures just below freezing (0 °C and -3 °C) and low levels of water vapor in the air. The reason is that at this temperature a straight edge of an ice crystal grows stably.

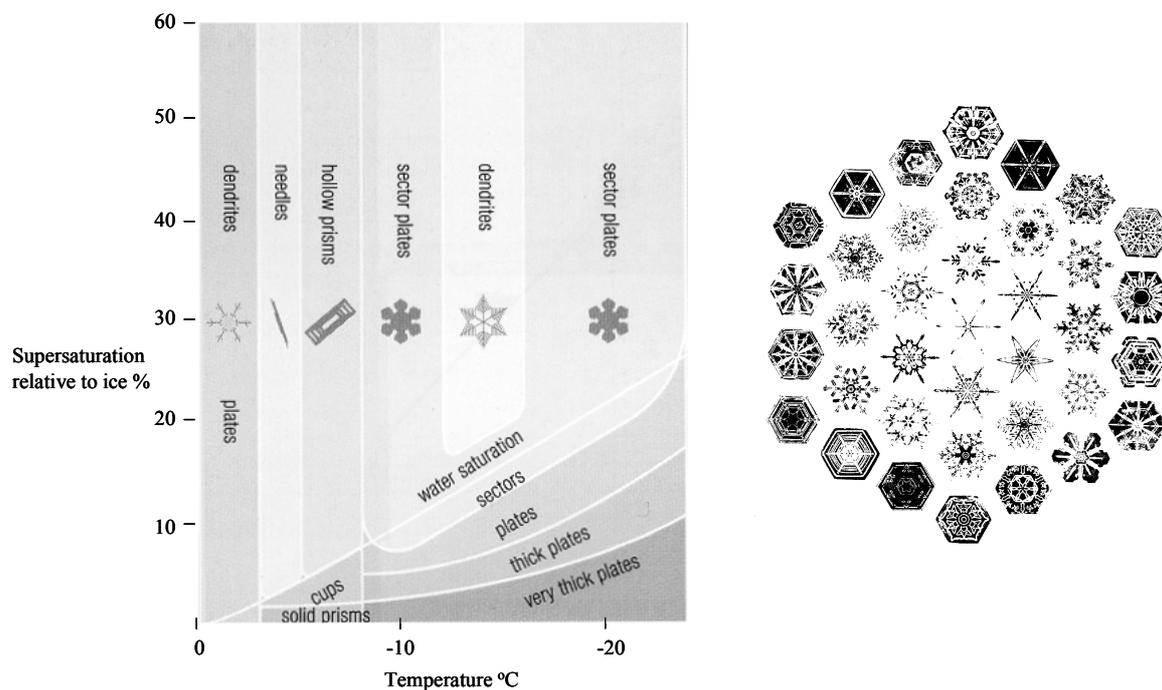


Figure 1.2 Atmospheric conditions leading to different shaped ice crystals.^{5,4}

The amorphous structures are the main topic of this thesis and will be introduced in the next section for the case of polymers, which are large molecules formed from repeated units (Greek *poly-* ‘many’ *meros* ‘share’). Also in the next section is explained the importance of studying the structure or morphology (Greek *morphē* ‘form’+ *logy* ‘study’) of these systems in a mesoscopic scale (Greek, *mesos* ‘middle’).

1.2 Morphology development in polymer systems

Polymers can present a broad range of morphologies ranging from crystallized systems and liquid crystalline mesophases to systems that phase separate macroscopically. Moreover, the fabrication, deformation and fracture of polymer systems can also modify the morphology and/or inducement morphology development.⁶ The prediction of the morphology on a mesoscopic scale is of great importance because it allows to bridge and to understand the relationship between microscopic parameters and macroscopic properties, which determine the final performance of a material. For example, the toughness of a polymer blend (figure 1.3) depends on the particle size, the uniformity, the dispersion and the interfacial adhesion between the particles and the matrix.⁷ These properties can be controlled by modifying the chemical composition of the blend or by inducing phase separation under specific conditions that lead to the formation of a connected structure as the one shown in figure 1.4.

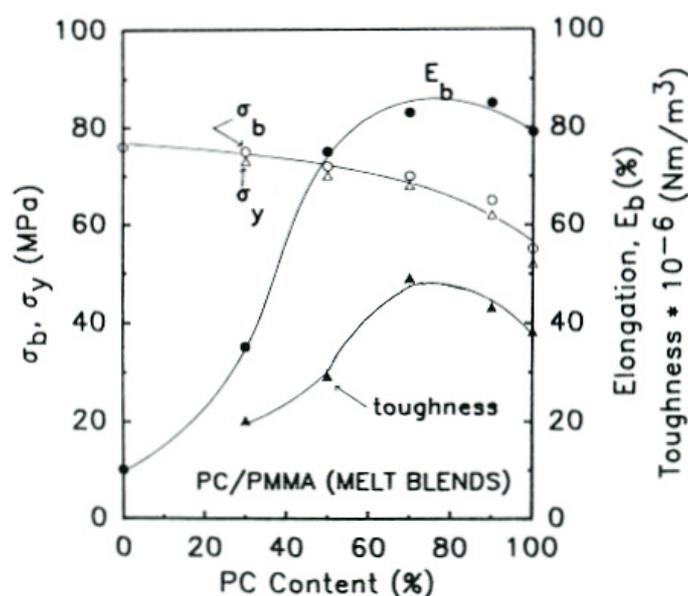


Figure 1.3 Tensile properties as a function of blend composition of PC / PMMA.⁷

PC = polycarbonate, PMMA = polymethylmethacrylate,

σ_b, σ_y = breaking stress (fracture strength) and yield strength.

When a polymer blend is spread on a substrate (rigid wall) a film is formed, the presence of this new boundary has an effect on the morphology developed due to the loss of geometry at the wall compared to the bulk. In this thesis, we focus on the morphology development induced by (macroscopic) phase separation in amorphous thin films made of binary polymer blends. Phase separation occurs due to the weak attraction between the (mostly) nonpolar molecules in polymer systems. The high energy of mixing cannot be overcome by the increase of entropy or randomness of the system caused by the mixing of two species. The interest in studying morphology development in polymer blends is not limited to films though is the main interest in this thesis;⁸ the specific case of microphase separation present in polymer blends containing block copolymer has been explored widely⁹ and is not studied here.

It is well known that phase separation can occur via two different mechanisms: nucleation and growth (binodal mechanism), where the system is metastable and spinodal decomposition, where the system is unstable and therefore quite sensitive to concentration fluctuations. Our study is carried out in the spinodal region around the critical point. The spinodal region is chosen because here it is possible to get the co-continuous structure illustrated in figure 1.4, which optimizes the adhesion between two different phases and therefore good mechanical properties are expected. The region around the critical point is chosen because the local concentration has large fluctuations that can be detected with light scattering¹⁰ (figure 1.4) and because the square-gradient theory considered in the energy functional to include the effect of concentration gradients to enthalpy and entropy of the system, is a good approximation in the partial miscible region of the phase diagram.^{11,12} Additionally, we limit our study to the early-stage of the spinodal decomposition because we think that important effects such as wetting that determine the final properties of a material develop within this stage.

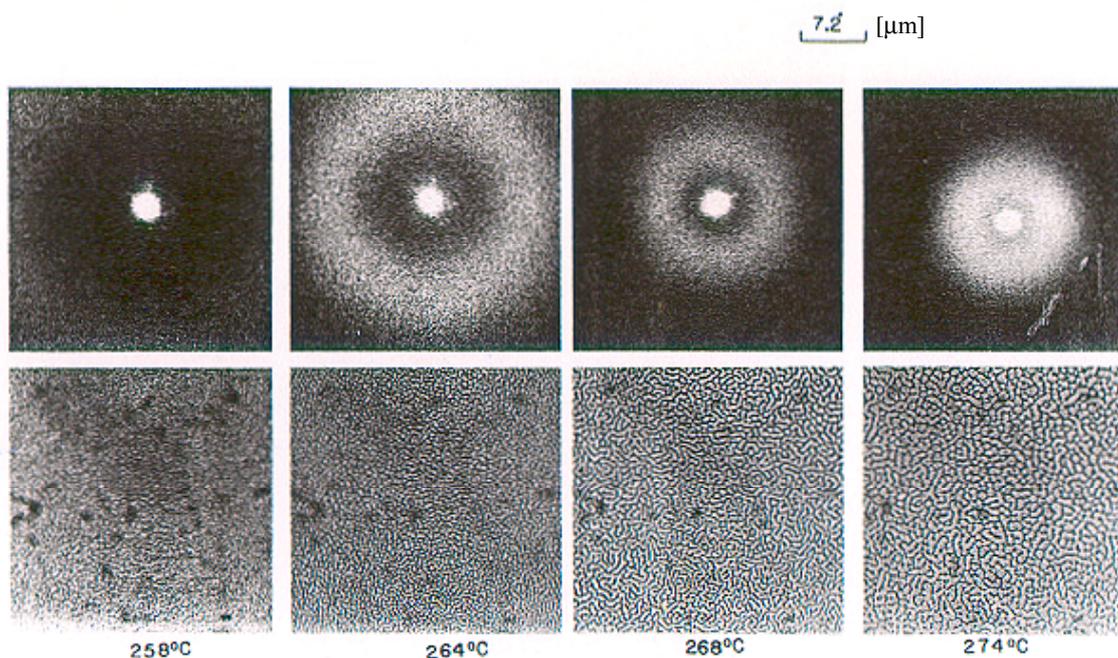


Figure 1.4 Optical micrographs and the corresponding scattering patterns of the 40/60 PC/PMMA blend as a function of temperature.⁸

1.3 Aim and outline of this thesis

This work has three main objectives:

- Establish a strategy to achieve and control stratification in thin films made of binary phase separating polymer blends.
- Extend a numerical method available for the prediction of morphology development in the bulk of a regular solution to polymer blends in the bulk and / or in the presence of a rigid wall.
- Understand the mechanism leading to a faster domain growth next to the wall for thin films of polymer blends, in the early-stage of the spinodal decomposition.

If you ever saw the movie *Before the rain* of Milcho Manchevski¹³ it will be easier for you as a reader to find the links between the way as this work is presented and its real temporal development. Briefly, in this movie that is a collaboration of three countries, a story is told in three parts linked by characters and events that alternate London and the countryside of Macedonia. This thesis is also the result of a good collaboration between two Departments and persons of three different groups within this University. The presentation of this research story starts in the second part of my time as a Ph. D. student, goes through an intermediate stage where coherent results between theory and experiments carried out in the early-stage of this project meet and finalizes in appendix II, which is the starting phase of this work. As circle stories are rather difficult to tell, I will introduce you in my work in the way as it is written.

In chapter 2 the coarse-grained model used in this thesis to describe a polymer chain is introduced; also a brief review on models used to study phase separation of incompressible

polymer blends at interfaces is presented. The justification of choosing a square-gradient or diffuse-interface model instead of a self-consistent field theory is made and the motivation that led us to investigate more in detail the early-stage of the spinodal decomposition is established.

In chapter 3, the analysis necessary to formulate a suitable model to study morphology development in an incompressible, density-matched, isothermal binary blend undergoing phase separation in the presence of a wall is presented. In this model, thermodynamics and hydrodynamics of the system are coupled via the introduction of a chemical potential (derived from an appropriate energy functional for polymer blends) in the conservation equations of the system. The energy functional used contains the Flory-Huggins energy of mixing, the de Gennes terms that consider concentration gradients to enthalpy and entropy and a third contribution due to the interaction of the blend components with the wall.

In chapter 4, the necessary re-scaling of the chemical potential and the conservation equations to dimensionless quantities that prevent from numerical instabilities is made, followed by the implementation of the model proposed into a finite element technique.

In chapter 5, the variation of parameters such as the number of segments in a polymer chain, the quench (upwards or downwards) in temperature within the miscibility gap of the phase diagram and the initial concentration at which the system is quenched are varied systematically to study the effect of these parameters on the morphology development in bulk conditions. For systems where a co-continuous morphology is observed in the bulk the wall effect is introduced and studied as a function of quench in temperature and magnitude of the wall-polymer interaction potential. A partial quantification of the morphology observed in the presence of the wall is done.

In chapter 6 the phase behavior of the binary system poly [methyl methacrylate-co-1H,1H,-perfluoroheptylmethyl methacrylate] / bisphenol-A-diglycidylether (Epikote 828) as a function of the molar mass, fluorine content in the copolymer and chain length extension of the Epikote 828 is studied. For one binary system, preliminary studies of the morphology development around the critical point and around the intersection point of the glass transition curves are carried out. The experimental results for this last region are compared with numerical results for morphology development obtained with the model proposed in this thesis.

In chapter 7, the conclusions of this work are presented followed by suggestions or future work. Appendix I is an extra support to the content of chapters 2 to 5 and in appendix II an experimental method is proposed to formulate homogeneous solutions of a polymer blend in one or more solvents.

1.4 References

¹ Kepler, J. *On the six-cornered snowflake* Published by Godfrey Tampach, Frankfort (1611)
Translated by L.L. Whyte, Oxford Univ. Press (1966)

² Toth, L.F *Regular figures* Pergamon Press Book, Macmillan, New York (1964)

³ Photo by Hoffman, S. *Apitec-Revista mexicana de apicultura* México (1997)

Chapter 1

- ⁴ Stewart, I. *What shape is a snowflake?* Freeman and Company, New York (2001)
- ⁵ Pearce, P. *Structure in nature is a strategy for design* The MIT press, USA (1978)
- ⁶ Woodward, A.E. *Understanding polymer morphology* Hanser, USA (1995)
- ⁷ Kyu, T.; Saldanha, J.M. and Kiesel, M.J. *Prog. Polym. Proc.* **2** (1991) 259
- ⁸ Kyu, T. and Saldanha, J.M. *J. Pol. Sc. Part C: Pol. Lett.* **26** (1988) 33
- ⁹ Knoll, A.; Horvat, A.; Lyakhova, K.S.; Krausch, G.; Sevink, G.J.A.; Zvelindovsky, V. and Magerle, R. *Phys. Rev. Lett.* **89**, no. 3 (2002) 035501-1
- ¹⁰ De Gennes, P.G. *Scaling concepts in polymer physics* Cornell Univ. Press, USA, (1979)
- ¹¹ Helfand, E. *Polymer compatibility and incompatibility: principles and practices* Ed. by Karel Šolc MMI Press Symposium Series **2** (1982) 143
- ¹² Lifschitz, M. and Freed, K.F. *J. Chem. Phys.* **98** (1993) 8994
- ¹³ Manchevski, M. *Before the rain* France/UK/Macedonia (1994)

CHAPTER 2

REVIEW

2.1 Introduction

In this chapter we briefly review the theories dealing with inhomogeneous systems. First in section 2.2, necessarily (due to the lack of standardization in the terminology used in polymer physics) the nomenclature used in this work to describe a polymer chain is introduced. In section 2.3 we give a historical review of the theories developed to study the phase behavior of inhomogeneous systems in bulk and at interfaces. In section 2.4 we justify the selection of a continuous model to study the dynamics of the phase behavior of a polymer blend in the presence of a wall, often denoted as surface directed spinodal decomposition. Subsequently, in section 2.5, we present a summary on experimental and theoretical work that motivated our study on surface directed spinodal decomposition, followed by arguments that have been given to explain this phenomenon. Section 2.6 contains final remarks and conclusions to this chapter.

2.2 Polymer chains

In this section, the nomenclature used throughout this thesis to describe a polymer molecule is introduced, to avoid any confusion with the rather non-standardized terminology found in the literature on physics of polymers.^{1,2,3}

Polymer chains are complex molecules; a simplified model to describe them is the random walk approximation. In this model, no constraints on bond angles, bond rotations, valence angles, etc., are considered. This results in a coil-like conformation and the term random coil is used; nevertheless, in reality, there are constraints. A further simplification to model a polymer chain is to create an effective, freely jointed random coil by combination of straight segments N_k ($N_k \leq N$), having a statistical length σ_k (Kuhn length); such a representation considers implicitly the stiffness of the chain and is called coarse-grained. In this latter scaled representation illustrated in figure (2.1), the real chain of N bonds is modelled as an equivalent chain of $N_k = N/b$, with b number of backbone atoms in the segment, and the Kuhn length as $\sigma_k = bl$, with l the bond length between two backbone atoms. The chain size $\langle r^2 \rangle^*$ of this modelled chain reads:²

* $\langle r^2 \rangle^{1/2}$ is the root-mean-square value of the end-to-end distance r

$$\langle r^2 \rangle = N_k \sigma_k^2 = b N l^2 \quad (2.1)$$

On the other hand the chain size for a random coil is:⁴

$$\langle r^2 \rangle = C_\infty N l^2 \quad (2.2)$$

where C_∞ is the characteristic ratio, which is related to the stiffness of the chain, higher values of C_∞ implies less flexibility. To ensure that the contour of both chain representations are equivalent the condition $b = C_\infty$ must be satisfied.

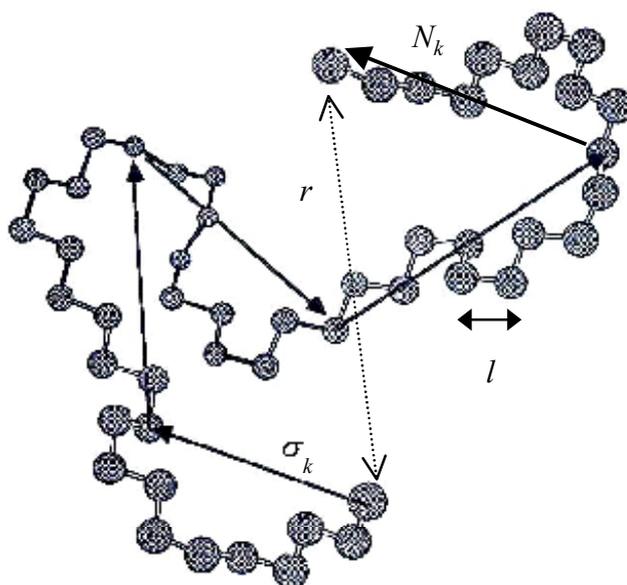


Figure 2.1 Freely jointed chain,⁴ r is the end-to-end distance, with l the bond length, σ_k the Kuhn length and N_k the total amount of Kuhn segments.

Another measure of the coil size is the radius of gyration R_g that provides information about diameter of a polymer chain is defined by⁴

$$R_g^2 = \frac{\langle r^2 \rangle}{6} = \frac{N_k \sigma_k^2}{6} \quad (2.3)$$

2.3 Historical review on the development of mean field and self-consistent field theories

Most of the theories on polymer physics developed to study the phase behavior of inhomogeneous systems in the bulk and at interfaces are an extension to the original lattice model of Flory⁵ and Huggins⁶ developed in 1941. The assumption of locality in the concentration and incompressibility in the system are the two main limitations of the Flory-Huggins lattice model that have motivated the development of different theories in the field of polymer physics. Below we present a brief historical review about the main contributions to the physics of polymers.

In 1957 more than one decade after the works of Flory and Huggins, Cahn and Hilliard,⁷ based on the work of van der Waals,⁸ introduced the gradient contribution to the free energy and for the first time it was possible to study the dynamics of phase separation for incompressible regular solutions in the binodal⁹ (1959) and the spinodal region¹⁰ (1965). For this last case, the effect of thermal fluctuations was added later by Cook¹¹ in 1969.

In the middle of 1960, Edwards¹² extended the classical work made earlier on mean field theories^{5,6,13} in his self-consistent field theory, where he found a direct analogy between the problem of interacting polymer chains and the classical problem of interacting electrons.

We can conclude that both contributions originated from different fields of physical chemistry (polymer and inorganic chemistry) and quantum physics and are the pillars on which the development of polymer physics stands. Still, the problems associated to polymer systems, such as the loss of conformational entropy that a polymer molecule experiences in the proximity of an interface and the effect of compressibility, were still unexplored until this point. It is then from here until our time, that a vast number of theories combining the fundamental ideas of earlier work have developed to study in detail the behavior of polymers at interfaces.

Early in the 70's, Helfand and co-workers gave a solution based on self-consistent field theories to describe the interfacial thickness of symmetric¹⁴ and asymmetric¹⁵ systems. However, Helfand's main contribution is not on the interfacial thickness determination, but on the extension of the lattice model to study the inhomogeneity of polymers at interfaces.¹⁶ In his model, he combines the original Flory lattice theory with anisotropy factors to account for the loss of the conformational freedom at an interface, resulting from molecules near the interface having to turn back from the opposite phase. Other contributions of Helfand and co-workers are the formalization of the Gaussian-random walk¹⁷ in terms of statistical mechanics and the application of his lattice model to the study of the behavior of a polymer melt against a rigid wall.¹⁸

At the end of the 70's, de Gennes¹⁹ developed the random phase approximation (RPA), a theory used to describe in a simple way the interaction between polymer chains. His method is based on the combination of the Flory lattice theory with the ideas of Edwards that allow computing all correlation functions in a dense mixture of strongly interacting polymer chains. In the next section, de Gennes work will be dealt within somewhat more detail. It should be mentioned that it has become clear^{20,21} that the square-gradient terms of de Gennes are appropriate to use in the limit of weak segregation. In the strong segregation limit this term is valid only for infinite molecular weights.

Contemporary to de Gennes are the contributions of Poser and Sánchez,²² who combined Flory's and the Cahn-Hilliard theory neglecting conformational effects in the entropy, and those of Scheutjens and Fleer²³ self-consistent field theory. The last is a rather independent theory applied initially to the study of homopolymers at interfaces, based on counting conformations and interactions of polymer chains on a lattice. The flexibility of this theory has allowed for extensions and modifications to study different effects in polymer systems.²⁴

Until this point, no compressibility effects are included. As in this thesis the same assumption is made, we stop here our review and refer the reader to other contributions that do include this effect.^{25,26,27}

2.4 Self-consistent field versus square-gradient theories

Before selecting a model to study phase behavior of polymer blends in the presence of a wall, we have to ask ourselves about the scale, the degree of accuracy, the numerical methods and even the time available to tackle the problem. In this section, we justify the selection of a continuous model instead of a discrete one.

If we want to know, for instance, the role of loops, trains and tails (illustrated in figure 2.2 (c)) on the properties of surfaces, or if we want to explain the effect of the orientation of a certain atom (see figure 2.2 (d)) within a molecule on the final properties of a material,²⁸ then a discrete²³ self-consistent field theory should be used; where the final equations for the energy are expressed in terms of the individual chain conformations. On the other hand, if we want to study the system from a mesoscopic to a macroscopic scale (figure 2.2 (b) and (a)), it is more convenient to use continuous models (Helfand¹⁶ and de Gennes¹⁹).

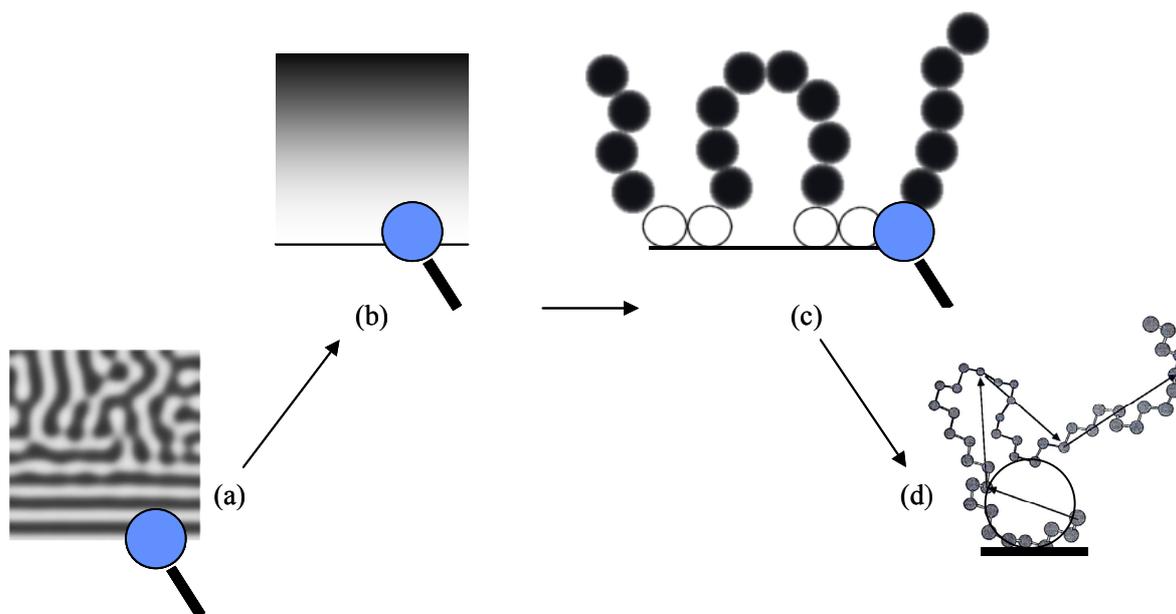


Figure 2.2 From a macroscopic to an atomic scale.

(a) Macroscopic phase separation, (b) mesoscopic scale, (c) coarse-grained scale (black spheres: loops and tails, white spheres: trains), (d) atomic scale.

From the theories presented in the brief historical review, we chose a diffuse-interface or square-gradient theory, since this choice was more compatible with the aim of this thesis and with the numerical methods available.

In the square-gradient approach initially developed for small molecules (Cahn-Hilliard), the free energy of a fluctuating system is assumed to depend not only on the local concentration, but also on derivatives of the free energy that give an excess energy. This fact is expressed by the Flory-Huggins-de Gennes equation. In the case of polymer molecules using the random phase approximation theory (RPA) and the linear response theory, there are two limiting

forms of the square-gradient pre-factor $\kappa(\phi)$ to be considered.[†] The first limit corresponds to the partially miscible region in the miscibility gap of the phase diagram where large wavelength fluctuations in comparison with the chain length dimensions are observed (diffuse interface), whereas the second limit corresponds to the highly segregated region where short wavelength fluctuations occur (sharp interface). In both cases one can write

$$\kappa(\phi) = a^2 kT \left(\frac{\chi}{6} + \frac{1}{\lambda \phi (1 - \phi)} \right) \quad (2.4)$$

where ϕ is the volume fraction of component one, χ is the Flory-Huggins^{5,6} interaction parameter, k is the Boltzmann constant, T the temperature, $\lambda = 36$ in the first limit and $\lambda = 24$ in the second one, and a is the lattice spacing calculated for a binary system as:⁴⁰

$$a^2 = \sigma_{k,1}^2 (1 - \phi) + \sigma_{k,2}^2 \phi \quad (2.5)$$

where $\sigma_{k,1}$ and $\sigma_{k,2}$ are the Kuhn lengths of components one and two, respectively. We focus our study on the partially miscible regime in the phase diagram of a binary polymer system ($\lambda = 36$) where the RPA has proved to give good predictions for phase behavior in polymers. The complete formulation of the Helmholtz free energy including the wall is given in chapter 3.

2.5 Surface-directed spinodal decomposition

In the previous sections, it was sorted out which theory was appropriate to study phase behavior of a binary polymer blend considering the contributions of concentration fluctuations to enthalpy and entropy. In this section we give a brief overview of experimental evidence^{29,30,31,32,33,34,35,36,37,38} on surface-directed spinodal decomposition, as well as the different models used^{39,40,41,42} and the possible mechanisms given so far^{43,44,45,46,47,48} to explain this phenomena.

Since the beginning of the 80's the study of surface-directed self-assembly in macro and micro phase separated binary polymer blends and solutions has been carried out.⁴⁹ For the first two cases, Krausch⁵⁰ presented a review.

Here, we focus on the study of surface effects in thin films of binary polymer blends within the spinodal region of the miscibility gap, the so-called surface-directed spinodal decomposition. The general features found experimentally on this subject are:

- Influence of the film thickness and of a boundary on the phase separation behavior induced by the polymer-surface interactions^{29,34,35,38}
- Formation of an oscillatory concentration profile²⁹⁻³⁷
- A modification of wetting induced by changing the wall^{29,32,36}
- Composition waves with wave vectors normal to the wall^{31,35}
- Difference in domain growth at the wall and in bulk^{30,37,46-48}

[†] See appendix I for the derivation of $\kappa(\phi)$.

The effect of film thickness on phase separation was rationalized by Cohen and Reich²⁹ in terms of a corrected Flory-Huggins interaction parameter with a reduced coordination number. The influence of a boundary on phase separation was explained by Ball and Essery⁵¹ in a theoretical approach modeling the phase behavior using a Ginzburg-Landau type of energy expression (4th expansion order of the Flory-Huggins mixing Gibbs energy). Their results showed formation of anisotropic domains instead of the usual isotropic order found in bulk. In addition, a correlation of a higher order in the domains formed with deeper quenches in temperature was established.

Puri and Binder⁵² reproduced theoretically the formation of an oscillatory concentration profile, found initially by Jones and co-workers³¹ experimentally. In their model, they used a phenomenological theory based on the work of Cahn and Hilliard, using two special boundary conditions that account for the preference of the wall for one of the blend components. So, by choosing certain boundary conditions, the preference for one or the other component for the wall is determined.

What are still not completely clear are the growth rate of the domains at the wall and in bulk and the mechanisms of formation of these domains. Different experimental and theoretical work on this field found contradicting results. Experimentally, Jones et al.³¹ found that the growth rate of phase separation close to the wall was slower than the growth rate in bulk. On the other hand Cumming and co-workers^{46,47,48} found the opposite, a high growth rate next to the wall and a smaller one in the bulk.

The theoretical work is also controversial; we have the following theoretical contributions supporting partially Jones and co-workers³¹ experiments: Brown and Chakrabarti,⁴² using the Ginzburg-Landau approximation for the energy plus terms including long-range effects found a power law proportional to $t^{1/3}$ for the domains growing parallel and perpendicular to the wall. The work of Marko⁵³ using the Cahn-Hilliard-Cook equation, also with a 4th order expansion in the energy, including surface interactions and non-linearities, agreed with the previous mentioned results. Other authors that also find only one length scale characterizing the composition waves are Koblinsky et al.⁴⁴ In their molecular dynamics simulations they integrate the equations of motion for an Ising spin system on a discrete lattice employing Kawasaki spin-exchange dynamics. Their equations reduce to the mean field approach of Puri and Binder⁵² on turning-off the noise or hydrodynamic effects.

The only theoretical work supporting the fast growth of the domains close to the wall was proposed by Troian.⁴³ She finds two length scales, one developing at early time with a scaling exponent t between 1 and 1.5, depending of the quenching in temperature and a second one developing later with a $t^{1/3}$ growth. Her argument to explain this accelerating growth of the domains at the surface is based on the analysis of domain coalescence with a Lifschitz-Slyozov type of growth, that is modified to include the geometrical constraints of growth introduced by the wall. Although the work of Troian is consistent with the experiments of Cumming et al.,^{46,47,48} it has received a severe criticism by Koblinsky et al.⁴⁴ due to the assumption of a higher radius of curvature for the domains growing deeper in the bulk than at the surface.

The general features in which all the mentioned work on surface directed spinodal decomposition agree are:

- The oscillatory behavior of the concentration profile caused by the wall
- The development of a wave vector q normal to the wall and therefore formation of anisotropic domains at the wall, compared to the formation of isotropic domains in the bulk.

The disagreements remaining, both in experiments and theory, motivated our study on surface-directed spinodal decomposition. Another motivation for our work was the rather low resolution of the morphology in the few publications where it is shown.^{42,34} Most of literature on surface-directed spinodal decomposition only show the concentration profiles for the early or late-stages of phase separation, but details of the order parameter or morphology that might give a better idea concerning the mechanism of surface-directed spinodal decomposition are omitted.

2.6 Conclusions

In this chapter, it was briefly presented the coarse-grained model used in the remainder of this thesis. We also outlined a historical review on mean field and self-consistent field theories developed to study polymers in bulk and at interfaces. Further, we gave the motivation to select a continuous square-gradient model instead of a discrete self-consistent field theory. Finally, we presented an overview on surface-directed spinodal decomposition, where we found that there is still a lot to do in this field to clarify contradictions and controversies given by different experimental results and theoretical approaches.

2.7 References

- ¹ Kuhn H. and Försterling H. *Principles of physical chemistry* Wiley & Sons, England (2000)
- ² Lyklema, J. *Fundamentals of Interface and Colloid Science. Vol. II: Solid-liquid interfaces* Academic Press, London (1995)
- ³ Strobl, G.R. *The physics of polymers: concepts for understanding their structure and behavior* 2nd ed. Springer, Berlin (1997)
- ⁴ Boyd, R.H. and Phillips, P.J. *The science of polymer molecules* Cambridge University Press, Great Britain (1993)
- ⁵ Flory, P.J. *J. Chem. Phys.* **9** (1941) 660
- ⁶ Huggins, M.L. *J. Chem. Phys.* **9** (1941) 440
- ⁷ Cahn, J.W. and Hilliard, J.E. *J. Chem. Phys.* **28**, no. 2 (1958) 258
- ⁸ Van der Waals, J.D. *J. Stat. Phys.* **20** (1979) 197 Translated by Rowlinson, J.S.
- ⁹ Cahn, J.W. and Hilliard, J.E. *J. Chem. Phys.* **31**, no. 3 (1959) 688
- ¹⁰ Cahn, J.W. *J. Chem. Phys.* **31**, no. 3 (1965) 688
- ¹¹ Cook, H.E. *Acta Metallurgica* **18** (1970) 297
- ¹² Edwards, S.F. *Proc. Phys. Soc.* **85** (1965) 613
- ¹³ Kuhn, W. *Kolloid Z.* **76** (1936) 258
- ¹⁴ Helfand, E. and Tagami, Y. *J. Chem. Phys.* **56**, no. 7 (1972) 3592
- ¹⁵ Helfand, E. and Sapse, A.M. *J. Chem. Phys.* **62**, no. 4 (1975) 1327
- ¹⁶ Helfand, E. *J. Chem. Phys.* **63**, no. 5 (1975) 2192

- ¹⁷ Helfand, E. *J. Chem. Phys.* **62**, no. 3 (1975) 999
- ¹⁸ Weber, T. and Helfand, E. *Macromolecules* **9**, no. 2 (1976) 311
- ¹⁹ De Gennes, P.G. *Scaling concepts in polymer physics* Cornell Univ. Press, USA (1979)
- ²⁰ Helfand, E. *Polymer compatibility and incompatibility: principles and practices* Ed. Karel Šolc MMI Press Symposium Series **2** (1982) 143
- ²¹ Tang, H. and Freed, K.F. *J. Chem. Phys.* **94** (1991) 1572
- ²² Poser, C.I. and Sánchez, I.C. *J. Colloid Interface Sci.* **69** (1979) 539
- ²³ Scheutjens, J.M.H.M. and Fleer, G.J. *J. Phys. Chem.* **83**, no. 12 (1979) 1619
- ²⁴ Fleer, G.J.; Cohen Stuart, M.A.; Scheutjens, J.M.H.M.; Cosgrove, T. and Vincent, B. *Polymers at interfaces* Chapman & Hall (1993)
- ²⁵ Hong, K.M. and Noolandi, J. *Macromolecules* **14** (1981) 1229
- ²⁶ Sánchez, I.C. and Lacombe, L.H. *Macromolecules* **11** (1978) 1145
- ²⁷ Lifschitz, M. and Freed, K.F. *J. Chem. Phys.* **98** (1993) 8994
- ²⁸ Van de Grampel, R.D. *Surfaces of fluorinated polymer systems* Ph. D. thesis. Eindhoven University of Technology, the Netherlands (2002)
- ²⁹ Reich, S. and Cohen, Y. *J. Pol. Sci. Pol. Phys.* **19** (1981) 1255
- ³⁰ Jones, R.A.L.; Kramer, E.J.; Rafailovich, M.H.; Sokolov, J. and Schwarz, S.A. *Mat. Res. Soc. Symp. Proc.* **153** (1989) 133
- ³¹ Jones, R.A.L.; Norton, L.J.; Kramer, E.J.; Bates, F.S. and Wiltzius, P. *Phys. Rev. Lett.* **66**, no. 10 (1991) 1326
- ³² Bruder, F. and Brenn, R. *Phys. Rev. Lett.* **69**, no. 4 (1992) 624
- ³³ Jones, R.A.L. *Phys. Rev. E* **47**, no. 2 (1993) 1437
- ³⁴ Krausch, G.; Dai, C.; Kramer, E.J.; Markov, J.F. and Bates, F.S. *Macromolecules* **26** (1993) 5566
- ³⁵ Kim, E.; Krausch, G.; Kramer, E.J. and Osby, J.O. *Macromolecules* **27** (1994) 5927
- ³⁶ Kraush, G.; Kramer, E.J.; Rafailovich, M.H. and Sokolov, J. *Appl. Phys. Lett.* **64**, no. 20 (1994) 2655
- ³⁷ Geoghegan, M.; Jones, R.A.L. and Clough, A.S. *J. Chem. Phys.* **103**, no. 7 (1995) 2719
- ³⁸ Karim, A.; Slawacki, T.M.; Kumar, S.K.; Douglas, J.F.; Satija, S.K.; Han, C.C.; Russell, T.P.; Liu, Y.; Overney, R.; Sokolov, J. and Rafailovich, M.H. *Macromolecules* **31** (1998) 857
- ³⁹ Nakanishi, H. and Pincus, P. *J. Chem. Phys.* **79** (1983) 997
- ⁴⁰ Schmidt I. and Binder, K. *J. Physique* **46** (1985) 1631
- ⁴¹ Chen, Z.Y.; Noolandi, J. and Izzo, D. *Phys. Rev. Lett.* **66**, no. 6 (1991) 727
- ⁴² Brown, G. and Chakrabarti, A. *Phys. Rev. A* **46**, no. 8 (1992) 4829
- ⁴³ Troian, S.M. *Phys. Rev. Lett.* **71**, no. 9 (1993) 1399
- ⁴⁴ Keblinski, P.; Ma, W.J.; Maritan, A.; Koplik, J. and Banavar, J.R. *Phys. Rev. Lett.* **72**, no. 23 (1994) 3738
- ⁴⁵ Ma, W.J.; Keblinski, P.; Koplik, J. and Banavar, J.R. *Phys. Rev. E* **48**, no 4 (1993) R2362
- ⁴⁶ Wiltzius, P. and Cumming, A. *Phys. Rev. Lett.* **66**, no 23 (1991) 3000
- ⁴⁷ Cumming, A.; Wiltzius, P.; Bates, F. and Rosedale, J. *Phys. Rev. A* **45**, no. 45 (1992) 885
- ⁴⁸ Shi, B.Q.; Harrison, C. and Cumming, A. *Phys. Rev. Lett.* **70**, no. 2 (1993) 206
- ⁴⁹ Guenoun, P. and Beysens, D. *Phys. Rev. Lett.* **65**, no. 19 (1990) 2406
- ⁵⁰ Krausch, G. *Mat. Sc. Eng.* **R14**, no. 1 (1995) 1
- ⁵¹ Ball, R.C. and Essery R.H.L. *J. Phys. Cond. Matt.* **2** (1990) 10303
- ⁵² Puri, S. and Binder, K. *Phys. Rev. A* **46**, no. 8 (1992) R4487
- ⁵³ Marko, J.F. *Phys. Rev. E* **48** (1993) 2861

CHAPTER 3

SPINODAL DECOMPOSITION IN A THIN POLYMER FILM INTERACTING WITH A RIGID WALL

3.1 Introduction

We study the morphology development of a binary polymer thin film on a substrate that undergoes phase separation within the spinodal region. Within this region, a homogeneous system is in non-equilibrium and is unstable to any infinitesimal concentration fluctuations. The fundamental balance equation in non-equilibrium or irreversible thermodynamics deals with entropy because there is always an entropy source present that is variable with time, given that as a basic rule in Nature entropy is always created and never destroyed. To relate the entropy source to the phenomena of our interest, that is the transport or diffusion of mass, we give in section 3.2 a brief description of the macroscopic conservation laws of mass, momentum and energy in a local or differential form.¹

In section 3.3, we formulate the total energy functional that is used in the remainder of this work. Three contributions are considered: the homogeneous part, the gradient contribution and the wall-polymer interaction. For the homogeneous part of the free energy, in section 3.3.1 we introduce the Gibbs mixing energy given by Flory² and Huggins³ in their mean field theory, plus terms allowing for non-mixing of the pure components. In section 3.3.2 equilibrium, spinodal and critical conditions are calculated. For the gradient contribution of the energy, in section 3.3.3 the additional terms proposed by de Gennes⁴ that consider the contribution of concentration gradients to enthalpy and entropy are taken into account. The minimization of the energy, considering only the homogeneous and the square-gradient term, is done in section 3.3.4 to obtain the bulk concentration profile and the interfacial thickness. This last physical property is of crucial importance in the scaling of the system discussed in chapter 4. The last, but not least important term to be introduced in the total free energy is the interaction of the blend components with the substrate, seen as a rigid wall. In section 3.3.5, we give a formulation of the total wall-polymer interaction potential. In the wall-polymer potential proposed in this thesis the short-range contribution is included as a hard-core potential. To finalize this chapter we give some conclusions in section 3.4.

3.2 Conservation equations

In this section we adhere to the so-called local approximation to obtain the differential form of the balance equations. This approximation implies that the laws governing macroscopic

systems remain valid for infinitesimally small parts of it followed along its center of gravity motion. These balance equations for mass, mass fraction, momentum, and energy in its local or differential form* for a binary system where no reactions take place read:^{1,5,6}

$$\frac{d\rho}{dt} + \rho \nabla \cdot \mathbf{v} = 0 \quad (3.1)$$

$$\rho \frac{dc_i}{dt} = -\nabla \cdot \mathbf{j}_i \quad (3.2)$$

$$\rho \frac{d\mathbf{v}}{dt} = \rho \mathbf{F} + \nabla \cdot \mathbf{P} \quad (3.3)$$

$$\rho \frac{du}{dt} = -\nabla \cdot \mathbf{j}_q - p \nabla \cdot \mathbf{v} - \mathbf{\Pi} : \nabla \mathbf{v} \quad (3.4)$$

with $-\nabla \cdot \mathbf{j}_q = \frac{dq}{dt}$

Equation (3.1) is the law of mass conservation where ρ is the total density, c_i the mass fraction defined by $c_i = \rho_i / \rho$, t the time, and \mathbf{v} the center of mass velocity. In the composition equation (3.2), as the mass of the system is conserved, the diffusion flow \mathbf{j}_i is the only contribution giving a temporal change in mass fraction within a volume element in the system. Equation (3.3) is the momentum or equation of motion, where \mathbf{F} contains all the external forces on the system or long-range interactions within the system and \mathbf{P} is the stress tensor deriving from short-range interactions between particles. Equation (3.4) is the first law of thermodynamics in its temporal form, where u is the specific internal energy and \mathbf{j}_q stands for the heat flux. The last two terms are derived by splitting the stress tensor in an isotropic part $p\mathbf{I}$ and a deviatoric part $\mathbf{\Pi}$, p is the equilibrium pressure and $\mathbf{\Pi}$ is the extra stress tensor ($\mathbf{P} = -p\mathbf{I} + \mathbf{\Pi}$). The equality $\mathbf{I} : \nabla \mathbf{v} = \nabla \cdot \mathbf{v}$ is used as well.[†]

Equations (3.1) to (3.4) in combination with the second law of thermodynamics or entropy law provide a set of equations that allows the study of non-equilibrium transformations. The balance equation for the entropy in its local form is given by:

$$\rho \frac{ds}{dt} = -\nabla \cdot \mathbf{j}_s + \sigma \quad (3.5)$$

where s is the specific entropy, \mathbf{j}_s is the entropy flow given by the difference of the total entropy flux and a convective term $\rho s \mathbf{v}$, and σ is the entropy production which is always positive according to the second law of thermodynamics.

To find expressions for the entropy production it is necessary to introduce a thermodynamic relation for the specific entropy s . In equilibrium the total differential for $s = s(u, v, c_i)$ is given by:

* For the interested reader details can be found in De Groot and Mazur,¹ Verschueren⁵ and van de Vosse.⁶

[†] The operator $:$ is the trace defined by $\mathbf{P} : \mathbf{Q} = P_{ij} Q_{ji}$

$$Tds = du + p dv - \sum_{i=1}^2 \mu_i dc_i \quad (3.6)$$

where p is the equilibrium pressure, v is the specific volume $v = 1/\rho$, $dv = -(1/\rho^2) d\rho$, μ_i is the specific chemical potential of the component i and c_i its mass fraction. Using once more the local approximation, it is possible to write the temporal form of equation (3.6) as:

$$T \frac{ds}{dt} = \frac{du}{dt} - \frac{p}{\rho^2} \frac{d\rho}{dt} - \sum_{i=1}^2 \mu_i \frac{dc_i}{dt} \quad (3.7)$$

where the substitution of the volume by the density was done. For the second term in (3.7) the following identity is used

$$-\frac{p}{\rho^2} \frac{d\rho}{dt} = -\frac{p}{\rho^2} (-\rho \nabla \cdot \mathbf{v}) = \frac{p}{\rho} \nabla \cdot \mathbf{v} \quad (3.8)$$

Substitution of (3.2), (3.4) and (3.8) into (3.7) results after some algebra in the following expression for the temporal change of the specific entropy

$$\rho \frac{ds}{dt} = -\frac{1}{T} \nabla \cdot \mathbf{j}_q + \sum_{i=1}^2 \nabla \cdot \frac{\mu_i}{T} \mathbf{j}_i - \frac{1}{T} \mathbf{\Pi} : \nabla \mathbf{v} - \sum_{i=1}^2 \mathbf{j}_i \cdot \nabla \frac{\mu_i}{T} + \mathbf{j}_q \cdot \nabla \frac{1}{T} \quad (3.9)$$

Under isothermal conditions, the term ∇T^{-1} vanishes. By comparing equation (3.9) with equation (3.5) the entropy flux \mathbf{j}_s and the entropy production σ are identified with:

$$\mathbf{j}_s = \frac{\mathbf{j}_q}{T} - \sum_{i=1}^2 \frac{\mu_i}{T} \mathbf{j}_i \quad (3.10)$$

$$\sigma = -\frac{1}{T} \mathbf{\Pi} : \nabla \mathbf{v} - \sum_{i=1}^2 \mathbf{j}_i \cdot \nabla \frac{\mu_i}{T} > 0 \quad (3.11)$$

Considering that $\sum_{i=1}^2 \mathbf{j}_i = 0$, that is $\mathbf{j}_1 = -\mathbf{j}_2$, the entropy production for a binary system simplifies to:

$$\sigma = -\frac{1}{T} \mathbf{\Pi} : \nabla \mathbf{v} + \mathbf{j}_1 \cdot \nabla \frac{\mu_1 - \mu_2}{T} \quad (3.12)$$

Still all the balance equations (3.1) to (3.4) and (3.12) are in terms of irreversible fluxes, which are unknown parameters. Therefore, it is necessary to introduce phenomenological equations which are linear relations of thermodynamic forces and irreversible fluxes, having the general form:

$$J_i = \sum_k A_{ik} X_k \quad (3.13)$$

where J_i and X_i are any of the Cartesian components of the independent fluxes and thermodynamic forces, Λ_{ik} are phenomenological coefficients, obeying the Onsager reciprocal relations. To write the entropy production in the form of equation (3.13), it is necessary to use a series of tensorial identities¹ that allow writing the dissipative term in equation (3.12) as

$$\mathbf{\Pi} : \nabla \mathbf{v} = \overset{\circ}{\mathbf{\Pi}} : (\overset{\circ}{\nabla} \mathbf{v})^s + \pi \nabla \cdot \mathbf{v} \quad (3.14)$$

where the deviators $\overset{\circ}{\mathbf{\Pi}}$ and $\overset{\circ}{\nabla} \mathbf{v}$ have zero trace and the quantity $\pi = 1/3 \mathbf{\Pi} : \mathbf{I}$. After substitution of (3.14) the entropy production is written as:

$$\sigma = -\frac{1}{T} \overset{\circ}{\mathbf{\Pi}} : (\overset{\circ}{\nabla} \mathbf{v})^s - \frac{\pi}{T} \nabla \cdot \mathbf{v} - \mathbf{j}_1 \cdot \nabla \frac{\mu_1 - \mu_2}{T} > 0 \quad (3.15)$$

Assuming Newtonian behavior, the corresponding Onsager relations for the fluxes in (3.15) are:

$$\begin{aligned} \overset{\circ}{\mathbf{\Pi}} &= -\frac{\Lambda_s}{T} \overset{\circ}{\nabla} \mathbf{v}, \text{ with } \frac{\Lambda_s}{2T} = \eta \\ \pi &= -\frac{\Lambda_b}{T} \nabla \cdot \mathbf{v}, \text{ with } \frac{\Lambda_b}{T} = \eta' \\ \mathbf{j}_1 &= -\Lambda_{11} \nabla \frac{\mu_1 - \mu_2}{T}, \text{ with } \Lambda_{11} \propto D \end{aligned} \quad (3.16)$$

where η is the shear viscosity, η' is the bulk viscosity, Λ_{11} is the diffusivity and D is the diffusion coefficient.

The local balance equations (3.1) to (3.4) together with the phenomenological equations (3.16) and the equations of state for pressure and internal energy, give a set of equations that describe the time behavior of an isotropic binary system, with specified boundary conditions. In our case, we will study the temporal evolution of an inhomogeneous, incompressible, density-matched, isothermal binary system. According to Verschueren⁵ the balance equations for this type of systems read for the mass conservation:

$$-\rho \nabla \cdot \mathbf{v} = 0 \quad (3.17)$$

This result comes from the fact that the difference in density in polymer systems is usually small, such that the Boussinesq approximation,⁷ where the difference in density between the two components is neglected ($\rho = \rho_2 = \rho_1$), can be used. The meaning of equation (3.17) is that the balance of outflow and inflow for a given element is zero any time.

For the mass fraction one obtains:

$$\begin{aligned} \rho \frac{dc}{dt} &= \frac{1}{T} \nabla \cdot \Lambda_{11} \nabla (\mu_1 - \mu_2) \text{ or} \\ \rho \frac{dc}{dt} &= \frac{\Lambda_{11}}{T} \nabla^2 \mu, \text{ with } \Lambda_{11} = \text{constant} \end{aligned} \quad (3.18)$$

where c is the concentration of component one. The non-homogeneity of the system is introduced via the chemical potential, which is by definition

$$\mu(T, c, \nabla c) = \mu_1 - \mu_2 = \left. \frac{\delta F}{\delta c} \right|_{T, V} \quad (3.19)$$

with $F[\phi] \approx F(\phi, \nabla \phi)$

For the momentum equation we have:

$$\frac{d\mathbf{v}}{dt} = -\nabla\left(f + \frac{p}{\rho}\right) + \mu\nabla c + \frac{\eta}{\rho}\nabla^2\mathbf{v} = 0 \quad (3.20)$$

where p is the pressure and η the shear viscosity.

3.3 Energy functional

For the formulation of the Helmholtz free energy, we follow the line of diffuse-interface theories.^{5,8,9,10} The main characteristic of these theories is that the interface has a non-zero thickness, allowing a continuous change in the properties of the system. In a previous study on morphology development in non-homogeneous systems, based on a diffuse-interface model,⁵ only the effect of concentration gradients to enthalpy was considered. Here, we also consider concentration gradients in the entropy, which are important in polymer systems.^{4,11} The Helmholtz energy functional used in this work to study the thermodynamics of a binary polymer thin film on a substrate, undergoing phase separation is:

$$F = \int_V dV [f_0(\phi) + \kappa(\phi)(\nabla\phi)^2 + \phi w(y)] \quad (3.21)$$

The first term of the integrand $f_0(\phi)$, represents the homogeneous contribution to the total Helmholtz energy functional. The square-gradient term $\kappa(\phi)(\nabla\phi)^2$ takes into account the effects of concentration gradients on enthalpy and entropy and the third term considers the interaction between the blend components and the substrate. Once having an expression for the total Helmholtz free energy of the system it is possible to obtain the chemical potential, which is by definition the functional derivative of the functional (3.21), considering the approximation done for F in equation (3.19).

$$\mu = \frac{\delta F}{\delta \phi} = \frac{\partial f}{\partial \phi} - \nabla \cdot \frac{\partial f}{\partial \nabla \phi} \quad (3.22)$$

where f is the integrand of equation (3.21). The first term of this differentiation includes the contributions from the homogeneous part of the Helmholtz energy $f_0(\phi)$ and the wall-polymer interaction potential. These contributions will be treated in detail in sections 3.3.1 and 3.3.5. The second term in equation (3.22) accounts for the concentration variations in entropy and enthalpy of the system (section 3.3.3).

3.3.1 Homogeneous contribution to the energy functional

The total Gibbs free energy for a binary system at constant temperature and pressure is given by:

$$G = \sum_{i=1}^2 n_i \bar{\mu}_i^0 + \Delta G \quad (3.23)$$

where n_i is the mole number of species i , $\bar{\mu}_i^0(T, p)$ is the molar chemical potential of pure species i and ΔG is the excess Gibbs free energy.

Dividing equation (3.23) by its total number of moles n , gives the molar Gibbs free energy ($g = G / n$), the molar excess Gibbs free energy ($\Delta g = \Delta G / n$) and the mole fractions $x_i = n_i / n$, with the mole fraction of component one $x_1 = x$ and the mole fraction of component two $x_2 = (1 - x)$. Considering that the system is incompressible, there are no changes in volume and g the total molar Gibbs free energy is equivalent to the total molar Helmholtz free energy f_0 , yielding

$$f_0 = x \bar{\mu}_1^0 + (1 - x) \bar{\mu}_2^0 + \Delta g \quad (3.24)$$

Instead of the molar excess Gibbs energy, we consider the expression proposed by Flory² and Huggins³ in their mean field lattice model for the free energy density $\Delta g_m(\phi)$

$$\Delta g_m(\phi) = kT \left[\frac{\phi}{N_1} \ln \phi + \frac{(1-\phi)}{N_2} \ln(1-\phi) + \chi \phi(1-\phi) \right] \quad (3.25)$$

with k the Boltzmann constant, T the temperature, $\phi = N_1 n_1 / n_i$ the volume fraction of component 1, $(1 - \phi) = N_2 n_2 / n_i$ the volume fraction of component 2, $n_i = N_1 n_1 + N_2 n_2$ is the number of lattice sites, with n_1 molecules of type 1 and n_2 molecules of type 2, having N_1 and N_2 Kuhn segments respectively[‡], these last quantities are calculated as $N_i = M_i / V_i \rho_i$, here M_i and ρ_i are the molar mass and the density of component i and V_i is the volume of one mole of lattice sites. χ the Flory-Huggins interaction parameter is given by $\chi = z \Delta w / kT$, where z is the number of nearest neighbors or coordination number of the lattice, and $\Delta w = \varepsilon_{12} - (\varepsilon_{11} + \varepsilon_{22}) / 2$ is the difference in contact interaction energy ε of pairs 1-2, 1-1 and 2-2. High values of Flory's interaction parameter lead to phase separation while sufficiently small positive values or negative values of χ indicate miscibility.

After re-writing molar fraction as volume fraction in equation (3.24), using $\phi_i = x_i \bar{V}_i / \sum x_i \bar{V}_i$, with \bar{V}_i is the molar volume of the species i , the homogeneous free energy takes the form:

$$f_0(\phi) = \phi \bar{\mu}_1^0 + (1 - \phi) \bar{\mu}_2^0 + kT \left[\frac{\phi}{N_1} \ln \phi + \frac{(1-\phi)}{N_2} \ln(1-\phi) + \chi \phi(1-\phi) \right] \quad (3.26)$$

[‡] For simplicity in the notation for the number of Kuhn segments N_i , only the component under consideration is explicitly written in the sub-index of this quantity, the label k used in chapter 2 is omitted.

where μ_i^0 is the chemical potential in kT units. For convenience in the literature and in this work the free energy of mixing instead of the total one is used,⁴ to get rid of linear ϕ terms. In appendix I it is shown that either quantity, total or mixing, leads to the same result for equilibrium concentrations and spinodal points.

3.3.2 Equilibrium, spinodal and critical conditions

Once having an expression for the homogeneous part of the free energy it is possible to calculate equilibrium, spinodal and critical conditions. These quantities are used in chapter 5 as an input for the numerical simulations.

According to Gibbs, the equilibrium conditions for a closed system at a fixed pressure and temperature correspond to a minimal free energy defined by:

$$\begin{aligned} d\Delta G \Big|_{T,p} &= 0 \\ d^2\Delta G \Big|_{T,p} &\geq 0 \end{aligned} \quad (3.27)$$

The first condition establishes the existence of an extremum and the second one makes clear that this extremum is a minimum. The excess Gibbs energy for a binary blend separating in two phases α and β , respectively, is sketched in figure 3.1.

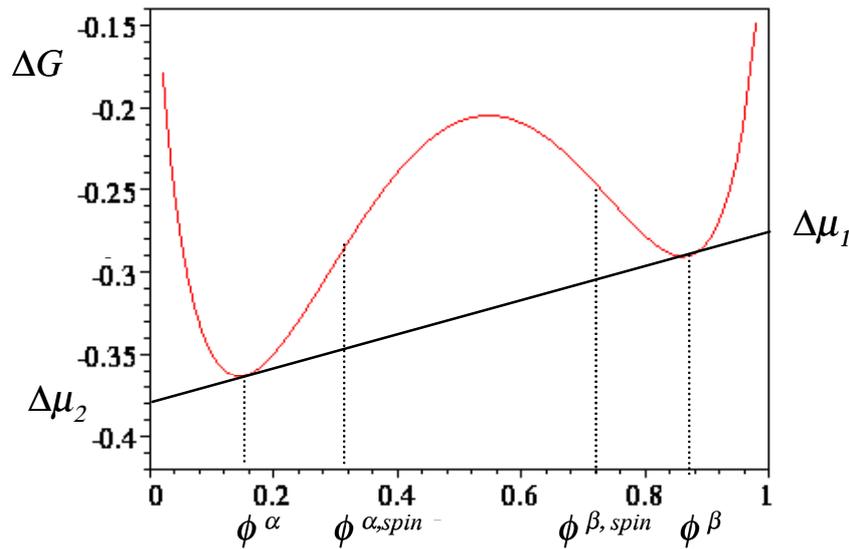


Figure 3.1 Behavior of the excess free energy ΔG in a phase-separated system and common tangent method. ϕ^α and ϕ^β are binodal points, $\phi^{\alpha, spin}$ and $\phi^{\beta, spin}$ are spinodal concentrations, $\Delta\mu_1$ and $\Delta\mu_2$ are chemical potentials of component 1 and 2, respectively.

The compositions of the coexisting phases ϕ^α and ϕ^β are called binodal points and can be determined by the common tangent method, as shown in the same figure. This method requires the solution of the following set of equations:

$$\begin{aligned}\Delta\mu(\phi)_1^\alpha &= \Delta\mu(\phi)_1^\beta \\ \Delta\mu(\phi)_2^\alpha &= \Delta\mu(\phi)_2^\beta\end{aligned}\quad (3.28)$$

where $\Delta\mu$ is the difference between the chemical potential in the mixture and the pure state. The intersections of the common tangent with the pure component axes yield the values of the chemical potentials $\Delta\mu_1$ and $\Delta\mu_2$. These quantities are related to the excess Gibbs energy according to:¹²

$$\begin{aligned}\Delta\mu_1(\phi) &= \left(\frac{\partial\Delta G(n_1, n_2)}{\partial n_1}\right)_{n_2} \\ \Delta\mu_2(\phi) &= \left(\frac{\partial\Delta G(n_1, n_2)}{\partial n_2}\right)_{n_1}\end{aligned}\quad (3.29)$$

where

$$\Delta G(n_1, n_2) = (N_1 n_1 + N_2 n_2) \Delta g_m(\phi) \quad (3.30)$$

After substitution of the free energy density Δg_m (equation (3.25)) in (3.30) is possible to write the following expressions for the chemical potentials of component 1 and 2 as a function of concentration:

$$\begin{aligned}\Delta\mu_1(\phi) &= N_1 \left[\Delta g_m + (1 - \phi) \frac{\partial \Delta g_m}{\partial \phi} \right] \\ \Delta\mu_2(\phi) &= N_2 \left[\Delta g_m - \phi \frac{\partial \Delta g_m}{\partial \phi} \right]\end{aligned}\quad (3.31)$$

From the set of equations in (3.31) in combination with the Gibbs-Duhem relation ($n_1 d\mu_1 + n_2 d\mu_2 = 0$) is derived:

$$\frac{\partial \Delta g_m(\phi)}{\partial \phi} = \frac{\Delta\mu_1(\phi)}{N_1} - \frac{\Delta\mu_2(\phi)}{N_2} \quad (3.32)$$

which gives the homogeneous contribution to the chemical potential in equation (3.22) and is introduced in the implementation of chapter 4 as:

$$\frac{\mu_0}{kT} = c_0 + c_1 \phi + c_2 \ln \phi + c_3 \ln(1 - \phi) + c_4 \phi^2 \quad (3.33)$$

where the coefficients c_0 , c_1 , c_2 , c_3 and c_4 are functions of $\chi(T)$, N_i and satisfy the conservation law explained in appendix I.

Back to figure 3.1 we can see that the Gibbs energy presents two inflection points with compositions $\phi^{\alpha, \text{spin}}$ and $\phi^{\beta, \text{spin}}$ (the super-index denotes the phase α or β in the spinodal points) that are calculated from

$$\left. \frac{\partial^2 \Delta g_m}{\partial \phi^2} \right|_{T, p} = 0 \quad (3.34)$$

in this region the free energy is convex and is called spinodal region. In the spinodal region the system is unstable and phase separation occurs spontaneously due to the negative

contribution to the free energy of the second derivative of the compositions in the range $\phi^{\alpha, \text{spin}} < \phi < \phi^{\beta, \text{spin}}$.

As our study of time dependence of morphology development is precisely in the spinodal region at different temperatures, it is necessary to construct the spinodal curve, which delimits the spinodal region in a representation T versus ϕ as it will be shown below.

Applying the spinodal condition (equation (3.34)) to equation (3.25), gives the following expression for the spinodal curve:

$$\chi = \frac{1}{2} \left(\frac{1}{N_1 \phi} + \frac{1}{N_2 (1 - \phi)} \right) \quad (3.35)$$

Substitution of the interaction parameter[§], $\chi = A + B / T$ (A and B are constants determined by e.g. scattering experiments or other measurement) in equation (3.35) leads to:

$$\frac{1}{T} = \frac{1}{2B} \left(\frac{1}{N_1 \phi} + \frac{1}{N_2 (1 - \phi)} \right) - \frac{A}{B} \quad (3.36)$$

A plot of $T = T(\phi, N_i)$ results in the spinodal curve as sketched in figure 3.2

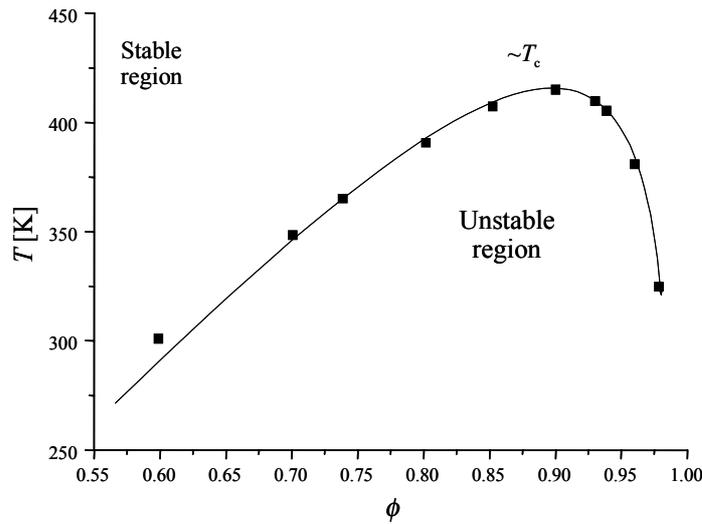


Figure 3.2 Spinodal curve for an asymmetric system.

■ ■ Spinodal curve, T_c is the critical temperature.

Morphological studies are carried out usually near the critical point, because it is in this region where the local concentration has large fluctuations that can be detected with light scattering.⁴ For this reason we calculate critical conditions.

The calculation of the critical concentration ϕ_c , the critical interaction parameter χ_c and the critical solution temperature T_c of a monodisperse system goes as follows. Differentiation of equation (3.35) with respect to ϕ and equalizing the result to zero, gives an extremum for the concentration in the spinodal curve, which is a maximum when the system presents an upper

[§] χ might have a more complicated form dependent on concentration and equation (3.21) changes.

critical solution temperature (UCST) and a minimum if the system has a lower critical solution temperature (LCST). One obtains that the critical concentration is

$$\phi_c = \frac{1}{\sqrt{\frac{N_1}{N_2} + 1}} \quad (3.37)$$

Substitution of equation (3.37) into (3.35) gives the value of the critical interaction parameter and implicitly the critical temperature.

$$\chi_c = \frac{1}{2} \left(\frac{1}{\sqrt{N_1}} + \frac{1}{\sqrt{N_2}} \right)^2 \quad (3.38)$$

For systems where the constants A and B are unknown, we calculate the spinodal curve using the critical conditions. The interaction parameter χ is expressed as $\chi = \chi_1 / T$, with $\chi_1 = \chi_c T_c$. χ_c calculated with equation (3.38) and the critical temperature T_c is interpolated from experimental light scattering data at the critical concentration ϕ_c , obtained with equation (3.37).

Once having the spinodal curve and the critical conditions, we will consider in chapter 5 different reduced quench depths in temperature ε , defined by

$$\varepsilon = (\chi - \chi_c) / \chi_c \quad (3.39)$$

3.3.3 Gradient contribution

In this section the interfacial thickness of a binary system having, either equal or different chain lengths of component one and two (symmetric and asymmetric system) is calculated. This quantity is of crucial importance in the scaling of our system in chapter 4 and therefore is an input parameter in the numerical simulations carried out in chapter 5.

To calculate the interfacial thickness in binary systems at a fixed temperature, we need an expression for the square-gradient term in equation (3.21). From the different theories that include the gradient contribution to the Gibbs energy,^{14,15} we considered the extension to the Flory-Huggins theory obtained by de Gennes the most convenient to use. In this formulation, a square-gradient term $\kappa(\phi)(\nabla\phi)^2$ is obtained using the random phase approximation theory⁴ (see appendix I). The parameter $\kappa(\phi)$ describes the free energy cost of concentration fluctuations and it has two sources: an enthalpic term relating to the effective range of interaction r_0 and a term whose origin is the configurational entropy of the Gaussian coils.^{17,16} The pre-factor of the square-gradient term is

$$\kappa(\phi) = kT \left[\frac{r_0^2}{6} \chi_{eff} + \frac{a^2}{\lambda\phi(1-\phi)} \right] \quad (3.40)$$

In polymer systems, usually the first term in $\kappa(\phi)$ is neglected; nevertheless, in this work we consider both contributions to make our model applicable to either polymer and/or monomer

systems. According to Cahn and Hilliard,⁸ and Binder,¹⁶ r_0 is of the same order as the lattice spacing a calculated with equation (2.5) and χ_{eff} is well represented by the critical interaction parameter χ_c ; therefore $\kappa(\phi)$ simplifies to

$$\kappa(\phi) = a^2 kT \left(\frac{1}{6} \chi_c + \frac{1}{\lambda \phi (1-\phi)} \right) \quad (3.41)$$

where $\lambda = 36$ when a partially miscible system is considered. In these kinds of systems, the wavelength of the concentration fluctuations is large. On the other hand $\lambda = 24$ holds for segregated systems where the wavelength of the concentration fluctuations is short.

By applying the second term of the functional differentiation in equation (3.22) one obtains the following gradient contribution to the chemical potential

$$\mu_{\text{grad}} = kT a^2 \left[\frac{1-2\phi}{\lambda \phi^2 (1-\phi)^2} \|\nabla \phi\|^2 - \left(\frac{1}{3} \chi_c + \frac{2}{\lambda \phi (1-\phi)} \right) \nabla^2 \phi \right] \quad (3.42)$$

Before introducing the wall interaction contribution, we discuss in the next section the minimization of the Helmholtz free energy considering only the homogeneous and the square-gradient term, to obtain the concentration profile and interfacial thickness.

3.3.4 Concentration profile and interfacial thickness

In equilibrium, there are three main important solutions for the concentration: the concentrations of the coexisting phases, obtained in section 3.3.2, and the concentration profile between these coexisting phases. To find the solution for the concentration profile, $\mu = 0$ must be solved in the one-dimensional case, which yields the following conservation law (see appendix I):

$$\frac{d\phi}{dy} = \pm \sqrt{\frac{f_0(\phi) - k_0}{\omega(\phi)}} \quad (3.43)$$

with $\omega(\phi) = \frac{1}{2} \kappa(\phi)$; $\kappa(\phi)$ and $f_0(\phi)$ are given by equations (3.41) and (3.26) respectively; k_0 is a constant determined by the values for ϕ and $d\phi/dy$ at the boundary. The solution of the conservation law in equation (3.43) is not trivial using the exact forms of $\omega(\phi)$ and $f_0(\phi)$. For this reason we use a Taylor expansion around $\phi = \frac{1}{2}$ in $f_0(\phi)$ and $\omega(\phi)$. This method has the advantage of giving an analytic solution for the concentration profile, but it is limited to symmetric systems in the critical region as shown below.

A Taylor expansion of the Flory-Huggins-de Gennes expression (equation (3.25) plus equation (3.41)) expanded around the concentration $\phi = \frac{1}{2}$ (which corresponds to the critical concentration for symmetric systems) and truncated after the first order term in $\kappa(\phi)$ gives:

$$\frac{f}{kT} = -\alpha \phi^2 + \frac{1}{2} \beta \phi^4 + \frac{1}{2} \kappa \left(\frac{d\phi}{dy} \right)^2 \quad (3.44)$$

where $\varphi = \phi - 1/2$ is the order parameter. The coefficients α , β and κ have the form

$$\alpha = \left(\chi - \frac{2}{N}\right) \quad (3.45)$$

$$\beta = \frac{8}{3N} \quad (3.46)$$

$$\kappa = a^2 \left(\frac{1}{6} \chi_c + \frac{1}{9}\right) \quad (3.47)$$

with $N = N_1 = N_2$ and λ equals 36 in equation (3.41). The solution of the inverse of (3.43) using (3.44) to (3.47) is

$$\varphi = \sqrt{\frac{\alpha}{\beta}} \tanh\left(\frac{y}{\xi}\right) \quad (3.48)$$

with

$$\xi = \sqrt{\frac{2\kappa}{\alpha}}, \quad (3.49)$$

$$\kappa > 0, \quad \alpha > 0, \quad \beta > 0$$

The definition of the interfacial thickness ξ is only valid if $\alpha > 0$, i. e. if $\chi > \chi_c = 2/N$. It must be kept in mind that equation (3.48) is obtained if κ is expanded to a first order, any other form of κ does not give the tangent hyperbolic function defining the profile shown in figure 3.3, which is that of our interest.

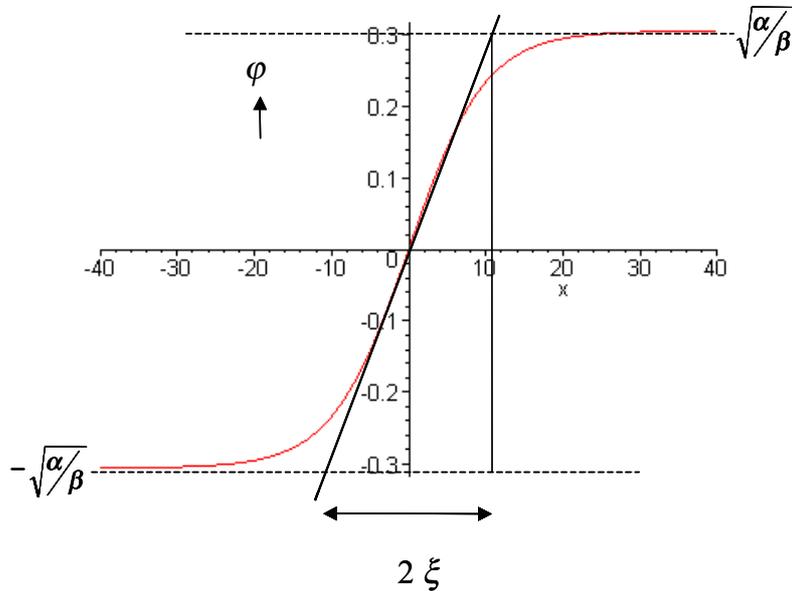


Figure 3.3 Interfacial thickness ξ .

$\varphi = \phi - 1/2, \pm(\alpha/\beta)^{1/2}$ are the equilibrium concentrations.

The interfacial thickness in equation (3.49) corresponds to a thickness going from one equilibrium concentration to the interface situated at $y = 0$. The total thickness for $y \rightarrow \pm \infty$,

$d\phi / dy = 0$, and the equilibrium concentrations $\phi = \pm (\alpha / \beta)^{1/2}$ is given by two times the value of ξ .

To obtain the interfacial thickness in terms of the chain length and thermodynamic quantities, substitution of κ and α into equation (3.49) gives:

$$\xi = a \left(\frac{1}{3} \chi_c + \frac{2}{9} \right)^{1/2} \left(\chi - \frac{2}{N} \right)^{-1/2} \quad (3.50)$$

After identifying $\chi_c = 2/N$ and multiplying by $(\chi_c^{-1/2} / \chi_c^{-1/2})$ one obtains

$$\xi = a \left(\frac{1}{3} + \frac{2}{9\chi_c} \right)^{1/2} \left(\frac{\chi}{\chi_c} - 1 \right)^{-1/2} \quad (3.51)$$

Equation (3.51) represents the form for the interfacial thickness considering both, enthalpy and entropy gradient contributions; depending on the polymer chain length and concentration either one or the other term dominates (see figure 3.4). For $N = 1$, we can neglect the gradient entropy contribution and consider equation (3.51) in the form:

$$\xi = \frac{a}{\sqrt{3}} \frac{1}{\sqrt{\frac{\chi}{\chi_c} - 1}} \quad (3.52)$$

for the case $\chi / \chi_c \gg 1$, i. e.

$$\sqrt{\frac{\chi}{\chi_c} - 1} \approx \sqrt{\frac{\chi}{\chi_c}} \quad (3.53)$$

one obtains after substitution of $\chi_c = 2/N = 2$

$$\xi = a \sqrt{\frac{\chi_c}{3\chi}} \equiv a \sqrt{\frac{2}{3\chi}} \quad (3.54)$$

which corresponds to the definition of interfacial thickness for small molecules in the highly segregated limit.^{9,17} Nevertheless, we have to make clear that equation (3.54) cannot be applied if the fourth order expansion of the energy density is used (equation (3.44)). Instead, the exact form of the Flory-Huggins-de Gennes equation must be considered; the reason is that when $\chi / \chi_c \gg 1$ (i.e. $N\chi \gg 2$), the equilibrium values for the order parameter ϕ , where $\phi = \phi - 1/2$ deviate from those obtained with the exact form of the Flory-Huggins equation, as shown in figure 3.4. An alternative method to obtain the interfacial thickness if the exact form of the Flory-Huggins equation is used is proposed in appendix I, section I.4.3.

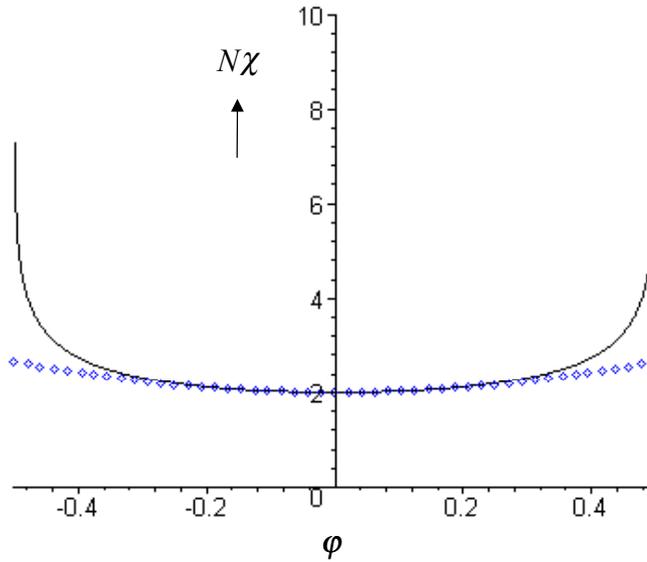


Figure 3.4 Binodal curve in terms of the order parameter φ for a symmetric system.
 — Exact form of the Flory-Huggins equation.
 ◇◇◇ Taylor expansion.

If we now assume that the gradient entropy contribution dominates the interfacial thickness, equation (3.51) is expressed as

$$\xi = a \sqrt{\frac{2}{9\chi_c}} \left(\frac{\chi}{\chi_c} - 1\right)^{-1/2} \quad (3.55)$$

partial substitution of $\chi_c = 2 / N$ gives the expression

$$\xi = \frac{a\sqrt{N}}{3} \left(\frac{\chi}{\chi_c} - 1\right)^{-1/2} \quad (3.56)$$

In the literature^{28,18} equation (3.56) is proposed to be valid around the critical point for systems with $N \rightarrow \infty$. To illustrate the effect of the concentration fluctuations in enthalpy and entropy on the pre-factor of the square gradient term, we considered a series of hypothetical systems with increasing N and a constant ratio χ / χ_c , with an arbitrary $\chi = 2.248$ for $N = 1$. For these systems, the following cases for κ were considered and substituted in the inverse of equation (3.43).

- 1) Only gradient enthalpy contribution in κ , $\kappa = \frac{1}{6} a^2 \chi_c$.
- 2) Only gradient entropy contribution in κ , $\kappa = \frac{1}{9} a^2$.
- 3) Both contributions considered in κ , $\kappa = a^2 \left(\frac{1}{6} \chi_c + \frac{1}{9}\right)$.

The results obtained are shown in figure 3.5 for $N = 1, 10, 100$ and 1000 , respectively.

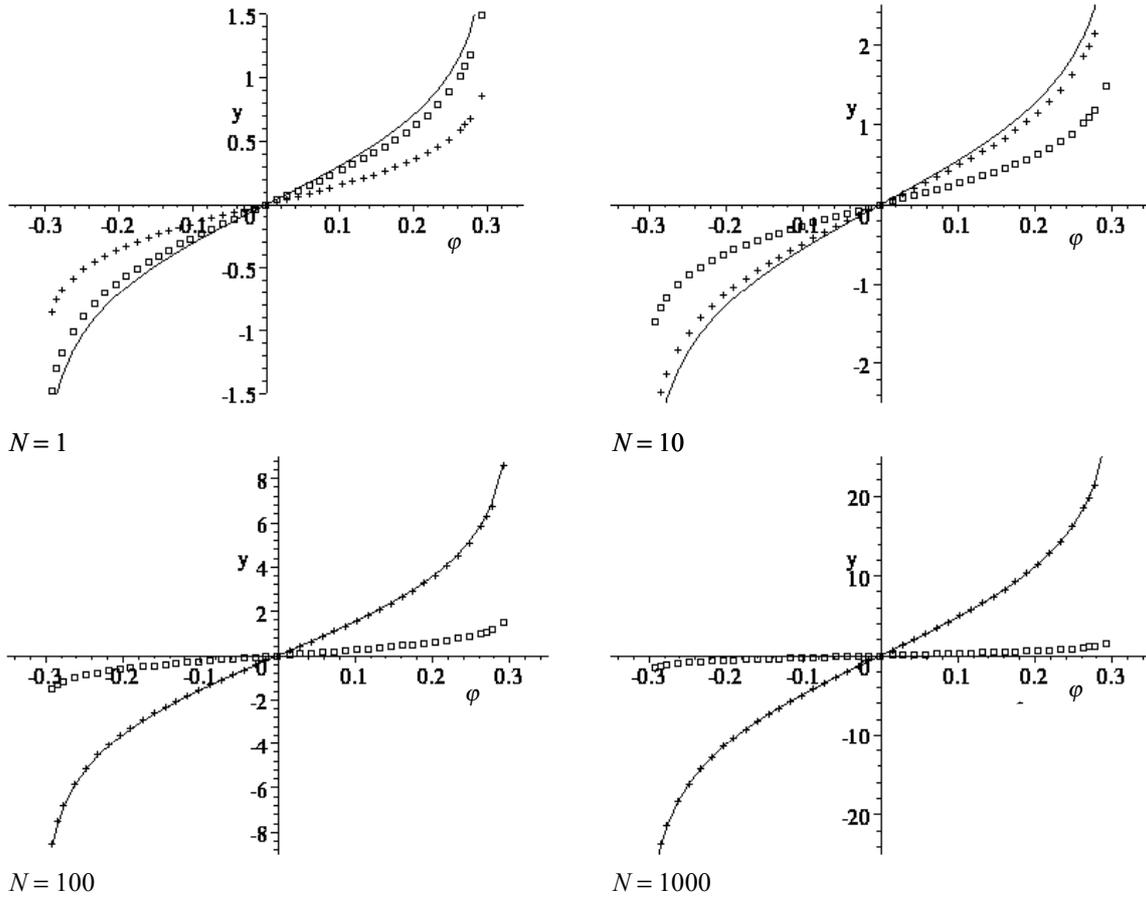


Figure 3.5 Interfacial thickness for different chain lengths.

□□ Enthalpic contribution, ++ entropic contribution, − enthalpic plus entropic contributions.
 $\phi = \phi - 1/2$, y represents the interfacial thickness.

It is clear that only for the case $N = 1$ the entropic contribution can be neglected; for any other situation the entropic term determines the thickness of the interface. In conclusion, the expressions for the interfacial thickness of a system of small molecules or large molecules, given by equations (3.54) and (3.56) respectively, are applicable to symmetric systems around their critical point or to partially miscible systems where the interfacial thickness becomes of the order of magnitude of the gyration radius R_g or larger.

In the case of immiscible or highly segregated systems with finite chain lengths equation (3.56) should not be used, because it predicts values for the interfacial thickness that deviate considerably from the ones known experimentally under this conditions.^{19,20,21} Instead the following analytical expression (Broseta et al.²²) obtained by considering $\lambda = 24$ in equation (3.40) should be used

$$\xi = \xi_{\infty} [1 + (1/\chi N_1 + 1/\chi N_2) \ln 2] \quad (3.57)$$

Here χN_i has typical values between 5 and 15 and ξ_{∞} is corrected for entropic effects and given by²¹

$$\xi_{\infty} = 2 \left[\frac{\rho_1^0 \sigma_1^2 + \rho_2^0 \sigma_2^2}{12\chi(\rho_1^0 \rho_2^0)^{1/2}} \right]^{1/2} \quad (3.58)$$

where σ_i is the statistical Kuhn length, ρ_i^0 is the monomer density of component i and χ is the interaction parameter.

So far, we were able to determine the concentration profile in the bulk when a Taylor expansion of the energy is done around the critical point for a symmetric system; nevertheless, it is known from experiments that this profile is no longer described with a tangent hyperbolic function when a wall is present; instead, a more complex behavior is obtained.²³ The concentration profile including the wall has no analytical solution, for this reason we use a numerical method explained in chapter 4. Before going to the numerical technique used to predict the concentration profile and morphology development in the presence of a wall, we formulate in the next section an expression for the wall-polymer potential used in this thesis.

3.3.5 Interaction potential of a polymer blend with a rigid wall

Intermolecular forces have different effects at short and long-range; short-range interactions have an effect in the order of magnitude below 1 nm, while long-range forces have a range to about 100 nm. It is known that the surface energy of nonpolar liquids including polymers arises from intermolecular van der Waals forces, rather than short-range surface interactions.²⁴ Because of this, we focus in formulating a wall potential in terms of the long-range forces and we include the short-range repulsion as a hard-core potential.

Although scientist have always looked for general laws to explain and to predict the behavior of Nature, intermolecular forces are too complex to summarize in a universal law the distance dependence of the interactions for any system. Instead, the use of semi-empirical expressions to explain the behavior of specific systems has been an alternative. Within the semi-empirical models, the first pair potential including attractive and repulsive interactions was proposed by Mie (1903) and has the form

$$w(y) = -\frac{C}{y^n} + \frac{D}{y^m} \quad (3.59)$$

where y is the intermolecular distance, C , D and the exponents n and m are parameters chosen according to the system considered. The repulsive part of this potential derives from electronic repulsions also known as steric repulsion. The range of these interactions for small atoms and molecules is the van der Waals diameter i. e. around 0.2 to 0.4 nm. The attractive part corresponds to the van der Waals forces;^{**} this term considers the long-range intermolecular interactions.

^{**} The name comes from the fact that Van der Waals was the first scientist in establishing the existence of attractive forces between molecules in 1874.

The Lennard-Jones potential is a good example of a Mie-type potential where the exponents m and n equal 6 and 12 respectively and the constants C and D are related to the molecular radii and potential depth. A sketch of this potential it is shown in figure 3.6.

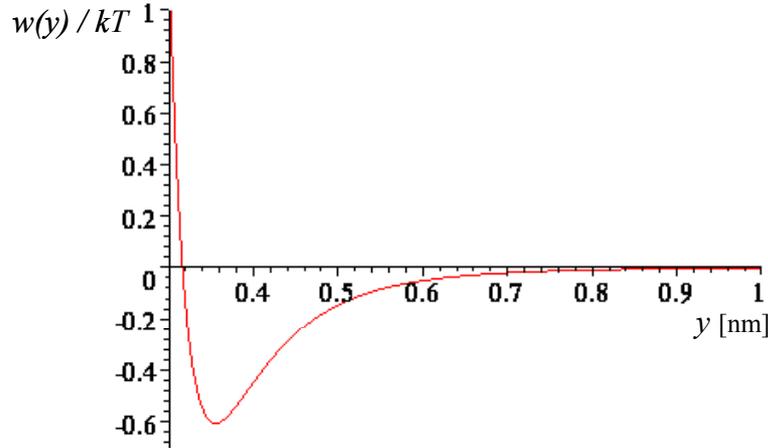


Figure 3.6 Lennard-Jones potential for a system²⁵ with $C = 10^{-23}$ [J nm⁶], $D = 10^{-26}$ [J nm¹²].

The success of this kind of potentials is that this mathematical form is rather simple and the energy of interaction can be adjusted well to experimental data.

Back to our problem, the system we want to study consists of molecules of type 1 and 2 undergoing phase separation and interacting with a wall at the same time. To approach this situation in the most simplified way, we consider initially the interaction of a molecule with a rigid wall, as depicted in the figure 3.7:

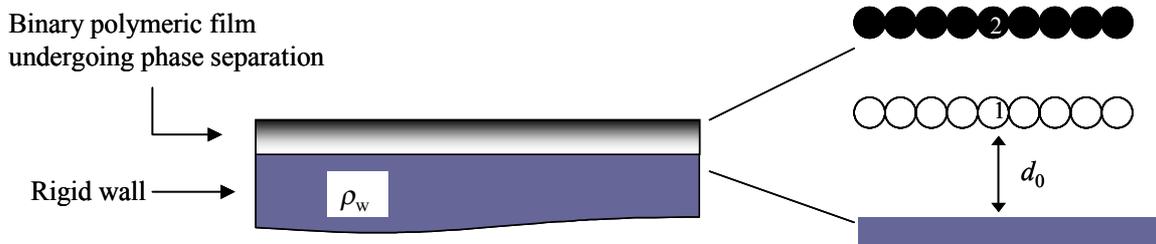


Figure 3.7 Surface-molecule interaction, ρ_w is the number density and d_0 the interfacial contact separation.

For this situation the interaction energy $w(y)$ for the attractive part of the total potential is calculated using pair wise additivity (Hamaker summation method) and according to Israelachvili²⁵ given by:

$$w(y) = -\pi C \rho_w / 6y^3 \quad (3.60)$$

where C is an interaction constant, y is the distance to the wall and ρ_w is the number density or atoms per unit volume in the wall. It is possible to relate the van der Waals interaction potential to the interfacial tension by recalling that the energy of two flat interfaces in terms of interfacial tension is given by:

$$w = \frac{A}{12\pi} \left(\frac{1}{d_0^2} - \frac{1}{d^2} \right) \quad (3.61)$$

at $d = d_0$ (two surfaces in contact), $w = 0$, and at $d = \infty$ (two isolated surfaces) we have

$$w = \frac{A}{12\pi d_0^2} = 2\gamma \quad (3.62)$$

or

$$\gamma_{1w} = \frac{A}{24\pi d_0^2} \quad (3.63)$$

In this last equation γ_{1w} is the interfacial tension between component one and the wall, A is the Hamaker constant defined as $A = \pi^2 C \rho^2$ and d_0 is the interfacial contact separation between the atoms of the two materials present at the interface; with a universal value of 0.165 nm.²⁵ At this point, we have to consider that we do not have only one component present interacting with the wall, but there is also a second component. For this reason we use the difference in interfacial tension of each component with the wall $\Delta\gamma_i = (\gamma_{2w} - \gamma_{1w})$, instead of γ_{1w} in equation (3.63). This new expression for $\Delta\gamma_i$ indicates the preferential adsorption of one component over the other (see appendix I, section I.5); therefore, when both components have the same interfacial energy with the wall no preferential adsorption is considered. After the previous considerations, we have for the attractive part of the wall-polymer potential the following expression

$$w(y) = -\frac{4d_0^2 \Delta\gamma_i}{\rho_w y^3} \quad (3.64)$$

The repulsive part or short-range interaction potential could be similar in form to the attractive part. However, differently to other authors,^{26,27,28,29} we use a hard-core potential radius d_0 that corresponds to the distance from the origin to the minimum of the total potential, as shown in figure 3.8. It is clear that for distances below d_0 the total potential goes to infinity, whilst for distances above d_0 it follows equation (3.64) and decays smoothly to zero.

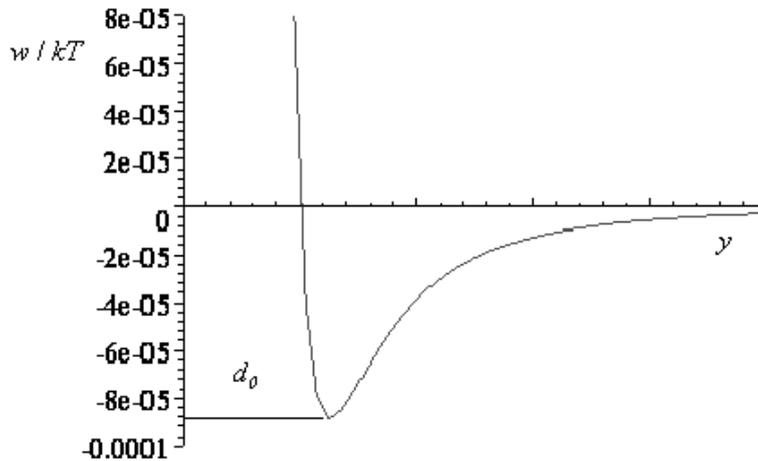


Figure 3.8 Total wall-polymer interaction potential, y is the distance to the wall, d_0 the interfacial contact separation.

Since the numerical technique used to solve our whole problem requires the same integration domain for each contribution; it is necessary to choose for the wall-polymer potential a range of integration that fairly represents the physical problem to describe and that does not give any singularity at or close to the wall. An approximation is used that avoids the blow-up of the potential to infinity at $y = 0$ and the vanishing of the interfacial tension at $d = d_0$ (equation (3.61)). This approximation, illustrated in figure 3.9, consists in shifting the origin of the potential to the position of the hard-core diameter d_0 ; after this shifting, the attractive term, y^3 , is replaced in the denominator of equation (3.64) by $(y + d_0)^3$; the only condition to be satisfied is that d_0 must be much smaller than the long-range interaction contribution. The area below d_0 , neglected by shifting the potential to d_0 , is compensated by the area in between the dashed-line and the original solid line of the potential, in this way the total value of the original potential is only slightly modified.

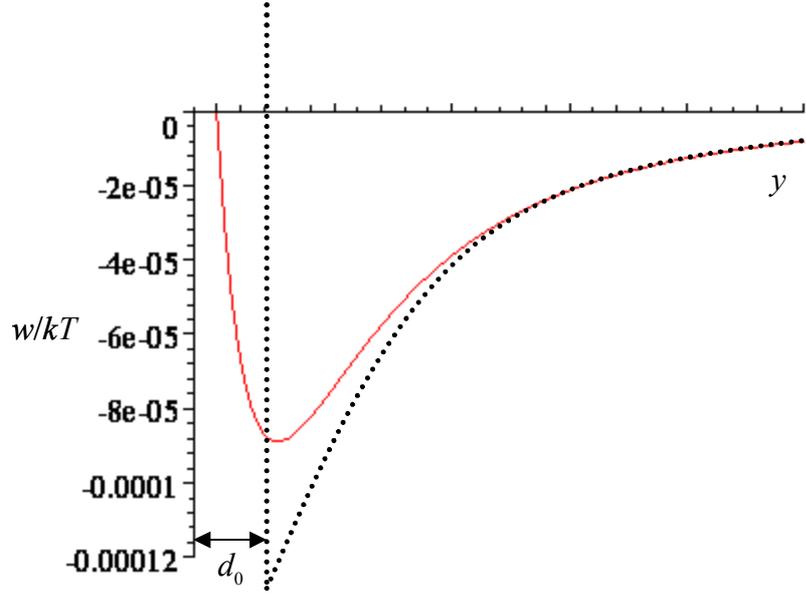


Figure 3.9 Shifting of the wall-polymer potential to the position of the hard-core diameter.

We thus conclude that the wall-polymer interaction potential takes the form

$$w(y) = -\frac{4d_0^2\Delta\gamma_i}{\rho_w(d_0 + y)^3} \quad (3.65)$$

With this final expression for the wall-polymer interaction potential, and the terms obtained in the previous sections for the homogeneous and the gradient contribution (equations (3.33) and (3.42)), the total chemical potential takes the form

$$\begin{aligned} \frac{\mu}{kT} = & c_0 + c_1\phi + c_2 \ln \phi + c_3 \ln(1-\phi) + c_4\phi^2 + \\ & a^2 \left[\frac{1-2\phi}{36\phi^2(1-\phi)^2} \|\nabla\phi\|^2 - \left(\frac{1}{3}\chi_c + \frac{1}{18\phi(1-\phi)} \right) \nabla^2\phi \right] + w(y^*) \end{aligned} \quad (3.66)$$

where $w(y^*)$ was made dimensionless by introducing the following dimensionless variables:

$$\begin{aligned}
 d_0^* &= d_0 / L^\dagger \\
 \Delta\gamma_i^* &= \frac{\Delta\gamma L^{\dagger 2}}{kT} \\
 \rho_w^* &= \rho_w L^{\dagger 3} \\
 y^* &= y / L^\dagger
 \end{aligned}
 \tag{3.67}$$

where L^\dagger is a numerical length defined by $L^\dagger = L / a_1$ with L the size of the system where the process takes place, and $a_1 = 100$ is a constant introduced for convenience to properly represent the wall-polymer potential in the numerical method used in the next chapter. Explicitly the dimensionless potential $w(y^*)$ is now:

$$w(y^*) = -\frac{4d_0^{2*}\Delta\gamma_i^*}{\rho_w^*(d_0^* + y^*)^3}
 \tag{3.68}$$

Below, we give the estimation we used for the interfacial energy as an input of this parameter in chapter 5. For simplicity, we omit the asterisk in the notation on each of the variables mentioned in equation (3.68).

Experimentally $\Delta\gamma_i = \gamma_{2w} - \gamma_{1w}$ is known only for a few systems^{30,31} and therefore we estimate this parameter using the Young equation and the concentration profile obtained in section 3.3.4. According to Young the interfacial tension of two liquids in contact with a wall are related by:

$$\gamma_{2w} = \gamma_{1w} + \gamma_{12} \cos\theta
 \tag{3.69}$$

where θ is the contact angle defined in the way shown in figure 3.10 and γ_{12} is the bulk interfacial tension that is straightforwardly calculated from the concentration profile given by equation (3.48), with¹⁸

$$\gamma_{12} = 2kT\rho \int_{-\infty}^{\infty} \kappa dy \left(\frac{d\phi}{dy} \right)^2
 \tag{3.70}$$

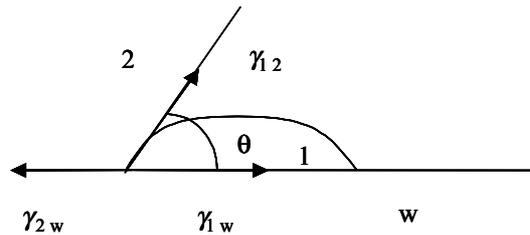


Figure 3.10 Definition of interfacial tensions for partial wetting $0 < \theta < 180^\circ$. γ_{12} , γ_w and γ_{2w} , are the interfacial tensions between components 1 and 2, component 1 and wall (w) and component 2 and wall, respectively.

Integration of equation (3.70) yields

$$\gamma_{12} = \frac{9}{a^2\sqrt{N}} \left(1 - \frac{\chi_c}{\chi} \right)^{3/2}
 \tag{3.71}$$

which is the interfacial tension for a symmetric system, where the Taylor expansion in f_0 and $\kappa(\phi)$ was used. For systems in which the exact form of the free Gibbs energy and $\kappa(\phi)$ is

used, the interfacial tension is obtained using the maximum slope method mentioned in appendix I, section I.4.3.

In our case, we assume total wetting therefore, $\theta = 0$ and one obtains that $\Delta\gamma_i = \gamma_{i2}$. For contact angles different from zero, a different way to calculate $\Delta\gamma_i$ must be followed, see appendix I, section I.5.1.

Until here, we analyzed the different contributions to the energy functional that describes phase behavior of our system either in bulk or in the presence of a wall. As a remark in equation (3.18) and (3.20), we have to fill in mass fraction instead of volume fraction and specific chemical potential instead of the molar property. The transformation from volume fraction to mass fraction is easily done using

$$c_i = \frac{\phi_i \rho_i}{\rho} \quad (3.72)$$

Nevertheless, the assumption done in this work on incompressibility implies a density-matched system and a non-distinction between mass and volume fraction. In that case the total expression for the specific chemical potential reads

$$\begin{aligned} \mu = \frac{\bar{\mu}M}{RT} = & c_0 + c_1c + c_2 \ln c + c_3 \ln(1-c) + c_4c^2 + \\ & a^2 \left[\frac{1-2c}{36c^2(1-c)^2} \|\nabla c\|^2 - \left(\frac{1}{3}\chi_c + \frac{1}{18c(1-c)} \right) \nabla^2 c \right] + w(y^*) \end{aligned} \quad (3.73)$$

where $\bar{\mu}$ is the molar chemical potential, M is the molar mass of the polymer blend, obtained from $M = M_1M_2 / (M_1(1-c) + M_2c)$, with M_1 and M_2 the molar masses of component one and two, respectively.

3.4 Conclusions

In this chapter, the local conservation equations for a binary isothermal, incompressible, density-matched polymer systems were obtained; these equations couple the dynamics and thermodynamics of the system allowing to follow any temporal transformation taking place. The introduction of phenomenological equations allowed the replacement of unknown irreversible fluxes by phenomenological coefficients which are physical properties characterizing the system. Further, to calculate the chemical potential the Helmholtz energy functional was introduced; formed by a homogeneous contribution, a square-gradient contribution giving the influence of concentration fluctuations in enthalpy and entropy, and the wall-polymer interaction contribution. Each of these contributions plays a different role: the homogeneous contribution determines the final bulk equilibrium conditions, the homogeneous plus the square-gradient terms determine the bulk concentration profile and the interfacial thickness, and it is expected that the wall has an influence on the morphology development, according to experimental observations. The analysis carried out in this chapter makes our model applicable to symmetric and asymmetric, having polymer chains with a large or a small number of segments.

3.5 References

- ¹ De Groot, S.R. and Mazur, P. *Non-equilibrium thermodynamics* Dover Publications, USA (1984)
- ² Flory, P.J. *Principles of polymer chemistry* Cornell University Press, USA (1953)
- ³ Huggins, M.L. *J. Chem. Phys.* **9** (1941) 440
- ⁴ De Gennes, P.G. *Scaling concepts in polymer physics* Cornell University Press, USA (1979)
- ⁵ Verschueren, M. *A diffuse-interface model for structure development in flow* Ph. D. thesis. Eindhoven University of Technology, the Netherlands (1999)
- ⁶ Van de Vosse, F.N. *Notes RPK course on polymer physics*, the Netherlands (2000)
- ⁷ Lowengrub, J. and Truskinovsky, L. *Proc. R. Soc. Lond. A* **454** (1998) 2617
- ⁸ Cahn, J.W. and Hilliard, J.E. *J. Chem. Phys.* **28**, no. 2 (1957) 258
- ⁹ Helfand, E. and Tagami, Y. *J. Chem. Phys.* **56**, no. 7 (1972) 3592
- ¹⁰ Van der Waals, J.D. *J. Stat. Phys.* **20** (1979) 197
- ¹¹ Helfand, E. *J. Chem. Phys.* **63**, no. 5 (1975) 2192
- ¹² Ten Brinke, G. *RPK notes on polymer physics* The Netherlands (1999)
- ¹³ Koningsveld, R. *Advan. Colloid Interface Sci.* **2** (1968) 151
- ¹⁴ Cahn, J.W. *J. Chem. Phys.* **42**, no. 1 (1965) 93
- ¹⁵ Fler G.J.; Cohen Stuart, M.A. and Scheutjens, J.M.H.M. *Polymers at interfaces* London: Chapman & Hall (1993)
- ¹⁶ Binder, K. *J. Chem. Phys.* **79**, no. 12 (1983) 6387
- ¹⁷ De Gennes, P. G. *J. Chem. Phys.* **72**, no. 9, (1980) 4756
- ¹⁸ Binder, K. *Acta Polymer.* **46** (1995) 204
- ¹⁹ Fernández, M.L.; Higgins, J.S.; Penfold, J.; Ward, C.; Shackleton, C. and Walsh, D.J. *Polymer* **28** (1988) 1923
- ²⁰ Russel, T.P.; Anastasiadis, S.H.; Menelle, A.; Felcher, G.P. and Satija, S.K. *Macromolecules* **24** (1991) 1575
- ²¹ Perrin, P. and Prud'homme, R. E. *Macromolecules* **27** (1994) 1852
- ²² Broseta, D.; Fredrickson, G.H; Helfand, E.; Leibler, L. *Macromolecules* **23** (1990) 132
- ²³ Bruder, F. and Brenn, R. *Phys. Rev. Lett.* **69**, no. 4 (1992) 624
- ²⁴ Jones, R.A.L. *Phys. Rev. E* **47**, no. 2 (1993) 1437
- ²⁵ Israelachvili, J. *Intermolecular and surface forces* 2nd ed. Academic Press limited, London (1992)
- ²⁶ Noolandi, J. and Chen, Z.Y. *Phys. Rev. Lett.* **66**, no. 6 (1991) 727
- ²⁷ Chakrabarti, A. and Brown, G. *Phys. Rev. A.* **46**, no. 8 (1992) 4829
- ²⁸ Jones, R.A.L. *Phys. Rev. E.* **47**, no. 2 (1993) 1437
- ²⁹ Krausch, G. *Mat. Sc. Eng.* **R14**, no. 1 (1995) 1
- ³⁰ Karim, A.; Slawacki, T. M.; Kumar, S. K.; et al. *Macromolecules* **31** (1998) 857-862
- ³¹ Jones, R.A.L.; Kramer, E.J.; Rafailovich, M.H. and Schwarz, S.A. *Mat. Res. Soc. Symp. Proc.* **153** (1989) 133

CHAPTER 4

MODEL IMPLEMENTATION

4.1 Introduction

In this chapter it is described how the numerical implementation of the extended diffuse-interface model proceeds; this extension includes the concentration gradient contribution of the concentration to entropy and the wall-polymer interaction potential.

In section 4.2, we consider a quasi-incompressible binary polymer blend undergoing phase separation in the presence of a rigid wall. A chemical potential derived from the Flory-Huggins-de Gennes mean field model is used, linking the thermodynamics and the kinetics, and allowing the study of transient morphology development. Since it is necessary to re-scale the system of equations to avoid numerical instabilities, in section 4.3 the chemical potential and the conservation equations are re-expressed in terms of non-dimensional quantities.

A finite element method is used and the temporal and spatial discretizations are presented in section 4.4. To finalize this chapter in section 4.5 the temporal and spatial validation of the model proposed is shown followed by a brief discussion and concluding remarks.

4.2 System definition

We consider a quasi-incompressible binary polymer blend in contact with a rigid wall; the total Helmholtz energy functional F for this system reads:

$$F = \int_V dV [f_0(\phi) + \kappa(\phi)(\nabla\phi)^2 + \phi w(y)] \quad (4.1)$$

where ϕ is the volume fraction of polymer one, $f_0(\phi)$ is the homogeneous part of the energy, $\kappa(\phi)$ the pre-factor of the concentration gradient in energy and entropy, and $w(y)$ the wall-polymer interaction potential, with y the distance to the wall. These three contributions were analysed and explained in detail in chapter 3.

In addition, in chapter 3 also the specific chemical potential, derived from the functional equation (4.1), and the simplified two-dimensional conservation equations (equations (4.3) and (4.4)) were obtained. It was shown that the phenomenological equations couple the

hydrodynamics and thermodynamics of the system. Therefore, the model introduced is general to study any system where hydrodynamic effects could play an important role. However, in this work, we study the early-stage of the spinodal decomposition, where hydrodynamic effects are minimal.¹

The chemical potential obtained in the previous chapter (see equation (3.73)) reads:

$$\begin{aligned} \mu = \frac{\bar{\mu}M}{RT} = c_0 + c_1 c + c_2 \ln c + c_3 \ln(1-c) + c_4 c^2 + \\ a^2 \left[\frac{1-2c}{36c^2(1-c)^2} \|\nabla c\|^2 - \left(\frac{1}{3} \chi_c + \frac{1}{18c(1-c)} \right) \nabla^2 c \right] + w(y^*) \end{aligned} \quad (4.2)$$

where $\bar{\mu}$ is the molar chemical potential, R is the gas constant, T the temperature, the coefficients c_0 , c_1 , c_2 , c_3 and c_4 contain implicitly the chain length N_i and the value of $\chi = \chi(T)$, a is the lattice spacing, χ_c is the critical interaction parameter, M is the molar mass of the polymer blend ($M = M_1 M_2 / (M_1(1-c) + M_2 c)$, with M_1 and M_2 the molar masses of component one and two respectively) and c is the mass fraction of component one.

After applying a Boussinesq approximation,² the local mass equation was reduced to:³

$$\nabla \cdot \mathbf{v} = 0 \quad (4.3)$$

Substitution of the irreversible fluxes by phenomenological quantities allowed writing the mass fraction conservation equation as:

$$\frac{dc}{dt} = \frac{\Lambda}{\rho_1 T} \nabla^2 \mu \quad (4.4)$$

where ρ_1 is the density of component one, t the time, μ the specific chemical potential, given by equation (4.2). Λ is a phenomenological coefficient related to the diffusion coefficient D , according to⁴

$$\begin{aligned} \Lambda = \frac{D\rho_1(1-c)T}{\mu_{11}^c}, \\ \text{with } \mu_{11}^c = \frac{RT}{c\{M_1(1-c) + M_2 c\}} \end{aligned} \quad (4.5)$$

Since we assumed incompressibility, it is convenient to eliminate the pressure term in equation (3.20). This can be done by writing the momentum equation in terms of a stream function ψ , defined by $\mathbf{v} = (\partial\psi / \partial y, -\partial\psi / \partial x)$, followed by application of the curl ($\nabla \times$). This operation yields the following momentum equation for ψ

$$\nabla^4 \psi = \frac{\rho}{\eta} \nabla \times \mu \nabla c \quad (4.6)$$

Using the full dimensional equations is possible in the finite element technique, but when numerical instabilities occur it is necessary to scale equations (4.2), (4.4) and (4.6), by introducing dimensionless variables. The next section is devoted to the scaling of the system.

4.3 Scaling chemical potential, mass balance and momentum equations

In the re-scaling of the chemical potential, mass balance and momentum equations two different lengths are used: the interfacial thickness (ξ) and the length of the domain in which the diffusion process is taking place (L). As a rule, quantities involving time such as diffusion and velocity, are scaled with the interfacial thickness, and quantities considering spatial coordinates, such as the wall potential, the stream function ψ , the gradient operator and the distance to the wall are scaled with a numerical length $L^\dagger = L/a_1$. The definition of this numerical length is necessary to properly represent the wall-polymer potential with the number of elements* used. A value of $a_1 = 100$ proved to be convenient to use.

The following set of dimensionless variables is introduced

$$\begin{aligned} y^* &= y / L^\dagger & \mu^* &= \frac{\mu M}{RT} & t^* &= \frac{tD}{\xi^2} \\ \nabla^* &= L^\dagger \nabla & a^* &= a / \xi & \psi^* &= \frac{\psi}{L^\dagger v} \end{aligned} \quad (4.7)$$

After re-writing equations (4.2), (4.4) and (4.6) in terms of the previous set of dimensionless variables one obtains for the chemical potential

$$\begin{aligned} \mu^* &= c_0 + c_1 c + c_2 \ln c + c_3 \ln(1-c) + c_4 c^2 + \\ &\left(\frac{a^* \xi}{L^\dagger} \right)^2 \left[\frac{1-2c}{36c^2(1-c)^2} \|\nabla^* c\|^2 - \left(\frac{1}{3} \chi_c + \frac{1}{18c(1-c)} \nabla^{*2} c \right) \right] + w(y^*) \end{aligned} \quad (4.8)$$

with $w(y^*)$ given by equation (3.68). Omitting the asterisk notation, the dimensionless equation for the diffusion reads

$$\frac{dc}{dt} = \left(\frac{\xi}{L^\dagger} \right)^2 \nabla^2 \mu \quad (4.9)$$

and for the rotation of the momentum equation the final result is

$$\nabla^4 \psi = \frac{\rho_1 RT \xi L^\dagger}{D \eta M} \nabla \times \mu \nabla c \quad (4.10)$$

*The small domains obtained after discretization of the system are called elements.

4.4 Spatial and temporal discretization of the conservation equations

In this section, we present the spatial and temporal discretization of the conservation equations. To discretize the governing equations we use a spectral element method,⁵ which is a combination of spectral and finite element methods resulting in a high order of accuracy of the spectral method combined with geometrical flexibility of the finite element method.⁶ The system under consideration is an inhomogeneous fluid in a closed area A , with a boundary S . From this area A we take an arbitrary area Ω , that has a boundary $\partial\Omega$ $\partial\Omega = (\partial\Omega^d + \partial\Omega^n)$ and an outer normal \mathbf{n} , as shown in figure 4.1.

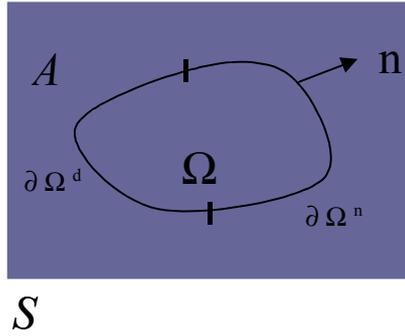


Figure 4.1 Domain to discretize.
 $\partial\Omega^d$, Dirichlet boundary conditions.
 $\partial\Omega^n$, Neumann boundary conditions.
 $\partial\Omega = (\partial\Omega^d + \partial\Omega^n)$.

This arbitrary area Ω represents our computational domain that is divided into N_{el} non-overlapping sub-domains Ω_e and a spectral approximation is applied on each element; the division of Ω into elements is called spatial discretization. The basis functions φ , which are used for the spatial discretization, are high-order Lagrange interpolation polynomials defined through the Gauss-Lobatto integration points per element.^{7,8,9}

The curl of the momentum equation (4.10) is a fourth-order differential equation in ψ , that we split into two-second order differential equations

$$-\nabla^2 Q = h \tag{4.11}$$

$$-\nabla^2 \psi = Q \tag{4.12}$$

where $h = -\frac{\rho_1 RT \xi L^\dagger}{D \eta M} \nabla \times \mu \nabla c$. Since the basis functions φ are elements of H^1 , that is

$$H^1(\Omega) = \{\varphi \mid \varphi \in L^2(\Omega), \nabla \varphi \in L^2(\Omega) \times L^2(\Omega)\} \tag{4.13}$$

The boundary conditions for Q and ψ are either homogeneous Neumann at $\partial\Omega^n$ or Dirichlet at $\partial\Omega^d$. The Galerkin weighted residual representation of the differential equation is

$$-(\nabla^2 Q, \omega)_\Omega = (h, \omega)_\Omega \tag{4.14}$$

$$-(\nabla^2 \psi, \omega)_\Omega = (Q, \omega)_\Omega \quad (4.15)$$

where the usual inner product $(a, \omega)_\Omega = \int_\Omega a \omega d\Omega$ is defined and ω is the standard Galerkin test function with the following property for the Dirichlet part of $\partial\Omega$ ($\partial\Omega^d$).

$$\omega \in H_0^1(\Omega) = \{\varphi \in H^1(\Omega) \mid \varphi|_{\partial\Omega^d} = 0\} \quad (4.16)$$

A partial integration of the integrals on the left-hand side of equations (4.14) and (4.15) yields the weak or variational form

$$(\nabla Q, \nabla \omega)_\Omega = (h, \omega)_\Omega + (\nabla \psi \cdot \mathbf{n}, \omega)_{\partial\Omega^n} \quad (4.17)$$

$$(\nabla \psi, \nabla \omega)_\Omega = (Q, \omega)_\Omega + (\nabla \psi \cdot \mathbf{n})_{\partial\Omega^n} \quad (4.18)$$

where the boundary integrals vanished because of the homogeneous boundary conditions. A next step is to decompose the total domain Ω in N_{el} non-overlapping sub-domains Ω_e and apply the spectral discretization on each element.

$$\mathbf{Q}_e = \sum_{l,m=1}^N Q_{lm} \varphi_{lm} \quad (4.19)$$

where φ_{lm} is the two-dimensional Lagrange interpolation through the Legendre-Gauss-Lobato integration points ($l, m = 1 \dots N$), which is the tensor product of the one-dimensional interpolation functions: $\varphi_{lm} = \varphi_l \varphi_m$. The values in the matrix Q_{lm} correspond to the value of \mathbf{Q} at the point lm giving after multiplication by φ_{lm} a vector \mathbf{Q}_e per element. Using similar discretizations for ψ , ω , h and assembling the elements we obtain the following discrete set of equations

$$\mathbf{S}\mathbf{Q} = \mathbf{M}\mathbf{h} \quad (4.20)$$

$$\mathbf{S}\boldsymbol{\psi} = \mathbf{M}\mathbf{Q} \quad (4.21)$$

where \mathbf{S} is the diffusion matrix, \mathbf{M} is the mass matrix and \mathbf{Q} , \mathbf{h} and $\boldsymbol{\psi}$ are the discrete vector representations of Q , h and ψ , respectively.

Further, mass balance and chemical potential compose a set of two second-order differential equations that are solved in a coupled way. Here it is necessary to apply besides spatial discretization also a temporal discretization. Prior to the temporal and spatial discretization of this set of equations, some algebraic manipulations of the chemical potential μ , given in equation (4.8), make it reduce to a polynomial in terms of c that simplifies the implementation.

If we multiply equation (4.8) by F^{-1} , the inverse of the Laplacian, given by

$$F^{-1} = \frac{18c(1-c)}{6\chi_c c(1-c)+1} = \frac{3c(1-c)}{(\chi_c c(1-c) + 1/6)}$$

$$\text{or } F^{-1} = \frac{3}{\chi_c + \frac{1}{6c(1-c)}} \quad (4.22)$$

and the non-linear terms are put on the right hand side, one obtains

$$F^{-1}(\mu - c_0 - c_1 c - c_4 c^2) + \left(\frac{a\xi}{L^\dagger}\right)^2 \nabla^2 c =$$

$$F^{-1}(c_2 \ln c + c_3 \ln(1-c) + w(y)) + \frac{(1-2c)}{12c^2(1-c)^2 + 2c(1-c)} \left(\frac{a\xi}{L^\dagger}\right)^2 \|\nabla c\|^2 \quad (4.23)$$

Once having this simplification of μ we carry out an Euler-backward temporal discretization. To do so we make use of $d/dt = \partial/\partial t + \mathbf{v} \cdot \nabla$ and re-write the mass fraction balance equation (4.9) as

$$\frac{\partial c}{\partial t} + \mathbf{v} \cdot \nabla c = \left(\frac{\xi}{L^\dagger}\right)^2 \nabla^2 \mu \quad (4.24)$$

Here μ is the chemical potential re-written in the form of equation (4.23) and

$$\frac{\partial c}{\partial t} \approx \frac{c_{i+1}^{n+1} - c_i^n}{\Delta t} \quad (4.25)$$

n indicates the concentration at time t and $n+1$ is equivalent to $t + \Delta t$. The subscript i corresponds to a Picard iteration step and is used to deal with the non-linear terms: the iteration starts using $c_1^{n+1} = c_0^n$ and as stopping criterion, is used $|c_i^n - c_{i+1}^{n+1}| < 10^{-4}$. By applying this iteration also to μ , and discretizing spatially (4.23) and (4.24) we obtain the Laplacian stiffness matrix \mathbf{S} and the convection matrix \mathbf{N} in the following system of equations

$$\mathbf{M}c_{i+1}^{n+1} - \Delta t \mathbf{N}c_{i+1}^{n+1} + \left(\frac{\xi}{L^\dagger}\right)^2 \Delta t \mathbf{S} \mu_{i+1}^{n+1} = \mathbf{M}c_0^n \quad (4.26)$$

$$F^{-1} \mathbf{M}(\mu_{i+1}^{n+1} - c_0 - c_1 c_i^{n+1} - c_4 (c_i^{n+1})^2) - \left(\frac{a\xi}{L^\dagger}\right)^2 \mathbf{S} c_{i+1}^{n+1} =$$

$$F^{-1} \mathbf{M}(c_2 \ln c_i^{n+1} + c_3 \ln(1 - c_i^{n+1}) w(y)) +$$

$$\frac{(1 - 2c_i^{n+1})}{12(c_i^{n+1})^2 (1 - c_i^{n+1})^2 + 2c_i^{n+1} (1 - c_i^{n+1})} \left(\frac{a\xi}{L^\dagger}\right)^2 \|\nabla \mathbf{M}c_i^{n+1}\| \quad (4.27)$$

Assembling of equations (4.26) and (4.27) give the following global stiffness matrix:

$$\begin{bmatrix} \mathbf{M} - \Delta t \mathbf{N}^n & \left(\frac{\xi}{L^\dagger}\right)^2 \mathbf{S} \\ -\frac{F^{-1}}{c_i^{n+1}} (c_0 + c_1 c_i^{n+1} + c_4 (c_i^{n+1})^2) \mathbf{M} - \left(\frac{a\xi}{L^\dagger}\right)^2 \mathbf{S} & F^{-1} \mathbf{M} \end{bmatrix} \begin{bmatrix} c_{i+1}^{n+1} \\ \mu_{i+1}^{n+1} \end{bmatrix} = \begin{bmatrix} \mathbf{M} c_0^n \\ \mathbf{M} f_2 \end{bmatrix} \quad (4.28)$$

where

$$\begin{aligned} f_2 = & F^{-1} (c_2 \ln c_i^{n+1} + c_3 \ln(1 - c_i^{n+1}) + w(y)) \\ & + \frac{(1 - 2c_i^{n+1})}{12(c_i^{n+1})^2 (1 - c_i^{n+1})^2 + 2c_i^{n+1} (1 - c_i^{n+1})} \left(\frac{a\xi}{L^\dagger}\right)^2 \|\nabla c_i^{n+1}\| \end{aligned} \quad (4.29)$$

After convergence, μ_{i+1}^{n+1} and c_{i+1}^{n+1} are used to compute a new h and move to the next time step.

4.5 Temporal and spatial validation of the model

Implementation of the model was checked in the first time step, and an arbitrary test function was introduced for the concentration

$$c(x, y) = \sin(x) \sin(y) \quad (4.30)$$

With this function, we calculated separately f_2 , the right hand side of the global stiffness matrix (4.29) using a Maple script. The results obtained were equivalent to those from the finite element model.

In the absence of a wall potential a direct comparison between the chemical potential obtained at the first time step in the finite element model and that given by the homogeneous contribution to this property is possible and convenient, to check whether both methods give the same output.

For the spatial validation of the model, we modified the order of the polynomial np used in the interpolation basis functions, in a finite element sub-routine that gives as output the residual or absolute value of the error between the real concentration and the calculated one $|c_r - c_c|$. This residual decreases monotonically as the finite element mesh is refined, due to the Galerkin assumption used. The results obtained are listed below in table 4.1. This matching of increase in polynomial order of the interpolation basis functions and the decrease of the error clearly shows the spatial consistency of our model.

Table 4.1 Error $|c_r - c_c|$ as a function of np , the polynomial order in the interpolation functions.

np	$ c_r - c_c $
2	0.1358
4	9.739×10^{-4}
6	6.974×10^{-14}
8	3.560×10^{-14}

In addition, in the calculation of the global stiffness matrix (4.29), the mesh, as well as the polynomial order in the interpolation functions were modified, giving the following results:

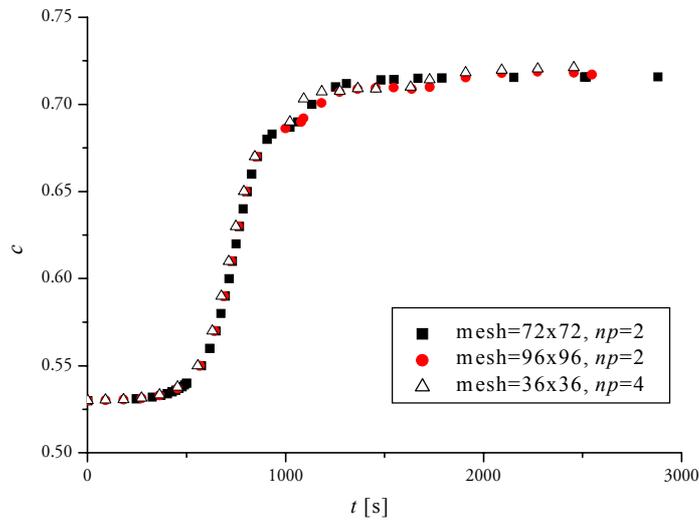
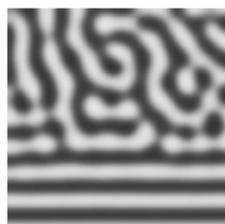


Figure 4.2 Concentration profile using different polynomial order np and mesh refinement ($\Delta t = 1 \times 10^{-5}$).

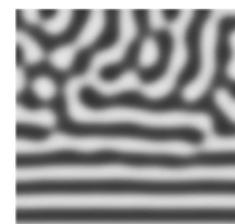
From figure 4.2 we see that increasing the polynomial order in the interpolation functions has the same effect as refining the mesh; nevertheless, the calculations are more time consuming when the polynomial order is higher. Figure 4.3 illustrates that the more refined the mesh, the better the definition in morphology.



$np = 2$, mesh = 72x72



$np = 2$, mesh = 96x96



$np = 4$, mesh = 36x36

Figure 4.3 Morphologies obtained for different polynomial order (np) and mesh refinement ($\Delta t = 1 \times 10^{-5}$, computational time equal to 0.016).

As always, a compromise between accuracy and computation time must be made. We chose for a mesh of 72 per 72 elements and a polynomial order of two for the interpolation functions.

To check temporal consistency of the model we tried three different time steps, a decrease in time step, implies an increase in accuracy of the calculation of the unknowns c and μ .

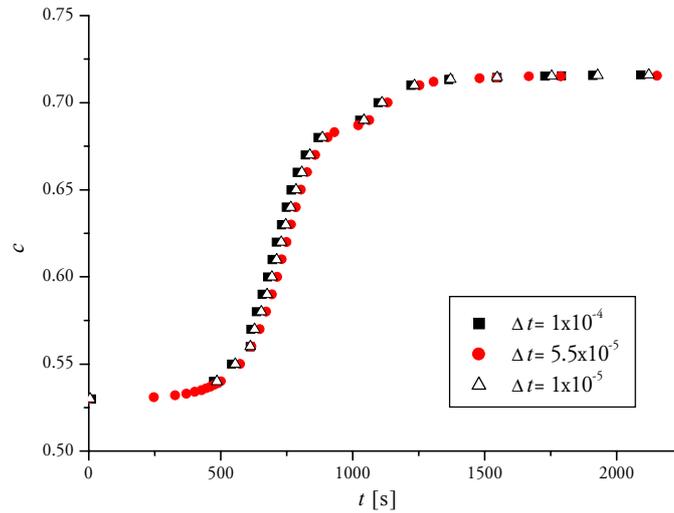


Figure 4.4 Concentration versus time for three different time steps.

Figure 4.4 shows the temporal consistency of our model, from the trend of the plots in this figure at different time steps we can conclude that a time step $\Delta t = 1 \times 10^{-5}$ is a good compromise between sufficient accuracy and acceptable computation time.

4.6 Conclusions

In this chapter, we presented the implementation of the extension to the diffuse-interface model that includes the gradient contribution to entropy and the wall-polymer interaction potential. In the re-scaling of the governing equations, it is necessary to introduce a numerical length L^\dagger to tune the effect of the wall potential. For the numerical implementation of the conservation equations, a Galerkin type spectral discretization, which ensures that the error of the residual is minimal, was used. Due to the dimensionality of the problem, the Gauss-Lobatto numerical integration or quadrature was also employed. Finally, we demonstrated the spatial and temporal consistency of the model.

4.7 References

- ¹Krausch, G. *Mat. Sc. Eng.* **R14**, no.1 (1995) 1
- ²Lowengrub, J. and Truskinovsky, L. *Proc. R. Soc. Lond. A* **454** (1998) 2617

- ³ Verschueren, M. *A diffuse-interface model for structure development in flow* Ph. D. thesis. Eindhoven University of Technology, the Netherlands (1999)
- ⁴ De Groot, S.R. and Mazur, P. *Non-equilibrium thermodynamics* Dover Publications, USA (1984)
- ⁵ Timmermans, L.J.P.; van de Vosse, F.N. and Mineev, P.D. *Int. J. Num. Meth. in Fluids* **18** (1994) 853
- ⁶ Canuto, C.; Hussaini, M.Y.; Quarteroni, A. and Zang, T.A. *Spectral methods in fluid dynamics* Springer-Verlag, New York-Berlin (1988)
- ⁷ Anderson, P.D. *Computational analysis of distributive mixing* Ph. D. thesis. Eindhoven University of Technology, the Netherlands (1999)
- ⁸ Hunter, P. *FEM/BEM notes* The University of Auckland, New Zealand (2002)
- ⁹ Timmermans, L.J.P. *Analysis of spectral element methods with application to incompressible flow* Ph. D. thesis. Eindhoven University of Technology, the Netherlands (1994)

CHAPTER 5

NUMERICAL RESULTS

5.1 Introduction

In chapter 3, we introduced a continuous diffuse-interface model to study morphology development of a polymer binary film undergoing phase separation in the presence of a rigid wall and in chapter 4 the implementation and validation of the model into a finite element technique was carried out. In this chapter, we apply the model to a series of polymer blends in bulk and in the presence of a rigid wall in the early-stage of spinodal decomposition. In section 5.2 the effect on morphology development of number of segments N_i , symmetry (or asymmetry) of the system, quench depth in temperature ε and initial concentration before quenching the system are investigated for the bulk. In section 5.3, we choose two symmetric and two asymmetric systems to study the wall effect for the conditions where co-continuous structures in bulk were observed. The effect of the magnitude of the wall-polymer potential and the quench depth in temperature is studied for one symmetric system. Further, in section 5.3.1 a quantitative analysis based on the root-mean-square deviation from the average concentration, the power spectral density function and the autocorrelation function of the wavelengths present in concentration profiles at different positions from the wall is carried out. To finalize this chapter, in section 5.4 we give some conclusions.

5.2 Morphology development in bulk

As a first application of the diffuse-interface model proposed in the previous chapters, we consider the series of binary polymer blends listed in table 5.1 without including the wall effect yet. The purpose of these simulations is to study the effect on the morphology development of initial concentration, reduced quenching gap in temperature ε , chain length N_i , and difference in chain lengths of the two components in the blend (symmetry or asymmetry).

For all systems shown in table 5.1, the necessary thermodynamic data to calculate equilibrium, spinodal and critical conditions (as explained in chapter 3, section 3.3.2) are known from the literature. Except for the system PMMA- d_8 / PTFPMA¹ that shows a lower critical solution temperature (LCST), the rest of the systems included show an upper critical solution temperature (UCST).

Table 5.1 Systems where bulk morphology is studied.

M_w , molar mass, N_1 and N_2 , number of Kuhn segments, χ_c , critical interaction parameter, ϕ_c , critical concentration, T_c , critical temperature, χ_1 , a constant (see section 3.3.2), χ , Flory-Huggins interaction parameter.

Blend	M_w [kg/mol]	N_1 / N_2	χ_c	ϕ_c	T_c [K]	χ_1	$\chi = \chi(T, \phi)$
dPS/P α MS ²	49 / 50	443 / 377	0.0049	0.48	418	--	$51 / T (0.0626 - 0.0018\phi - 5.16 \times 10^{-5}T)$
dPS / PBr _x S ³ $x = 0.119$	123.2 / 162	1098 / 1285	0.0017	0.52	569.8	0.96	
PS / dPS ⁴	903.6/1290	8700/11500	0.0002	0.47	407.4	--	$-0.00029 + 0.2/T$
x MMA-(1- x)FHMA / Epikote 828, $x = 0.9128$	32 / 0.67	47 / 1	0.656	0.13	403.2	264	---
PMMA-d ₈ / PTFPMA ¹	570 / 100	4009 / 737	0.0014	0.30	487.7	---	$0.14398 - 69.54576 / T$

For each system, the conditions listed in table 5.2 are investigated. When the initial concentration ϕ_0 equals the critical concentration ϕ_c three different reduced quenches in temperature, ε (equation (3.39)), are tried, whilst for initial concentrations $\phi_0 = \phi_c \pm \Delta\phi$ only two. Equation (3.51) is used to calculate the interfacial thickness ξ in symmetric systems, whilst the method of the maximum slope presented in appendix I (section I.4.3) is used for asymmetric systems. The value for η , the viscosity, is an estimation calculated according to van Krevelen⁵ for a polymer melt.

Table 5.2 Summary of the parameters used as input for the simulations.

System	ϕ_0	ε	T [K]	ξ [nm]	η [kg/nm s]
dPS / P α MS ²	0.48	0.05	404.8	16.9	1.1×10^{-7}
	0.33,0.48,0.63	0.25	359.5	7.6	7.0×10^{-7}
	0.33,0.48,0.63	0.45	323.3	5.7	7.0×10^{-7}
dPS / PBr _x S ³ $x = 0.119$	0.52	0.05	542.6	34.5	1.6×10^{-6}
	0.37,0.52,0.67	0.25	453.2	15.2	1.8×10^{-6}
	0.37,0.52,0.67	0.45	393.0	11.5	6.4×10^{-6}
PS / dPS ⁴	0.53	0.05	399.2	95.4	2.5×10^{-4}
	0.38,0.53,0.68	0.25	369.6	44.2	1.4×10^{-3}
	0.38,0.53,0.68	0.45	344.0	33.0	1.4×10^{-3}
x MMA-(1- x)FHMA / Epikote 828, $x = 0.9128$	0.127	0.05	384.0	2.3	1.1×10^{-8}
	0.08,0.127,0.32	0.25	322.6	1.0	1.7×10^{-8}
	0.08,0.127,0.32	0.45	278.1	0.8	1.7×10^{-8}
PMMA-d ₈ / PTFPMA ¹	0.2,0.3,0.45	0.25	488.9	10.9	3.2×10^{-5}
	0.2,0.3,0.45	0.45	489.9	7.9	3.2×10^{-5}

In figure 5.1, the results for the system dPS / P α MS² are shown. It should be mentioned that this binary polymer blend was chosen to modify systematically N_i in symmetric systems; nevertheless, an experimental morphological study for this system is not possible, because the miscibility gap lies below the glass transition temperature. In the captions of figures 5.1 to 5.5 a is the lattice spacing, calculated with equation (2.5).

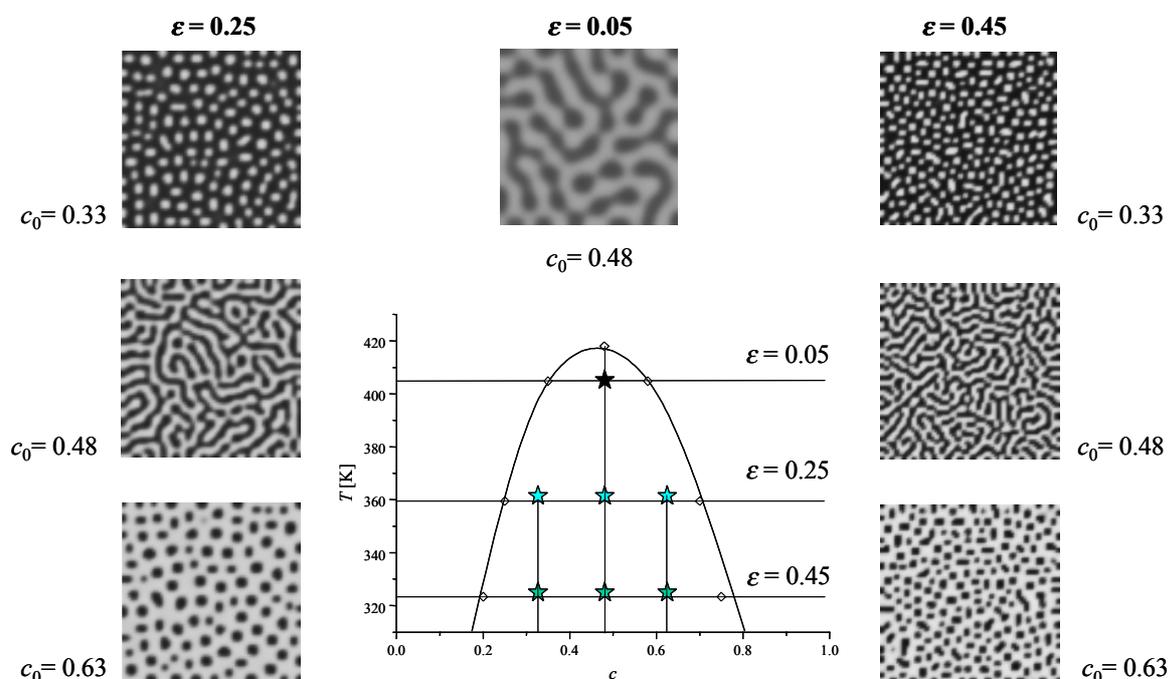


Figure 5.1 System dPS / P α MS², $L = 3500$ nm, $a = 0.561$ nm.
 ◇◇ Spinodal curve.

From figure 5.1, we observe that the concentration at which the system is quenched has an effect on the structure developed. For quenches departing from $\phi_0 = \phi_c$, co-continuous domains are formed. On the other hand, for quenches departing from $\phi_0 = \phi_c \pm 0.15$ the co-continuous or lamellar structure is lost. As anticipated, from the interfacial thickness values obtained in table 5.2, deeper quenches in temperature give smaller domain sizes in the morphology; this is due to the increase of the bulk interfacial tension.

For the systems dPS / PBr_xS and PS / dPS similar results in morphology were found and are shown in figures 5.2 and 5.3. Only the domain size increases by increasing the chain length of the polymers, as expected from the interfacial thickness values.

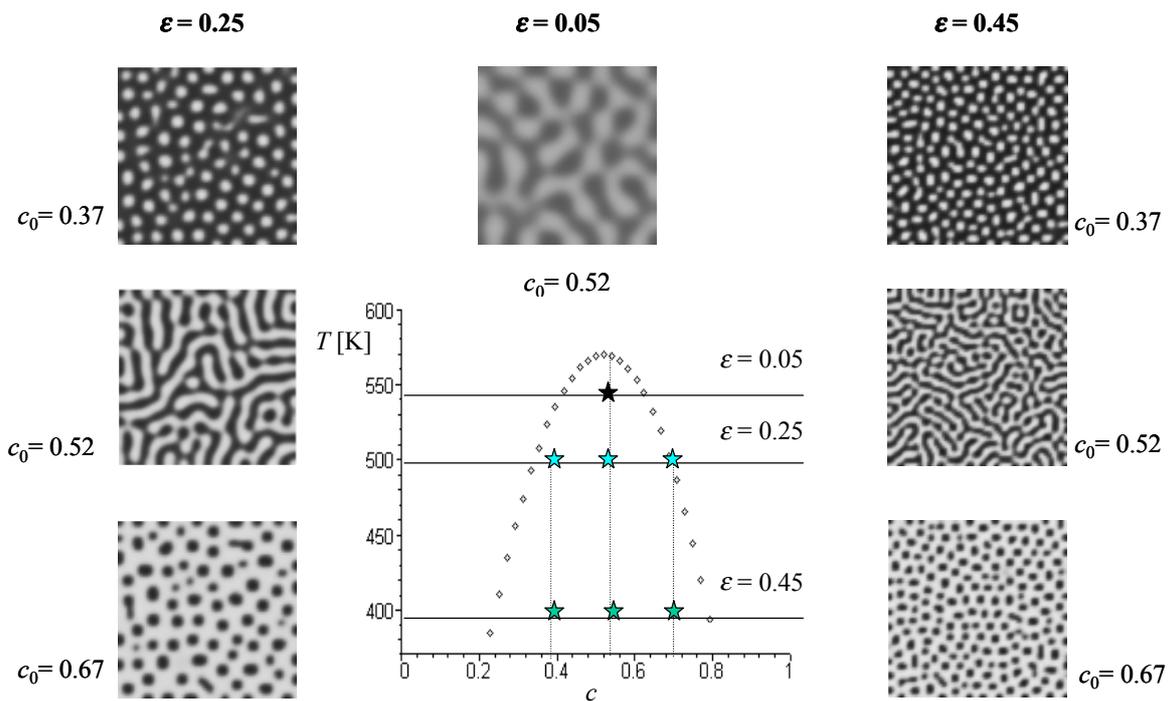


Figure 5.2 System dPS / PBr_xS₃, $x = 0.119$, $L = 3000$ nm, $a = 0.67$ nm.
 ◇◇◇ Spinodal curve.

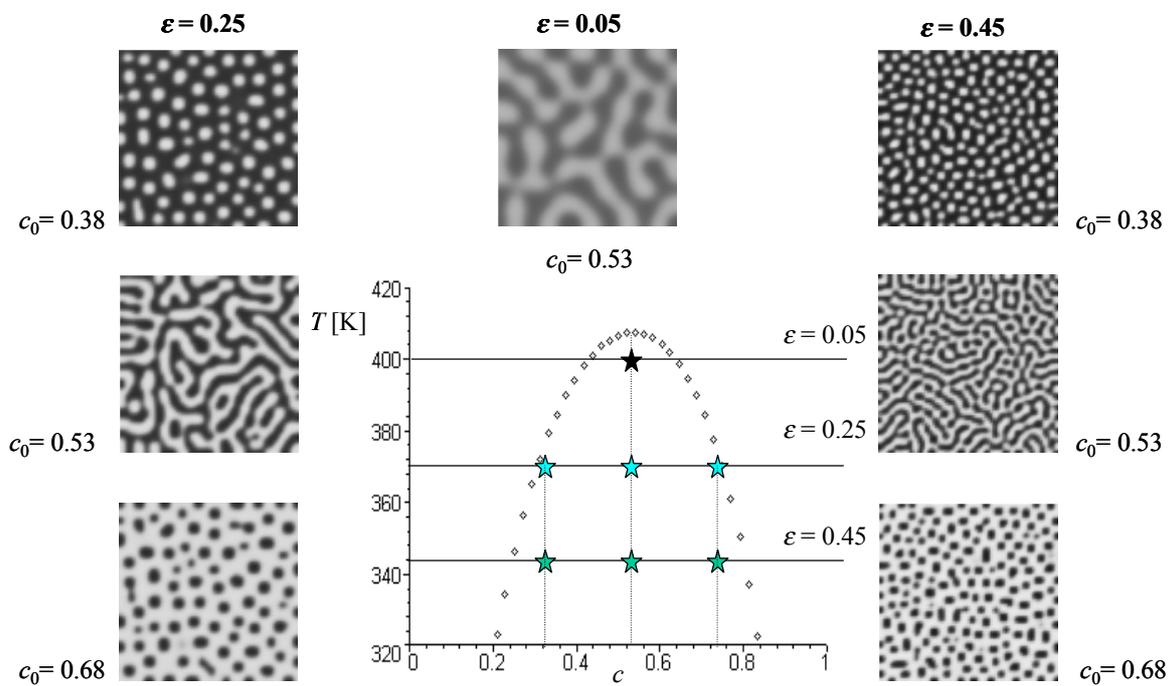


Figure 5.3 System PS / dPS,⁴ $L = 5000$ nm, $a = 0.67$ nm.
 ◇◇◇ Spinodal curve.

To study effect of symmetry of the system on morphology development, two highly asymmetric systems were chosen, one presenting an upper critical solution temperature (UCST) and a second one presenting a lower critical solution temperature (LCST).

The system with the UCST shown in figure 5.4 is of particular interest to us, because we carried out experimental work on the phase behavior (see chapter 6). Therefore, the predictions obtained with the model are useful in understanding more of the kinetic and thermodynamic behavior of this system.

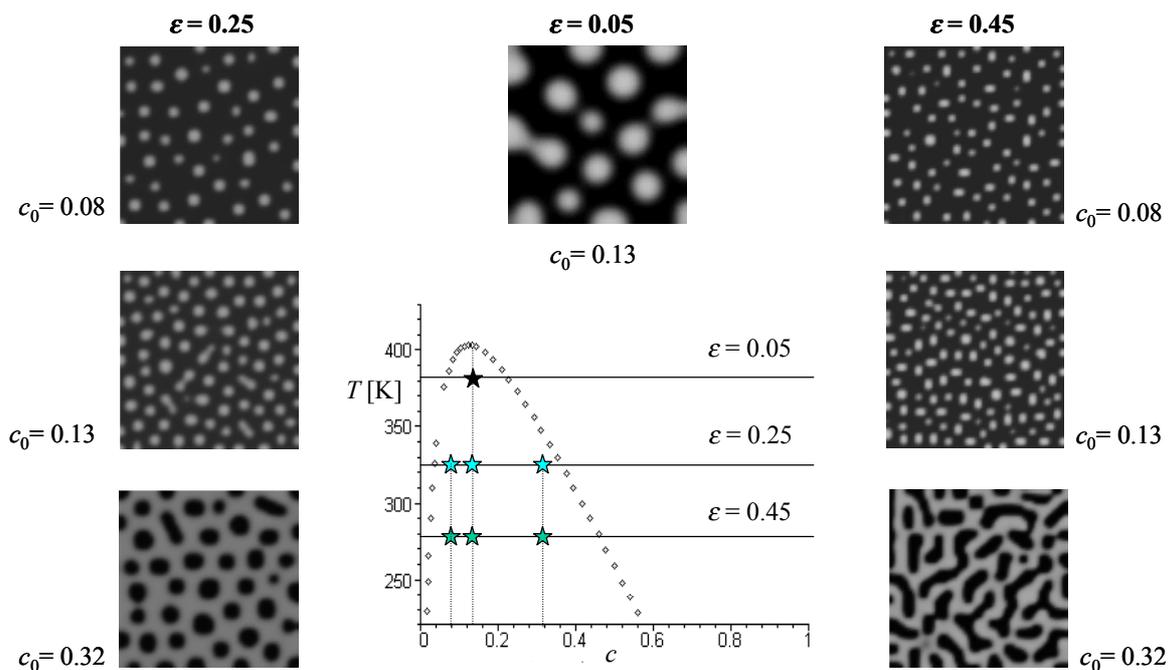


Figure 5.4 x MMA-(1- x)FHMA / Epikote 828, $x = 0.9128$, $L = 1000$ nm, $a = 0.67$ nm.
 $\diamond\diamond$ Spinodal curve.

The results obtained in figure 5.4 show that the symmetry of the blend has definitely an effect on morphology development. In this case, the temperature and the concentration at which the system is quenched are important factors to obtain a co-continuous structure in the bulk morphology. Once more, chain length is not an important parameter in the connectivity of the morphology developed, as shown for the second asymmetric system in figure 5.5.

For the LCST system, the behavior of the interfacial thickness with temperature is inverted, as expected. At higher temperatures, the interfacial thickness decreases and therefore the domain size as shown in figure 5.5. These results clearly show that our model is not limited to UCST systems, but can be applied within the spinodal region of any type of phase diagram.

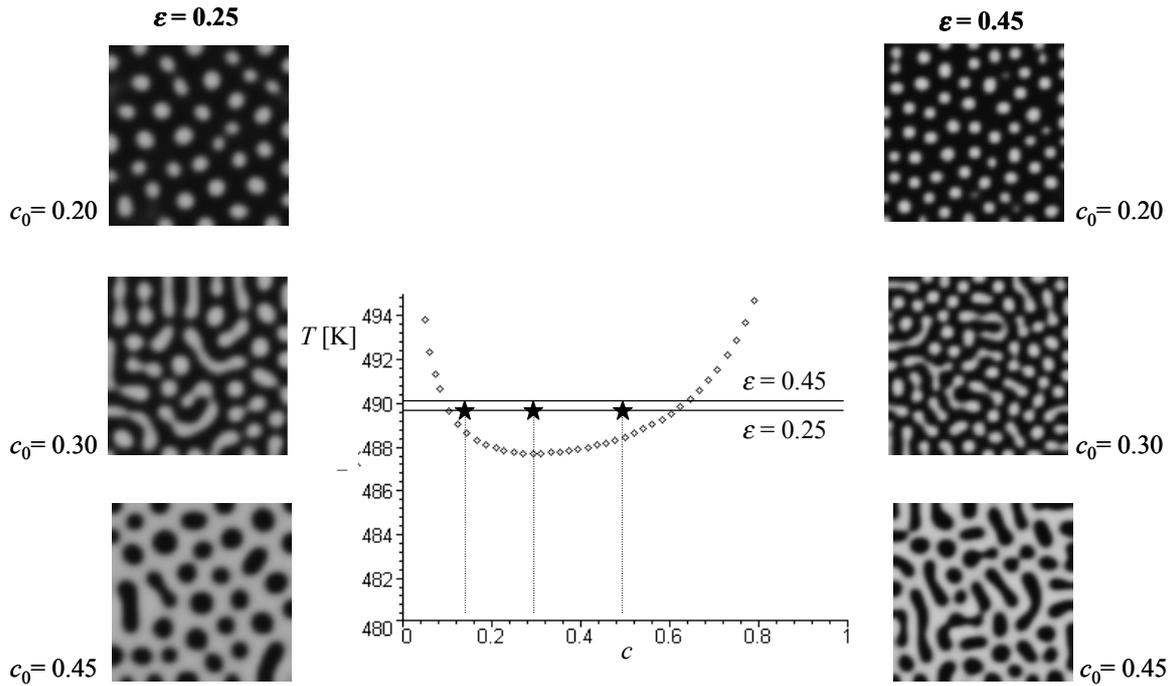


Figure 5.5 System PMMA- d_8 / PTFPMA,¹ $L = 1500$ nm, $a = 0.584$ nm.
 ◇◇◇ Spinodal curve.

In the next section, we focus on systems with a co-continuous morphology to study the wall effect. Experimentally this structure would be easily detected with light scattering and the connectivity observed in co-continuous structure has a direct effect on the mechanical properties of a film, which is an important property in a practical application.

5.3 Morphology development in the presence of a rigid wall

The investigation carried out in the previous section allowed us to refine the selection of systems where the study of the wall effect on morphology development is of interest. All the selected systems present co-continuous morphology in bulk; the conditions chosen are summarized in table 5.3.

We warn beforehand that the time in which the morphology develops, must be taken as a qualitative indication, because of the assumptions made for some parameters that are characteristic for each system such as the viscosity⁵ and the diffusion coefficient ($D = 0.1 \text{ nm}^2 / \text{s}$).

Table 5.3 Systems considered in the study of wall effect.
 γ_{12} is the interfacial tension between component 1 and component 2.

System	ϕ_0	ε	T [K]	ξ [nm]	γ_{12} [J / nm ²]
PS/dPS ⁴	0.53	0.05	399.2	95.4	1.3×10^{-23}
	0.53	0.25	369.6	44.2	9.4×10^{-23}
dPS/PBr _x S ³ , $x = 0.119$	0.52	0.25	453.2	15.2	3.4×10^{-22}
x MMA-(1- x)FHMA / Epikote 828, $x = 0.9128$	0.32	0.45	278.1	0.8	2.7×10^{-21}
PMMA-d ₈ / PTFPMA ¹	0.45	0.45	489.9	7.9	3.5×10^{-22}

For the first symmetric listed in table 5.3, we obtained the results as shown in figure 5.6 for the morphology development in the presence of a rigid wall.

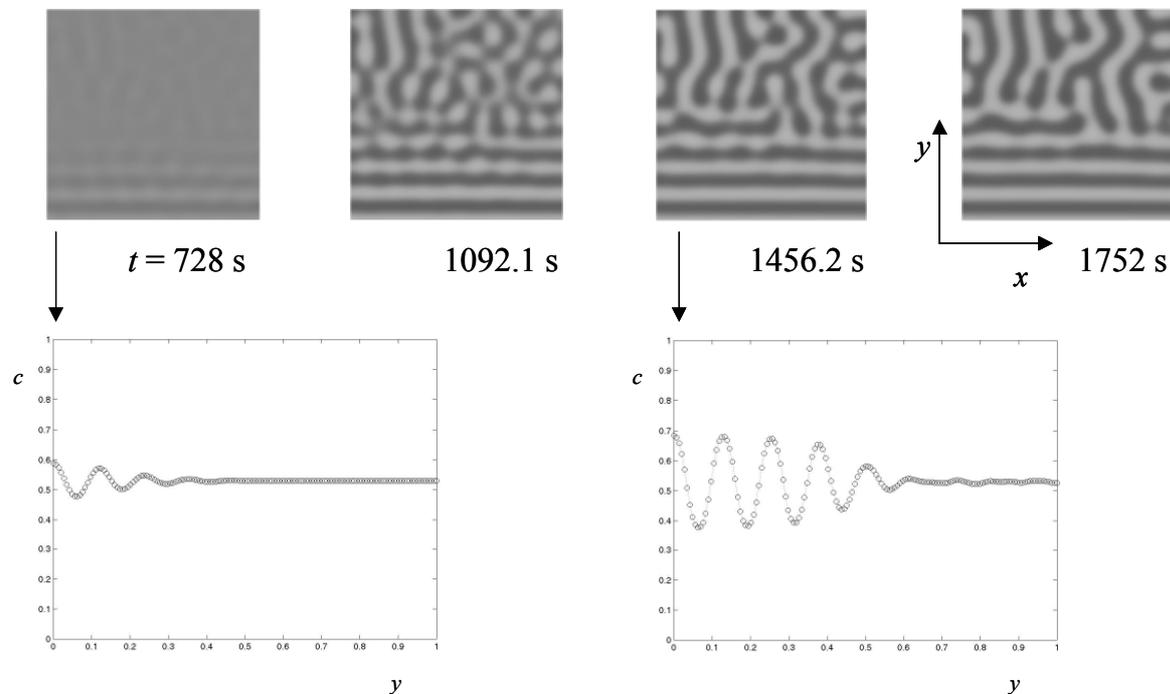


Figure 5.6 Morphology development for the system PS / dPS,⁴ $\varepsilon = 0.05$, $L = 5000$ nm.
 (Lower picture: Typical concentration profile perpendicular to the wall).

The morphology as shown in figure 5.6 presents the following striking features:

- The formation of a macroscopic layer at the wall, as earlier observed.^{2-4,6,7,8,9,10,11}
- An oscillatory concentration profile with oscillations decreasing in amplitude with increasing distance from the wall. The values for the concentration at the wall are determined by the equilibrium conditions; this fact is consistent with other theoretical^{12,13} and experimental^{3,4,9,10} results on surface-directed spinodal decomposition.
- An anisotropic domain growth close to the wall. Guenoun has observed also this experimentally at critical compositions¹⁴ in binary fluids and Cumming¹⁵ in polymer blends.

- Two different domain sizes, parallel and perpendicular to the wall are clearly observed, and this feature was also found in the work of Brown and Chakrabarti.¹⁶
- A faster domain growth close to the wall compared to the bulk consistent with the experimental work of Cumming et al.^{15,17,18} and the theoretical predictions of Troian.¹⁹

Especially this last feature is of relevance because it contributes to clarify which is indeed the domain growth at the early-stage of the spinodal decomposition in the presence of a wall, a problem that has been controversial for one decade. This controversy originated from the contradictions in the experimental evidence found on one hand by Jones and coworkers¹⁰ and on the other hand by Cumming et al.¹⁵ Theoretically, besides the work of Troian, there is no explanation of the fast domain growth at the early-stage of the spinodal decomposition, because either the focus is on the late-stage regime of the spinodal decomposition (which is not investigated in this work) or the wetting effects are simply sub-estimated.

The two main arguments given in the literature to explain the fast domain growth are a hydrodynamic process with geometric limitations due to the presence of the wall, and van der Waals forces leading to wetting effects and therefore to an earlier coalescence at the wall. Our results are in agreement with the last argument, since our model includes hydrodynamic effects but they are minimal due to the large viscosity of polymer blends and besides we are in the early-stage of the spinodal decomposition where it is known that hydrodynamic effects do not have a large contribution. The only extra contribution we introduced in the Helmholtz energy functional compared to the bulk one, is precisely the interaction of the wall with the blend components, which is defined in terms of van der Waals forces (see chapter 3). The coalescence mechanisms near the wall could be compared to the growth mechanism of a drop on a solid surface explained by Rogers et al.²⁰ with the difference that in our case the adsorbed layer on the wall acts as a diffusion sink for the flux of monomers close to it.

Continuing further with our investigation, to check the effect of the magnitude of the wall-polymer potential at constant temperature, we decreased systematically this parameter by one and two orders of magnitude. The results obtained are shown in figure 5.7. The formation of a macroscopic layer at the wall is not observed for smaller interactions of the wall with the blend components. This feature and the corresponding wall potentials shown in figure 5.8 for the morphologies of figures 5.6 and 5.7, show that the magnitude of the wall potential is a factor that determines the formation of a macroscopic wetting layer at the wall.

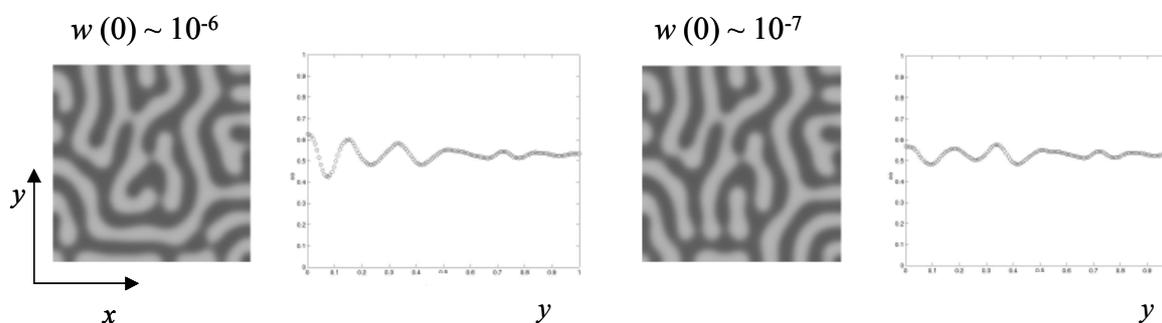


Figure 5.7 Effect of the wall-polymer interaction potential at constant temperature, $\varepsilon = 0.05$, $L = 5000$ nm.

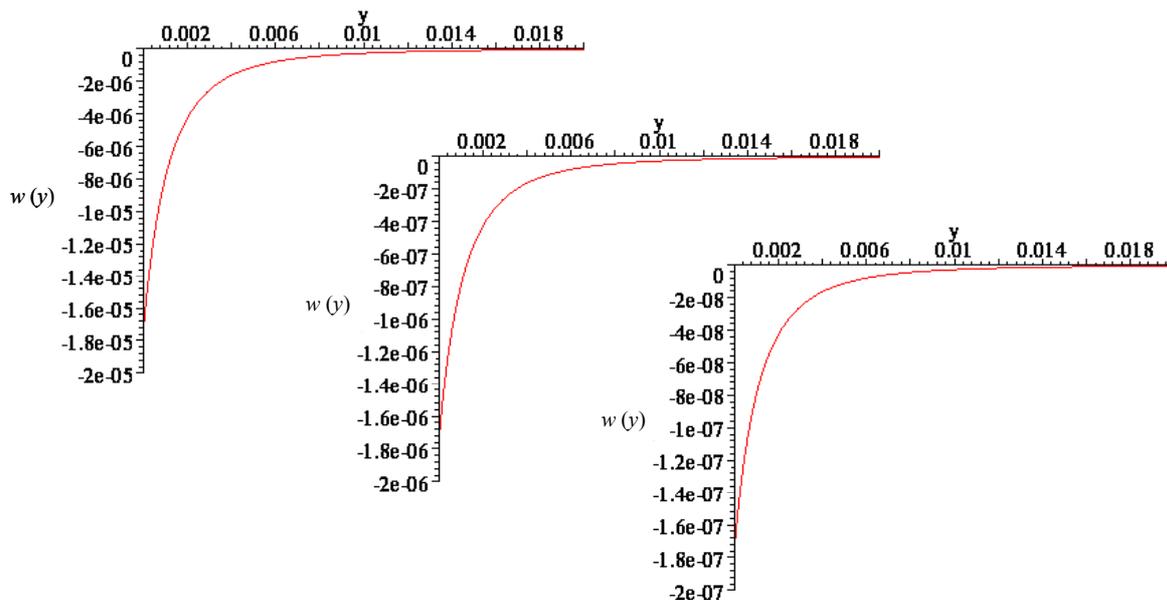


Figure 5.8 Wall-polymer potentials for the morphologies shown in figures 5.6 and 5.7. System PS / dPS⁴, $\epsilon = 0.05$.

The extension of the wetting layer into the bulk seems to have another reason, due not only to long-range interaction of the wall with the blend components. To find out which is the second factor playing a role in the extension of this layers into the bulk, we considered the same system of figure 5.6 (PS / dPS⁴) at a deeper quench in temperature ($\epsilon = 0.25$) to obtain the morphologies as shown in figure 5.9.

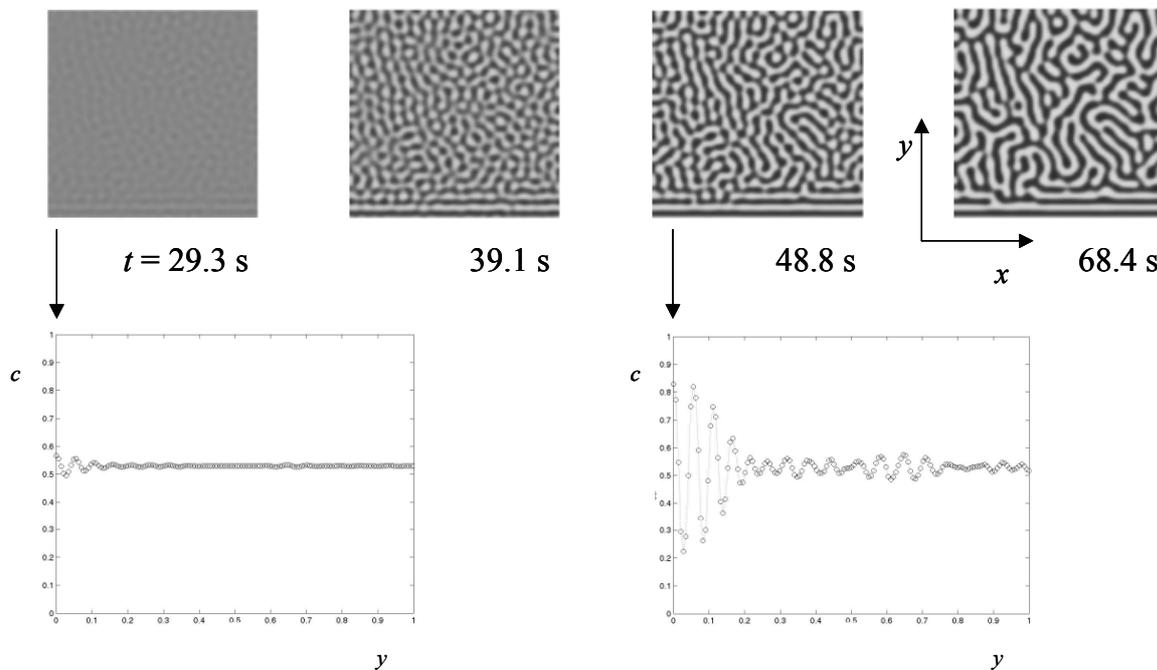


Figure 5.9 Morphology development for the system PS / dPS⁴, $\epsilon = 0.25$, $L = 5000$ nm. (Lower picture: Typical concentration profile perpendicular to the wall).

The slight decrease in amount of layers next to the wall in figure 5.9, can be explained in terms of the ratio $r = \mu / w(0)$, where $\mu = (\Delta\mu_l - \Delta\mu_2)|_{\phi^{\alpha,\text{spin}}} - (\Delta\mu_l - \Delta\mu_2)|_{\phi^{\beta,\text{spin}}}$, and $w(0)$ is the wall-polymer potential evaluated at the wall ($y = 0$ where the maximum contribution of this property occurs). From the values obtained in table 5.4, we can see that a quench in temperature increases the order of magnitude of the chemical potential; therefore, the relative contribution of the wall to the bulk morphology is smaller. This speculation is confirmed by the results obtained in figures 5.10 to 5.12 for the rest of the systems tabulated in table 5.4. The larger the value of r (or contribution of the bulk chemical potential), the smaller the layer formation at the wall.

Table 5.4 Difference in chemical potential, wall potential at $y = 0$, and their ratio r , at a quench depth ε .

System	ε	$w(0)$	μ	r
PS/dPS ⁴	0.05	-1.77×10^{-5}	0.0300	1695
	0.25	-1.38×10^{-4}	0.3178	2303
dPS/PBr _x S ³ , $x = 0.119$	0.25	-4.09×10^{-4}	0.3262	816
x MMA-(1- x)FHMA / Epikote 828, $x = 0.9128$	0.45	-5.29×10^{-3}	6.562	1241
PMMA-d ₈ / PTFPMA ¹	0.45	-3.89×10^{-4}	1.341	3477

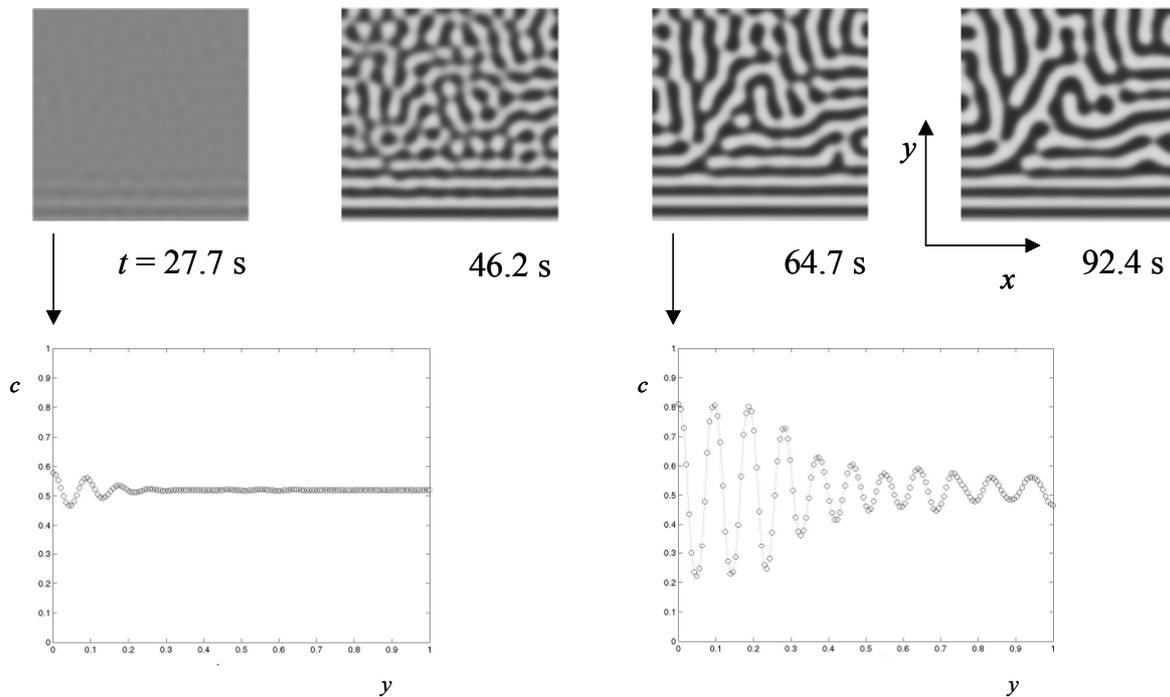


Figure 5.10 Morphology development for the system dPS / dPBr_xS³, $\varepsilon = 0.25$, $L = 3000$ nm. (Lower picture: Typical concentration profile perpendicular to the wall).

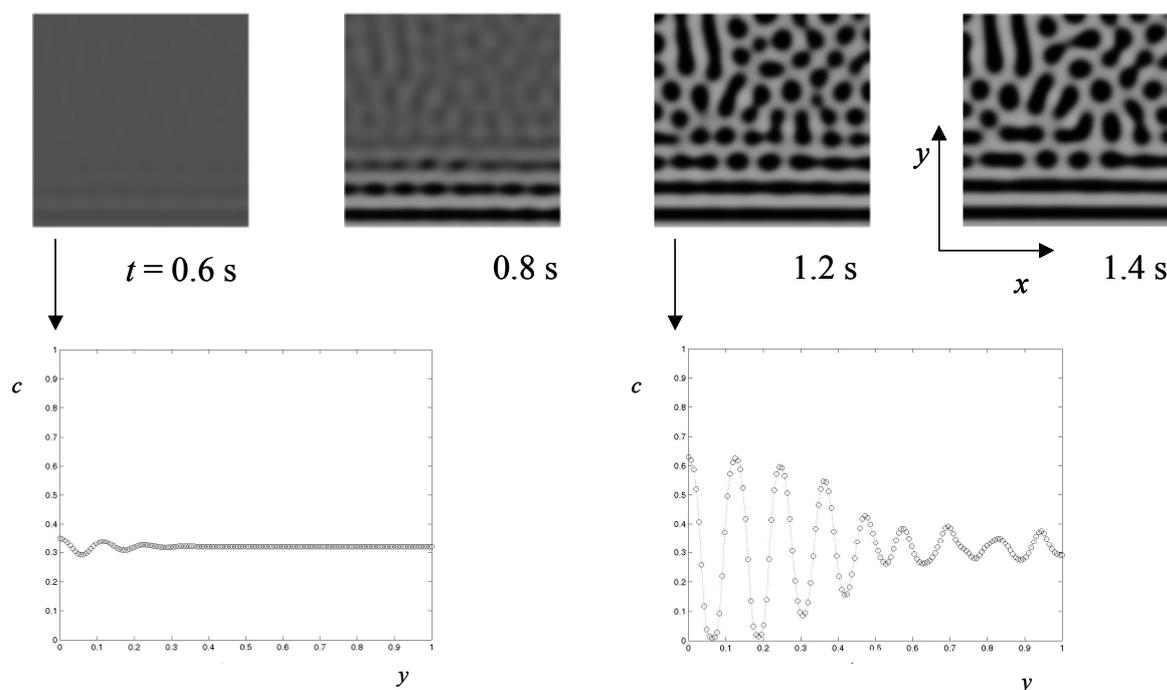


Figure 5.11 x MMA-($1-x$)FHMA / Epikote 828, $x = 0.9128$, $\varepsilon = 0.45$, $L = 1000$ nm.
(Lower picture: Typical concentration profile perpendicular to the wall).

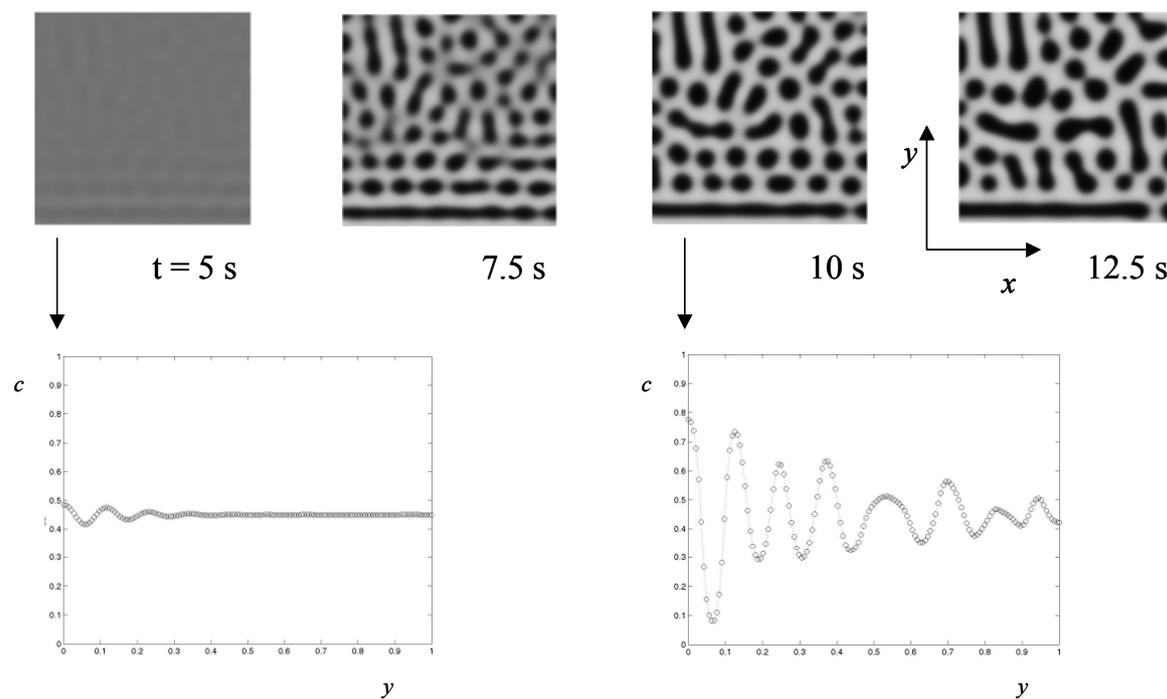


Figure 5.12 System PMMA- d_8 / PTFPMA, $\varepsilon = 0.45$, $L = 1500$ nm.
(Lower picture: Typical concentration profile perpendicular to the wall).

The results obtained in this section show that when the wall effect is switched on, a striking change in morphology is observed. The impact of this effect farther from the wall depends on two factors: the magnitude and extension into the bulk of the wall-polymer interaction potential and the magnitude of the difference in chemical potentials of the blend components.

5.3.1 Quantification of the morphology

In this section our intention is to quantify mainly two features relevant in the morphology found in the presence of a wall: the fast growth of the domains at the wall and the difference in domain size at the wall and in the bulk. To do so, we took, for one symmetric and one asymmetric system, a series of concentration profiles parallel to the wall at different time steps. With these data we performed an analysis in one dimension on the morphology of one symmetric and one asymmetric system in terms of the following parameters: R_q , the root-mean-square deviation from the average, $G(\omega)$, the power spectral density function and $\rho(x)$, the correlation function. Each of these parameters is explained in more detail below.

First, we start with the analysis of the symmetric system PS / dPS at $\varepsilon = 0.05$ and $t = 1092.1$ s; at this time the system has phase separated (see figure 5.6.). In figure 5.13, for clarity, we show only the sampling done for the concentration profile at two distances y , close to ($y = 0.125$) and far away from the wall ($y = 0.875$), x corresponds to the position of the concentration running in a line parallel to the wall and z is $\phi_y - \langle \phi \rangle$.

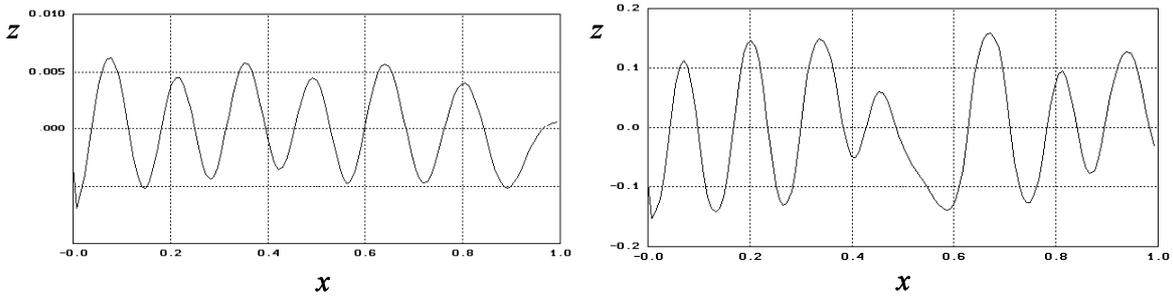


Figure 5.13 Sampled concentration profile for the system PS/ dPS at $\varepsilon = 0.05$ and $t = 1092.1$ s, for two fixed distances to the wall. Left plot $y = 0.125$, right plot $y = 0.875$.

The first main feature we see in figure 5.13 is that close to the wall the difference of the concentration from the mean value is very small, and further in the bulk is around 25 times larger. This is consistent with the fact that close to the wall there are flat layers which concentration from an average value fluctuates very little, whilst further from the wall there is a co-continuous morphology with high concentration fluctuations.

With the sampled concentration profile it is possible to calculate the root-mean-square deviation, defined by²¹

$$R_q = \left\{ \frac{1}{L} \int_0^L z^2 dx \right\}^{1/2} \quad (5.1)$$

Physically, R_q is the standard deviation of the sampled concentration profile. The behavior of R_q as a function of time, from the moment when oscillations in the concentration profile are visible (see figure 5.6) is shown in figure 5.14. It can be concluded that until the time when the concentration fluctuations in the bulk are small, R_q remains practically constant at any distance from the wall. As soon as the concentration fluctuations grow considerably and the system starts to coarsen or phase separate, R_q stays around the same value close to the wall and jumps to a higher value deeper in the bulk. This is consistent with the temporal change in morphology observed in figure 5.6.

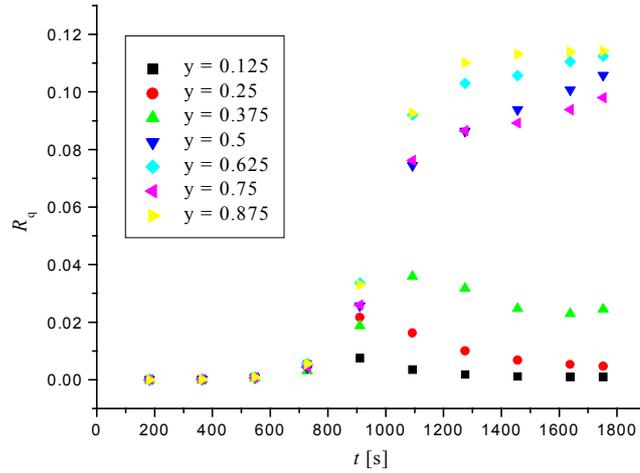


Figure 5.14 Root-mean-square deviation for sampled concentration profiles at increasing distances y from the wall.

To determine the different wavelengths present in the concentration profiles of figure 5.13 we plot the power spectral density function or power spectrum, which is proportionally the one-dimensional version of the structure factor $S(q)$ used in light scattering. This parameter is obtained from the surface profile after a Fourier transform of $z(x)$, and is defined by

$$G(\omega) = (1/2\pi) \int_{-\infty}^{\infty} z(x) \exp(-i\omega x) dx \tag{5.2}$$

where ω is a radial frequency (cycles / distance) $2\pi / \lambda$ with λ the wavelength. The power spectrum of the profiles shown in figure 5.13 is sketched in figure 5.15. For the profile close to the wall, a single frequency band results while for the sample farther from the wall at least two bands with different amplitude are involved.

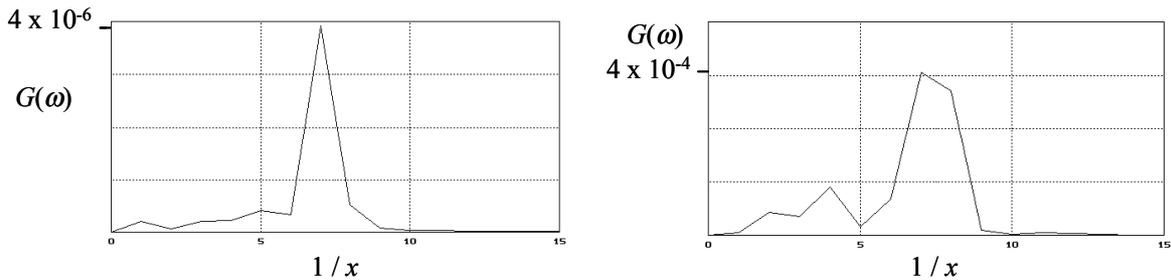


Figure 5.15 Power spectrum for the two different concentration profiles of figure 5.13. Left picture $y = 0.125$ and right picture $y = 0.875$.

It is clear from figure 5.15 that the discrimination between a peak or band and the noise in the spectrum is not always evident and for this reason (and for extracting extra information about the correlation of the present wavelengths), it is convenient to calculate the autocovariance $R(x)$, this function is related to the power spectrum according to

$$R(x) = \int_0^{\infty} G(\omega) \cos(\omega x) d\omega \tag{5.3}$$

where the Euler formula $\exp(i\omega x) = \cos\omega x + i\sin\omega x$ has been used, and only the real part of the function has been considered. A plot of the autocovariance function of the concentration profiles of figure 5.13 is shown in figure 5.16. The high degree of correlation shows that a rather limited number of wavelengths are involved for both profiles. The slightly lower correlation for the profile farther from the wall indicates that a somewhat wider frequency range is involved; this is consistent with the presence of a second and a third tiny frequency (band) as observed in the power spectrum in figure 5.15.

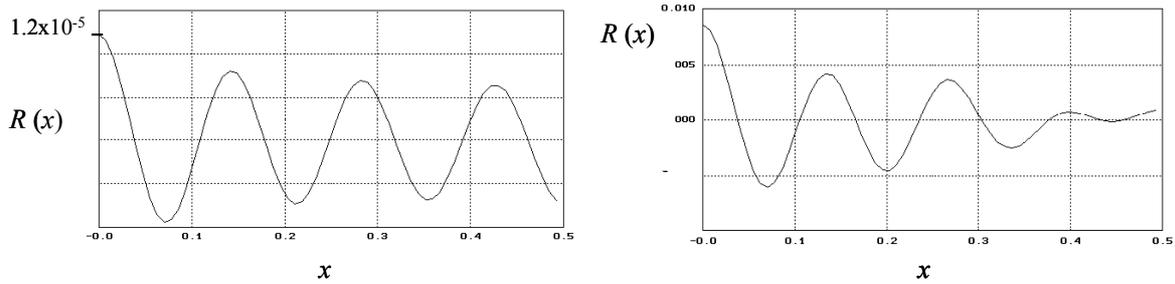


Figure 5.16 Autocovariance function for the two different concentration profiles of figure 5.13. Left picture $y = 0.125$ and right picture $y = 0.875$.

With the support obtained from the autocovariance function, we distinguish the presence of three bands of different amplitude in the power spectrum, one at $1/x = 1$, the second one at $1/x = 4$ and a third one at $1/x = 7$. If we now plot the amplitude of these three different bands as a function of time, we obtain the result as shown in figure 5.17. The trend observed indicates that the mentioned bands in the power spectrum are associated to the bulk phase separation. All the different frequencies are present at any time both close and further from the wall, but only one dominant frequency grows in amplitude at a distance farther from the wall. This frequency would be associated to the characteristic wavelength of the domains in the bulk.

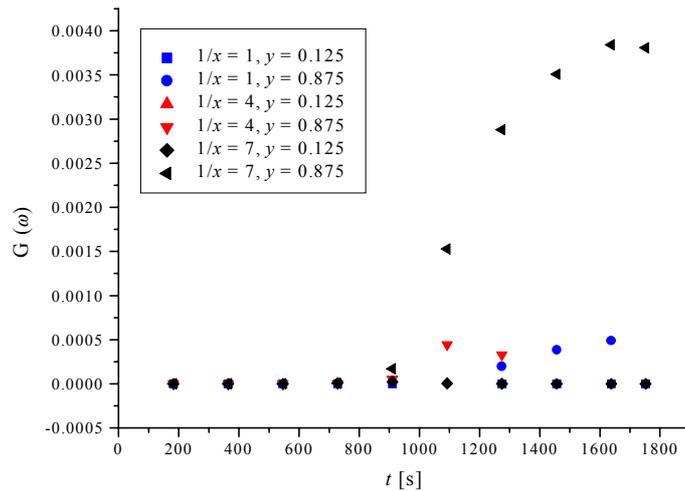


Figure 5.17 Amplitude of the different bands in the power spectrum of figure 5.15.

To obtain relative correlations, it is convenient to take the normalization of the autocovariance function by R_q^2 that results in the autocorrelation function $\rho(x)$, such that $\rho(0) = 1$.

$$\rho(x) = R(x) / R_q^2 \tag{5.4}$$

If we look at the temporal behavior of the autocorrelation function for the frequencies at $1/x = 4$ and $1/x = 7$ we find in figure 5.18 a trend that is coherent with the results extracted from figure 5.17. Close to the wall, the correlation is higher before phase separation takes place whilst far from the wall the correlation is higher after the bulk phase separation.

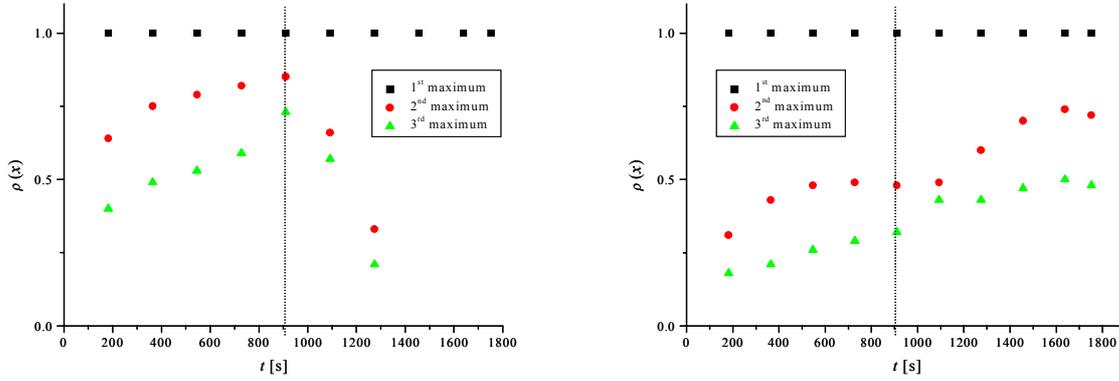


Figure 5.18 Maxima heights in the correlation function versus time for the concentration profiles of figure 5.13. Left picture $y = 0.125$ and right picture $y = 0.875$.

The first maximum equals R_q^2 .

For the asymmetric system figure 5.19 show the same trend as for the symmetric system previously analyzed.

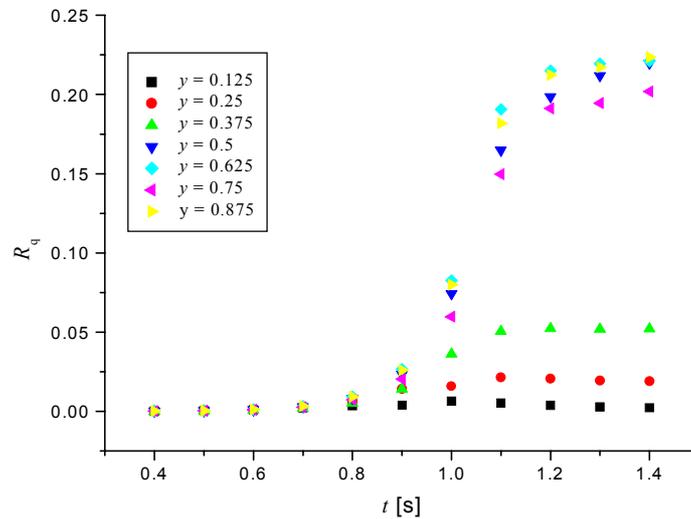


Figure 5.19 Root-mean-square deviation for sampled concentration profiles at increasing distances y from the wall.

From this analysis, we conclude that for the bulk morphology it was possible to determine the presence of three different frequencies. Only one dominant frequency at $1/x = 7$ is associated to the characteristic wavelength of spinodal morphology in the bulk. The smaller frequency(s) we expected to find, corresponding to the wall domains was not observed.

5.4 Conclusions

We can conclude that the model proposed is applicable to binary polymer blends having a phase diagram with either upper critical solution temperature or lower critical solution temperature. The results provided by the diffuse-interface model implemented in this thesis are qualitatively in good agreement with experimental evidence on surface-directed spinodal decomposition. From the parameter variation, it was found that the symmetry of the system is what mainly affects the connectivity of the bulk morphology. When the wall is included, we find the formation of a macroscopic wetting layer and a faster domain growth at the wall; these findings contribute to clarify the early-stage of the spinodal decomposition. The extent of the development of layers deeper in the bulk is determined by two factors: the range of the interaction of the wall with the blend components and the ratio between the difference in chemical potential of the blend components and the magnitude of the wall-polymer interaction potential. The analysis carried out in the last section allowed a partial quantification of the morphology developed deep in the bulk.

5.5 References

- ¹ De Graaf, M. *Transmissive and emissive polymer waveguides for communication and illumination* Ph. D. thesis. Eindhoven University of Technology, the Netherlands (2002)
- ² Geoghegan, M.; Jones, R.A.L. and Clough, A.S. *J. Chem. Phys.* **103** No. 7 (1995) 2719
- ³ Bruder, F. and Brenn, R. *Phys. Rev. Lett.* **69**, no.4 (1992) 624
- ⁴ Bates, F.S. and Wignall, G.D. *Phys. Rev. Lett.* **57** No.12 (1986) 1429
- ⁵ Van Krevelen, D.W. *Properties of polymers* 3rd ed. Elsevier, the Netherlands (1997)
- ⁶ Jones, R.A.L.; Kramer, E.J.; Rafailovich, M.H. and Schwarz, S.A. *Mat. Res. Soc. Symp. Proc.* **153** (1989) 133
- ⁷ Kraush, G.; Dai, C.; Kramer, E.J. and Markov, J.F. *Macromolecules* **26** (1993) 5566
- ⁸ Kim, E.; Krausch, G. and Kramer, E.J. *Macromolecules* **27** (1994) 5927
- ⁹ Krausch, G.; Kramer, E.J.; Rafailovich, M.H. and Sokolov, J. *Appl. Phys. Lett.* **64**, no. 20 (1994) 2655
- ¹⁰ Jones, R.A.; Norton, L.J.; Kramer, E.J.; Bates, F.S. and Wiltzius P. *Phys. Rev. Lett.* **66**, no. 10 (1991) 1327
- ¹¹ Karim, A.; Slavecki, T.M.; Kumar, S.K.; Douglas, J.F.; Satija, S.K.; Han, C.C.; Russell, T.P.; Liu, Y.; Overney, R.; Sokolov, J.; and Rafailovich, M.H. *Macromolecules* **31** (1998) 857
- ¹² Puri, S. and Binder, K. *Phys. Rev. A* **46**, no. 8 (1992) R4487
- ¹³ Binder, K. *Acta Polymer.* **46** (1995) 204
- ¹⁴ Guenoun, P. and Beysens, D. *Phys. Rev. Lett.* **65**, no. 19 (1990) 2406
- ¹⁵ Wiltzius, P. and Cumming, A. *Phys. Rev. Lett.* **66**, no 23 (1991) 3000
- ¹⁶ Brown, G. and Chakrabarti, A. *Phys. Rev. A* **46**, no.8 (1992) 4829
- ¹⁷ Shi, B.Q.; Harrison, C. and Cumming, A. *Phys. Rev. Lett.* **70**, no. 2 (1993) 206
- ¹⁸ Cumming, A.; Wiltzius, P.; Bates, F. and Rosedale, J. *Phys. Rev. A* **45**, no. 45 (1992) 885
- ¹⁹ Troian, S.M. *Phys. Rev. Lett.* **71**, no. 9 (1993) 1399
- ²⁰ Rogers, T.M.; Elder, K.R. and Rashmi, C.D. *Phys. Rev. A* **38**, no. 10 (1988) 5303
- ²¹ Thomas, T.R. *Rough surfaces* Longman, USA (1982)

CHAPTER 6

PHASE BEHAVIOR OF THE BINARY SYSTEM POLY [METHYL METHACRYLATE-CO-1H,1H-PERFLUOROHEPTYLMETHYL METHACRYLATE] / BISPHENOL-A-DIGLYCIDYLETHER

6.1 Introduction

In this chapter we investigate the fundamental aspects of fluoro-modified epoxy-based coatings for metals. The polymers used are a thermosetting epoxy resin and a thermoplastic hybrid fluorinated copolymer; this combination seems to be ideal in a formulation for coatings. On the one hand, epoxy resins have a good adhesion on different substrates and good mechanical properties, they shrink slightly during curing, their curing kinetics can be controlled easily and they are easily processed.¹ On the other hand, the fluorinated thermoplastic polymers have a chemical and mechanical stability over a wide range of temperatures, a high outdoor durability, but with the disadvantage of having low solubility in most of the common organic solvents.²

The first problem to face when two polymers of different chemical nature are mixed is the miscibility between them. Therefore in section 6.2 the phase behavior is studied of the binary systems poly [methyl methacrylate-co-1H,1H-perfluoroheptylmethyl methacrylate] and bisphenol-A-diglycidylether abbreviated as x MMA-(1- x)FHMA and Epikote 828, respectively, as a function of: 1) molar mass and fluorine content in the copolymer, x MMA-(1- x)FHMA and 2) chain length extension of the epoxy resin.

In section 6.3 studies on morphology development of a film and a drop (bulk) are carried out for the binary system x MMA-(1- x)FHMA / Epikote 828, $(1-x) = 0.0872$ in two regions: 1) around the critical point and 2) around the intersection point of the glass transition and the cloud-point curves. The results experimentally observed are compared with numerical simulations using the model presented in this thesis. In section 6.4 we give final conclusions to this chapter.

6.2 Phase behavior

In this section we present the results obtained on phase behaviour of the binary systems poly [methyl methacrylate-co-1H,1H-perfluoroheptylmethyl methacrylate] and

bisphenol-A-diglycidylether, by modifying the molar mass, the fluorine content in the copolymer x MMA-(1- x)FHMA and for one binary system also the effect of the chain length extension of the epoxy resin.

6.2.1 Materials

The fluorinated copolymers poly [methyl methacrylate-co-1H,1H-perfluoroheptylmethyl methacrylate], with a different ratio of each monomer, were synthesized in our laboratories.³ For simplicity the short notation x MMA-(1- x)FHMA will be used, to refer to these compounds; x is the molar ratio of monomer MMA and (1- x) of monomer FHMA. A bisphenol-A-diglycidylether (DGEBA, Epikote 828) abbreviated as Epikote 828 was obtained from Shell Chemicals (Amsterdam, the Netherlands) and used without further purification. To prepare oligomers of Epikote 828 a polyoxipropylenediamine (Jeffamine D-230) obtained from Huntsman (Everberg, Belgium) was used. The chemical formulas of the compounds and the fluorinated copolymers used are shown in figure 6.1 and table 6.1, respectively.

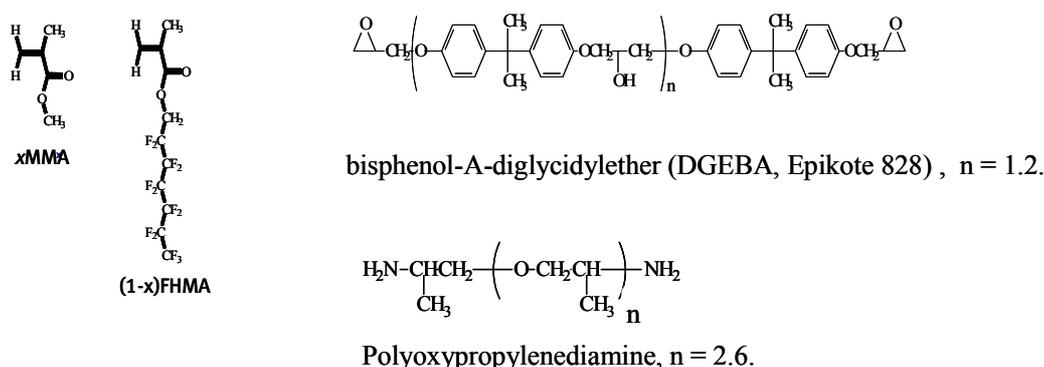


Figure 6.1 Chemical formulations of the compounds used.

Table 6.1 Copolymers used.

[x MMA / (1- x)FHMA]	M_w [kg/mol]
0.9000 / 0.1000	7.7
0.8760 / 0.1240	32
0.9128 / 0.0872	32
0.9320 / 0.0680	32
0.9467 / 0.0533	32

6.2.2 Methods

The cloud-point curves were determined experimentally by a hot-stage light scattering technique, using a heating rate of 10 degrees per minute. Following the procedure as explained in chapter 3, the Flory-Huggins theory^{4,5} was fitted to the experimental data, to obtain the spinodal curves, as well as critical parameters for each system.

Oligomers of Epikote 828 were obtained by reacting in a round bottom flask the Jeffamine with the epoxy compound for one hour, using magnetic stirring at two different temperatures, 373.15 and 393.15 K. The amount of Jeffamine necessary to obtain a certain degree of polymerization was calculated according to Gordon.⁶ Matrix Assisted Laser Desorption Ionization-Time off Flight (MALDI-TOF) gave a qualitative identification of the reaction products.

6.2.3 Results

Using equations (3.35) to (3.38) the spinodal curve, the critical concentration and critical temperature were calculated. The constant $\chi_1 = \chi_c T_c$ was estimated, as explained in see section 3.3.2 for each system. This makes possible to predict, at least qualitatively, the phase behavior for any other binary system with fluorine content between 0.0872 and 0.1240. These data are listed in table 6.2.

Table 6.2 Critical conditions and maximum experimental solution temperature for systems $x\text{MMA}-(1-x)\text{FHMA}$ / Epikote 828.

$x/(1-x)$	M_w [kg/mol]	ϕ_{\max}	T_{\max} [K]	χ_1	ϕ_c	T_c [K]
0.9000 / 0.1000	7	0.07	495.2	357.6	0.23	423.7
0.8760 / 0.1240	32	0.10	524.2	335.3	0.13	520.8
0.9128 / 0.0872	32	0.04	415.2	264.4	0.13	403.2
0.9320 / 0.0680	32	-	Miscible	-	-	-
0.9467 / 0.0533	32	-	Miscible	-	-	-

From figure 6.2 it is clear that the calculated critical points appear on the right-hand branches of the cloud-point curves. This feature has been observed earlier⁷ and is attributed to the polydispersity (M_w/M_n) of the blend. Epikote 828 is a mixture of monomers and dimmers, as the number $n=1.2$ indicates, and the fluorinated copolymers have a ratio $M_w / M_n = 1.8$.

In addition, in figure 6.2 it can be seen that fluorine content in the copolymer is the main contribution to the blend immiscibility; at higher fluorine concentration the miscibility gap becomes broader, shifting to more elevated temperatures and higher copolymer composition. No phase separation is observed at room temperature when fluorine content in the copolymer is equal to or below 0.068. The copolymer molar mass is a secondary effect in the shift of the miscibility gap.

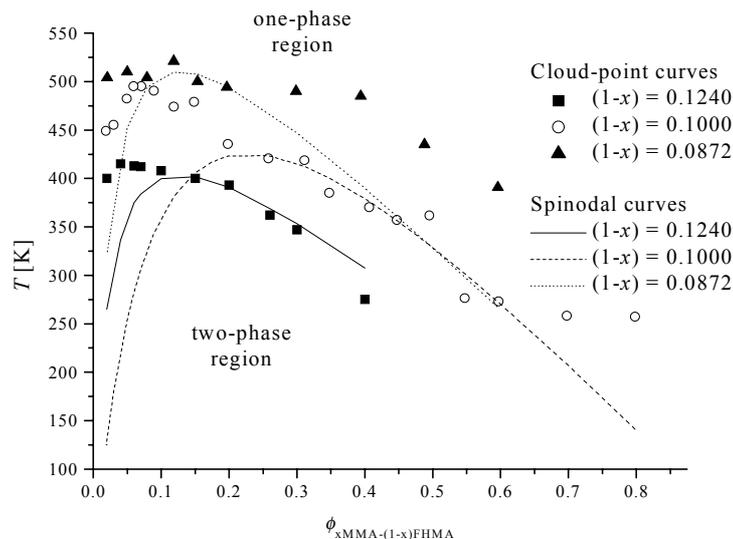


Figure 6.2 Phase diagrams of the binary systems $x\text{MMA}-(1-x)\text{FHMA}$ / Epikote 828.

To complete the study on phase behavior of the binary systems $x\text{MMA}-(1-x)\text{FHMA}$ / Epikote 828, the chain length extension of the epoxy resin was modified by reacting this component with Jeffamine-D230. The only phase diagram measured was for the polymer blend $x\text{MMA}-(1-x)\text{FHMA}$ / (n-mer)Epikote 828, with a fluorine content in the copolymer $(1-x) = 0.0872$, because of experimental limitations.

Dimers and trimers were identified in the MALDI-TOF spectra illustrated in figure 6.3. Due to the high polydispersity of the system, no further quantification of the monomers synthesized or calculations of the χ Flory-Huggins interaction parameter were done. For this last point extended theories in thermodynamics,^{7,8} where χ depends not only on composition but also on polymer size, should be applied and it is not within the scope of this work to go into detail of this extension of the Flory-Huggins lattice theory.

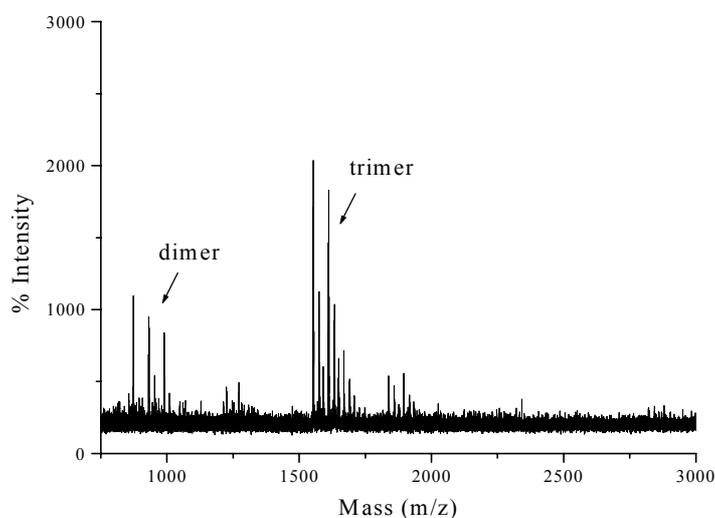


Figure 6.3 MALDI-TOF spectra of Epikote 828 oligomers prepared at $T = 373.15\text{ K}$.

The phase diagram was determined to study the influence of the chain length extension of the epoxy resin on the miscibility gap (figure 6.4). Reliable results for the cloud-point curves are obtained only at diluted conditions, since the low diffusion and high viscosity made experimental data at higher concentrations inaccurate. Miscibility is highly reduced by increasing chain length of the epoxy resin, having even a more drastic effect than the modification of fluorine content in the copolymer.

Summarizing, in this section we established that the main contributions to the broadening of the miscibility gap in the binary systems $x\text{MMA}-(1-x)\text{FHMA}$ / Epikote 828 are: the chain length extension of the epoxy resin and fluorine content in the copolymer, whilst the increment in molar mass of the fluorinated copolymer is a secondary effect.

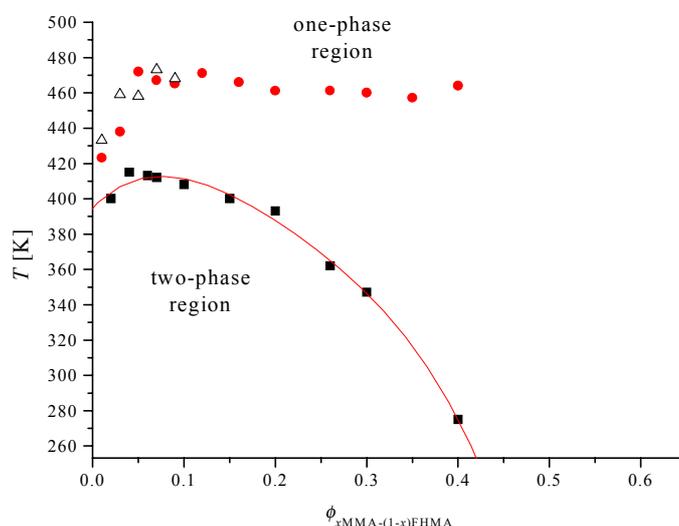


Figure 6.4 Phase diagrams of systems $x\text{MMA}-(1-x)\text{FHMA}$ / (n-mer) Epikote 828, $(1-x) = 0.0872$.
 ■ ■ Monomer, ● ● oligomer prepared at $T = 373.15$ K, △△ oligomer prepared at $T = 393.15$ K.
 (Lines drawn to guide the eye).

6.3 Morphology development

Preliminary studies in a drop and in a film were performed to elucidate the relationship between copolymer composition and morphology development. The regions of interest are around the critical point, where concentration fluctuations are large, and around the intersection point of the glass transition and the cloud-point curves, where due to the proximity to the vitrification region of the system, the morphology developed by the polymer blend can be frozen-in and easier to identify (figure 6.5). Because these regions were more easily accessed in the binary system containing $x\text{MMA}-(1-x)\text{FHMA}$ / Epikote 828, $(1-x) = 0.0872$, this system was chosen.

The glass transition curve plotted in figure 6.5 was estimated using the Fox equation.⁹

$$\frac{1}{T_g} = \frac{c}{T_{g1}} + \frac{(1-c)}{T_{g2}} \quad (6.1)$$

with T_g , the glass transition of an ideal homogeneous system, c , the mass fraction of component one ($c \approx \phi$), T_{g1} and T_{g2} , the glass transition of component 1 and 2, respectively. In this work the measured glass transition temperatures are for the copolymer $x\text{MMA}-(1-x)\text{FHMA}$, $(1-x) = 0.0872$, $T_{g1} = 370.5$ K and for the Epikote 828, $T_{g2} = 257.85$ K.

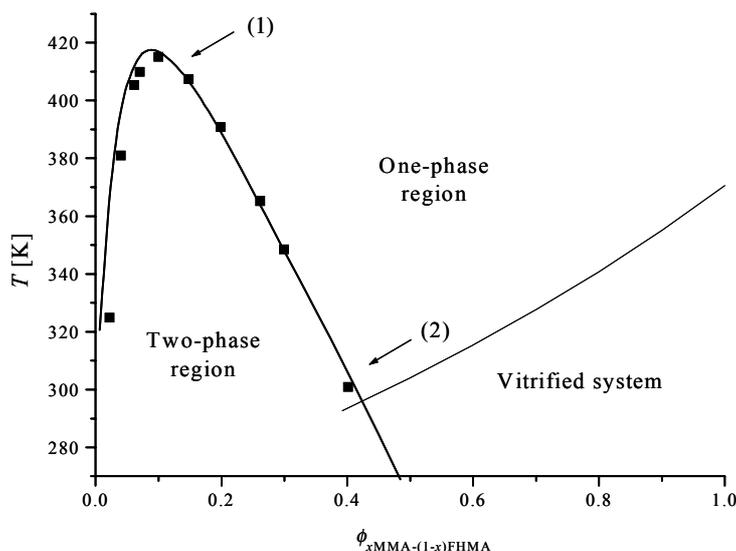


Figure 6.5 Phase diagram of the binary system $x\text{MMA}-(1-x)\text{FHMA}$ / Epikote 828, $(1-x) = 0.0872$.
 ■■ Cloud-point curve, — glass transition temperature curve.

E-SEM, AFM, SALS and SAXS techniques were tried around the critical conditions of the system in region (1) but no experimental features on the morphology were discerned. To check whether the size of the domains formed was a factor not allowing spotting the morphology in this region, a solution in toluene of the binary blend was casted at 393.15 K on a clean silicon wafer and spin-coated to obtain a layer 1 μm thick. This thin layer was cured at 373.15 K for one hour with the Jeffamine D-230 in order to produce larger domain sizes. The results of this treatment are shown in figure 6.6 and 6.7. Even after this chemical modification, it was not possible to identify clearly the spinodal decomposition; instead, it was obtained a kind of honeycomb structures that have been observed previously in systems where precipitation of water vapor drops on a polymer layer was done.¹⁰ Therefore, another factor must be linked to the difficulty of observing the morphology of this binary blend around the critical point.

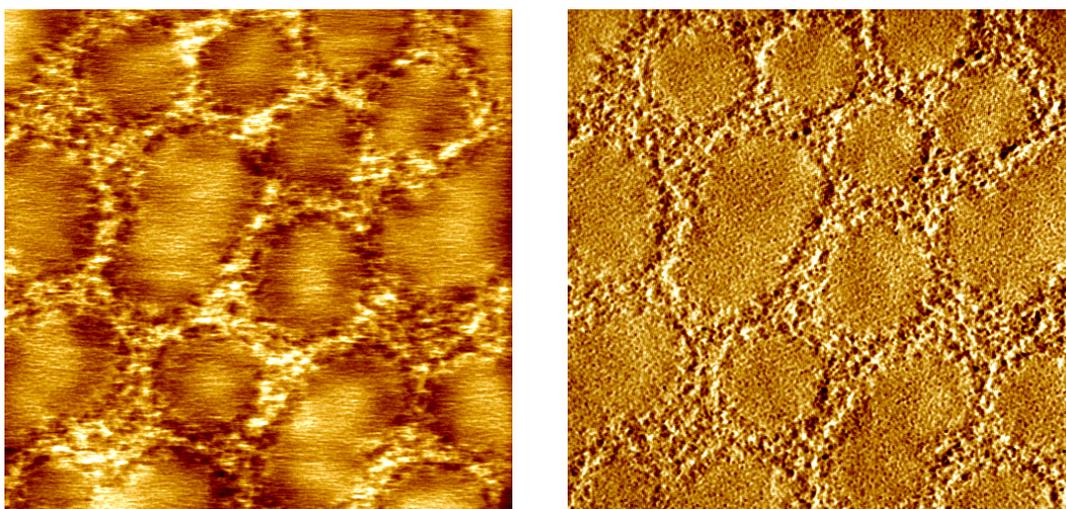


Figure 6.6 AFM pictures, tapping mode.
Binary system x MMA-(1- x)FHMA / Epikote 828, (1- x) = 0.0872.
Blend composition 0.1 / 0.9 in volume fraction.

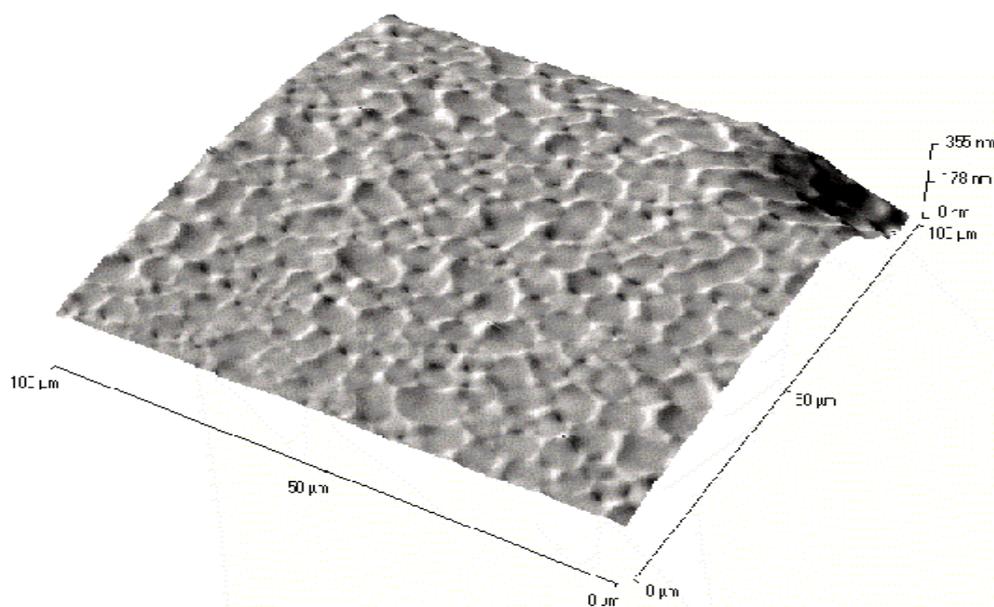


Figure 6.7 AFM picture, contact mode.
Binary system x MMA-(1- x)FHMA / Epikote 828, (1- x) = 0.0872.
Blend composition 0.1 / 0.9 in volume fraction.

For region (2), the phase transition process is very slow, due to the high viscosity of the system. E-SEM experiments carried out after one week on two semi-transparent samples a drop (bulk) and a film around 0.5 mm thick with the same blend composition show that nucleation takes place. The aggregate size depends of the sample thickness, for the drop the aggregate size was around 0.5 μm and more homogeneously distributed (figure 6.8 (a)), while for the film the aggregate size is between 0.1-1 μm (figure 6.8 (b)).

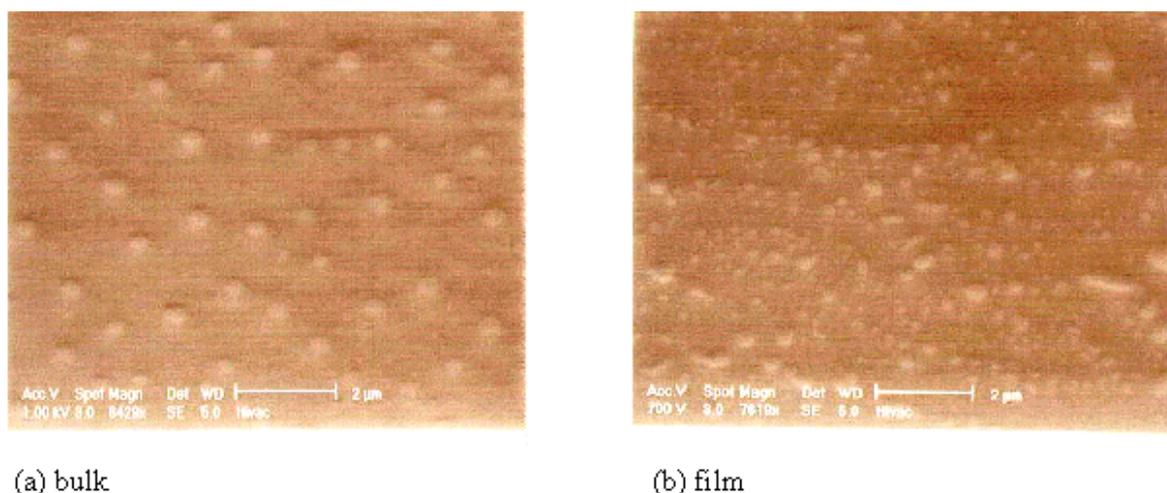


Figure 6.8 E-SEM pictures at $T = 293.15$ K.
 Binary system x MMA-(1- x)FHMA / Epikote 828, (1- x) = 0.0872.
 Blend composition 0.4 / 0.6 in volume fraction.

The morphology developed in region (2) is neat and it raised one more question: why are the sizes of the domains in the drop (bulk) and in the film different?

Motivated by the results obtained in the simulations presented in the previous chapter, we decided to use the model introduced in this thesis to study morphology development and to apply it to this specific case to find the answers to the questions raised from experimental results in region (1) and (2) of figure 6.5.

Figure 6.9 presents the phase diagram and morphology obtained from numerical simulations for the binary system x MMA-(1- x)FHMA / Epikote 828, (1- x) = 0.0872. The simulations suggest that a larger content of fluorinated copolymer in the blend (equal to 0.32 in volume fraction) was needed to experimentally observe the co-continuous morphology.

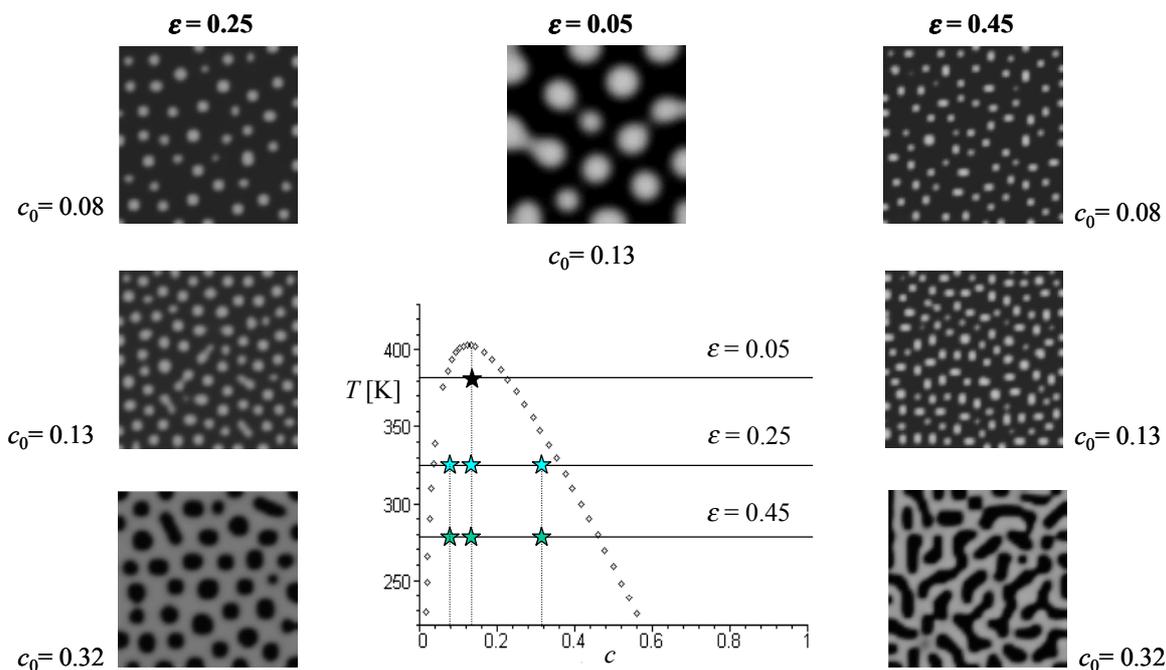


Figure 6.9 Simulations results for the binary system $x\text{MMA}-(1-x)\text{FHMA}$ / Epikote 828, $(1-x) = 0.0872$.

To find out why the domain sizes in region (2) are different in a drop (bulk) and in a film with the same concentration, we did a couple of numerical simulations quenching the system to a temperature of 293.15 K, using an initial blend composition equal to the experimental one ($c \approx \phi_0 = 0.4$); the results are shown in figure 6.10. The morphologies obtained in the numerical simulations match qualitatively with the experimental ones. We can see that in the bulk larger and more homogeneously distributed aggregates are formed. On the other hand, in the presence of the wall, the size of the droplets formed decreases as a function of the distance to the wall, due to the lower amount of copolymer available deeper in the bulk of the system, as illustrated by the concentration profile in figure 6.10. This feature is consistent with E-SEM picture in figure 6.8 (b).

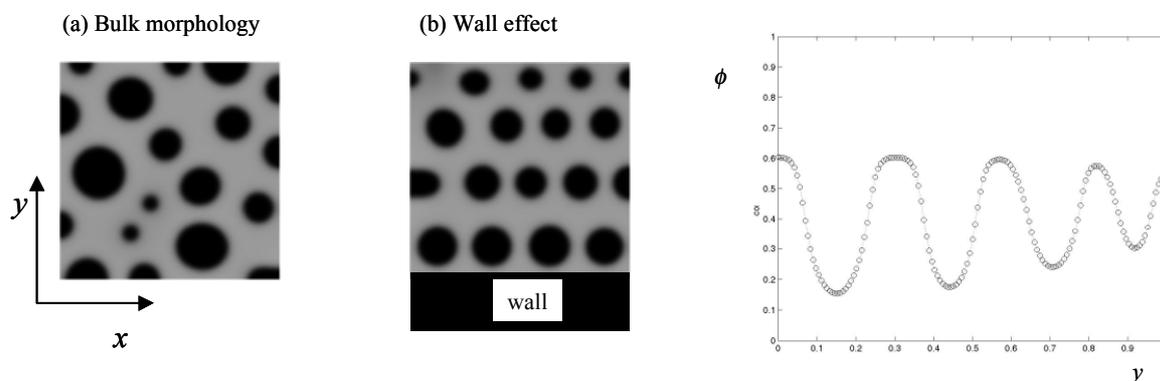


Figure 6.10 Numerical simulations for bulk and film morphologies.

System $x\text{MMA}-(1-x)\text{FHMA}$ / Epikote 828, $(1-x) = 0.0872$.

Blend composition 0.4 / 0.6 in volume fraction, $T = 293.15$ K, $L = 1000$ nm.

Right figure: concentration profile corresponding to (b) Wall effect.

6.4 Conclusions

In this chapter we established that fluorine content in the copolymer and chain length extension of the epoxy resin mainly determines the phase behavior in the binary blends; molar mass of the fluorinated copolymer is a secondary effect in the shift of the miscibility gap. With the χ_1 parameters obtained, qualitative predictions of the miscibility gap for binary systems with fluorine content between 0.0872 and 0.1240 are possible.

The numerical simulations allowed a better understanding of experimental results. No co-continuous spinodal morphology around the critical point was found due to the small amount of copolymer present in the binary polymer blend. The smaller sizes of the domains in the presence of the wall are explained in terms of the lower amount of fluorinated copolymer available in the bulk as the distance to the wall increases.

6.5 References

- ¹ Potter, W.G. *Uses of epoxy resins* Newnes-Butterworths, London (1975)
- ² Paul, S. *Surface coatings. Science and technology* 2nd ed., John Wiley & Sons, England (1985)
- ³ Van de Grampel, R.D.; van Geldrop, J. and van der Linde R. *J. Appl. Polym. Sci.* **79** (2001) 159
- ⁴ Flory, P.J. *J. Chem. Phys.* **9** (1941) 660
- ⁵ Huggins, M.L. *J. Chem. Phys.* **9** (1941) 440
- ⁶ Dobson, G.R. and Gordon, M. *J. Chem. Phys.* **43**, no.2 (1965) 705
- ⁷ Koningsveld, R. *Adv. Coll. Int. Sc.* **2** (1968) 151
- ⁸ Schulz, M. and Frisch, H.L. *J. Chem. Phys.* **101**, no. 6 (1994) 5013
- ⁹ Fox, T.G. and Flory, P.J. *J. Appl. Phys.* **21**, (1950) 581
- ¹⁰ Govor, L.V.; Bashmakov, I.A.; Kaputski, F.N., Pientka, M. and Parisi, J. *Macromol. Chem. Phys.* **201**, no.18 (2000) 2721

CHAPTER 7

EPILOGUE

7.1 Facts

The study of stratification in a thin film requires an understanding of thermodynamics and kinetics or diffusion of mass of the components in the system. It is not enough to choose a polymer blend where we know beforehand that stratification will occur due to difference in surface energy of the components (as is described in appendix II). Therefore, if we aim to control the final morphology and to achieve certain final macroscopic properties in a material, we have to know the temporal evolution of the thermodynamic properties, and to count with information on physical parameters of the system, such as diffusion coefficient, interfacial tension, viscosity, etc., as a function of temperature, and pressure if necessary.

The investigation of the diffusion process of any specific system is achieved by solving the balance equations of the system, which is a problem involving the solution of thermodynamics and hydrodynamics in a coupled way. The property linking these two fields is the chemical potential and therefore it is important for this quantity to consider in detail the thermodynamics and physics involved. Here, to derive the chemical potential of a thin film of a binary blend undergoing phase separation in the spinodal region, a Helmholtz free energy functional is used containing local contributions to the energy (Flory-Huggins lattice model), gradient concentrations in enthalpy and entropy (RPA, de Gennes), and the interactions of the blend components with the wall. In this last term, the short-range interactions are included as a hard-core potential and the long-range ones as attractive van der Waals interactions (Israelachvili).

The analysis of the Helmholtz energy functional carried out shows that the magnitude of the interfacial thickness is determined by the entropic contribution in the square-gradient term for polymer systems. This quantity is of importance not only because it is needed in the re-scaling of the balance equations, but also because it determines the interfacial tension, which plays an important role in the domain size of the system.

The results obtained with the model proposed, show that the connectivity of the co-continuous spinodal morphology is mainly determined by the symmetry or ratio of number of segments of the chains contained in the polymer blend. The initial concentration of the blend before quenching the system within the miscibility gap is another important factor to obtain a co-continuous structure. When the wall effect is switched on, a striking change in the morphology is observed. The impact of this effect farther from the wall depends on two

factors: the magnitude and extension into the bulk of the wall-polymer interaction potential and the magnitude of the chemical potential.

It was possible to clarify the early-stage of the spinodal decomposition when a boundary or rigid wall is present. Two processes are involved in this stage: wetting and phase separation. We found, as Cumming and co-workers reported experimentally,^{1,2} that for a system where one of the components prefers the substrate, there are indeed two different growth rates for the domains close and farther from the wall. The domains at the wall form faster and have a larger magnitude than those forming deeper in the bulk. The fast growth at the wall is associated to wetting effects; this fact closes the open question posed by Troian.³ In the case of non-preference for any of the blend components towards the wall, is expected that the fast domain growth is inhibited and the surface domains present only an anisotropic growth due to the geometric constraint introduced by the wall.

The model implemented in this thesis, allowed also explaining morphological results observed here experimentally. Consequently, it was possible to obtain a better understanding of the relationship between phase and morphological behaviors of a system difficult to resolve experimentally.

We conclude that the extension of the diffuse-interface model (Verschueren) as presented in this thesis resulted in a useful tool to predict morphology development of a polymer (or monomer) blend in a mesoscopic scale both in bulk and in the presence of a rigid wall. In addition, the model proposed can be applied to the temporal study of morphology of symmetric and asymmetric systems, having either an upper or a lower critical solution temperature.

7.2 Constraints of the model used

When a model is proposed it is important to indicate its range of applicability. The model proposed here is limited to the study of morphology development in partially miscible systems where the RPA approximation gives good predictions for the phase behavior of polymers. Other assumptions done in the models are: incompressibility and isothermal conditions. The introduction of compressibility would require a reformulation of the balance equations (see chapter 3) and the Helmholtz energy functional (Sánchez and Lacombe, Lifschitz and Freed) whilst the effect produced by thermal fluctuations has already been studied in other work (Verschueren).

A feature present commonly in polymer systems is polydispersity. This fact is not a basic limitation but it was not studied here and therefore if a polydisperse system is considered, it must explicitly expressed in the formulation of the free energy functional (Koningsveld).

Polymer blends are very viscous systems and therefore hydrodynamic effects do not play a main role in their morphology development, as it can be deduced by inspection of the momentum equation. Nevertheless, if the diffuse-interface model proposed here is applied to monomer systems having large diffusion coefficients, hydrodynamic effects are relevant and their effect should be studied in more detail.

7.3 Suggestions

Once something is achieved, we can propose ideas for future work. In fact, a series of extensions can be done. It is necessary to develop a method of analysis for small values of the wave vector q in the early-stage of the spinodal decomposition. This would allow the quantification of the domain growth at the wall and a direct comparison with experiments. In addition, to determine and to quantify the domain growth due to bulk phase separation it is necessary to extend this study to the late-stage of the spinodal decomposition.

It is known from the literature (Reich and Cohen) that the film thickness plays a role in the phase separation and final shape of the concentration profile of the system. To be able to study this effect, it would be necessary to introduce in the model the interaction of the blend components with a second interface vapor-polymer blend (free interface).

A very attractive application of the spinodal phase separation in thin films has been the creation of lateral order on patterned substrates, proposed by Kraush et al.⁴ and re-taken by Böltau et al.⁵ The modeling of this phenomenon is of interest because it allows tailoring the morphology in a very small scale at a very low cost, which has a large technological impact. In principle, the model proposed here could be extended to study patterned surfaces. To do so is necessary to introduce a wall-polymer interaction potential that is different for each domain in the pattern and software that implements this differentiation.

As mentioned in the introduction of this thesis, chemical treatment is another way of inducing development of structure in a system. In the coatings field a frequent practice is curing, which means drying and cross-linking of the system. The model proposed could be extended to study this kind of process by keeping the reactive terms in the balance equations (de Groot and Mazur).

7.4 References

¹ Wiltzius, P. and Cumming A. *Phys. Rev. Lett.* **66**, no. 23 (1991) 3000

² Cumming, A.; Wiltzius, P.; Bates, F.S. and Rosedale, H. *Phys.Rev. A.* **45**, no. 2 (1992) 885

³ Troian, S. *Phys. Rev. Lett.* **71**, no. 9 (1993) 1399

⁴ Krausch, G.; Kramer, E.; Rafailovich, M.H.; Sokolov, J. *Appl. Phys. Lett.* **64**, no. 20 (1994) 2655

⁵ Böltau, M.; Walheim, S.; Mlynek, J.; Kraush, G.; Steiner, U. *Nature* **391**, no. 26 (1998) 877

After the introduction of Lagrange multipliers, the free energy takes the form:

$$\begin{aligned} \frac{F^{inh}}{n_s kT} = & \sum_K \sum_l \phi_{IK} \{ [1-2m] g_{IK}^0 \log g_{IK}^0 + m g_{IK}^+ \log g_{IK}^+ + m g_{IK}^- \log g_{IK}^-] \\ & + (\xi_{IK} - 1)(1-2m) g_{IK}^0 + m g_{IK}^+ + m g_{IK}^- - 1] + m \lambda_{IK} g_{IK}^+ - m \lambda_{1-l,K} g_{IK}^- \\ & + \frac{1}{2} \chi [\phi_{IK'} + m(\phi_{l+1,K'} - 2\phi_{1K'} + \phi_{l-1,K'})] + w_{\zeta,l} \} - \sum_l w_{\zeta,l} \end{aligned} \quad (I.4)$$

this equation is to be minimized with respect to the g_{IK}^v and ϕ_{IK} . The result after minimization and partial substitution of the constraints is

$$\begin{aligned} g_{IK}^0 &= \exp[-\xi_{IK}], \\ g_{IK}^+ &= \exp[-\xi_{IK} - \lambda_{IK}], \\ g_{IK}^- &= \exp[-\xi_{IK} + \lambda_{1-l,K}], \\ \xi_{IK} - \chi [\phi_{IK'} + m(\phi_{l+1,K'} - 2\phi_{1K'} + \phi_{l-1,K'})] - w_{\zeta,l} &= 0 \end{aligned} \quad (I.5)$$

Inserting this set of equations into the constraints conditions we get:

$$\begin{aligned} \exp(\xi_{IK}) &= 1 + m [\exp(-\lambda_{IK}) + \exp(\lambda_{1-l,K}) - 2] \\ \exp(-2\lambda_{IK}) \frac{1 + m [\exp(-\lambda_{l+1,K}) + \exp(\lambda_{l,K}) - 2]}{1 + m [\exp(-\lambda_{IK}) + \exp(\lambda_{1-l,K}) - 2]} &= \frac{\phi_{l+1,K}}{\phi_{IK}} \end{aligned} \quad (I.6)$$

The set of equations (I.4) to (I.6) are solved numerically, giving the following solution, which corresponds to the lowest free energy

$$\phi_{l2} = \phi_{1-l,1} \quad (I.7)$$

$$g_{l2}^v = g_{1-l,1}^{-v} \quad (I.8)$$

There is no doubt that this procedure might lead to a more accurate calculation of the equilibrium conditions including the effect of loss of entropy at an interface than the random phase approximation, but definitely is more time consuming.

I.2 Derivation of the pre-factor of the square-gradient term

The pre-factor $\kappa(\phi)$ (equation (2.4)) of the square-gradient term in equation (3.41) is obtained by following a formulation based on the random phase approximation (RPA) combined with the Flory-Huggins lattice model. According to de Gennes,¹ the inverse structure factor for the interacting system is defined by:

$$\frac{1}{S_T^{coll}(q)} = \frac{1}{S_{non-int}(q)} - V(q) \quad (I.9)$$

with q is the amplitude of the scattering wave vector (equal to $4\pi\lambda^{-1} \sin \theta / 2$ where λ is the wavelength and θ is the scattering angle), the first term in the right hand side is the non-interacting part of the structure factor and the second is the interacting contribution. By considering interactions between closest neighbors in a cubic lattice, the interacting term takes the form:

$$V(q) = 2\chi\left(1 - \frac{1}{6}q^2r_0^2\right) \quad (\text{I.10})$$

where χ is the Flory-Huggins pair interaction parameter and r_0 is a measure of the range of intersegment forces, with an order of magnitude of the segment size.

The non-interacting term is defined by

$$\frac{1}{S_{non-int}(q)} = \frac{1}{\phi g_D(N_1, q)} + \frac{1}{(1-\phi)g_D(N_2, q)} \quad (\text{I.11})$$

where ϕ and $(1-\phi)$ are the volume fractions of segments of component one and two, respectively and $g_D(N_i, q)$ is the Debye function, which considers single chains and indicates the number density of other monomers at a distance r from the first segment, N_i ($i = 1$ or 2) refers to the number of segments in component 1 or 2. Substitution of (I.10) and (I.11) into (I.9), gives:

$$\frac{1}{S_T^{coll}(q)} = \frac{1}{\phi g_D(N_1, q)} + \frac{1}{(1-\phi)g_D(N_2, q)} - 2\chi\left(1 - \frac{1}{6}q^2r_0^2\right) \quad (\text{I.12})$$

In the short-range limit (when $qR_g \ll 1$), by considering only pair interactions between molecules of type 1 and 2, and recalling that in the critical point and along the spinodal curve, the Debye function simplifies to N_i , the structure factor form at the spinodal for the simple Flory-Huggins lattice model is recovered and given by

$$\frac{1}{S_T^{coll}(q)} = \frac{1}{\phi N_1} + \frac{1}{(1-\phi)N_2} - 2\chi \quad (\text{I.13})$$

When q approaches zero, $q \rightarrow 0$, the Debye function takes the form

$$g_D(N_i, q \rightarrow 0) = N_i\left(1 - \frac{1}{3}q^2R_g^2\right) \quad (\text{I.14})$$

with R_g the radius of gyration given by

$$R_g^2 = \frac{N_i a^2}{6} \quad (\text{I.15})$$

and the parameter a refers to the lattice spacing. Substitution of equations (I.14) and (I.15) into (I.12), gives

$$\frac{1}{S_T^{coll}(q)} = \frac{1}{\phi[N_1(1 - \frac{1}{18}q^2N_1a^2)]} + \frac{1}{(1-\phi)[N_2(1 - \frac{1}{18}q^2N_2a^2)]} - 2\chi(1 - \frac{1}{6}q^2r_0^2) \quad (\text{I.16})$$

If we consider for a moment $x_1 = \frac{1}{18}q^2a^2N_1$, $x_2 = \frac{1}{18}q^2a^2N_2$ and keep in mind that we are in the short-range limit (where $qR_g \ll 1$), it is possible to apply the approximation $\frac{1}{1-x} = 1+x$; this yields a simplification of (I.16) in the form

$$\frac{1}{S_T^{coll}(q)} = \frac{1}{\phi N_1} + \frac{1}{(1-\phi)N_2} + \frac{q^2a^2}{18\phi(1-\phi)} - 2\chi(1 - \frac{1}{6}q^2r_0^2) \quad (\text{I.17})$$

This form of the structure factor corresponds to an extended Flory-Huggins model called in this work the Flory-Huggins-de Gennes energy of mixing, given by:

$$f_{FHG} = \Delta g_m(\phi) + \kappa(\phi)(\nabla\phi)^2 \quad (\text{I.18})$$

where Δg_m is the Flory-Huggins energy of mixing² and $\kappa(\phi)$ is:

$$\kappa(\phi) = \frac{r_0^2}{6}\chi_c + \frac{a^2}{\lambda\phi(1-\phi)}, \quad (\text{I.19})$$

with $\lambda = 36$. On the other hand $\lambda = 24$, is obtained for a long-range limit, where the Debye function has the form

$$g(q) = \frac{2N_i}{q^2R_g^2} \quad (\text{I.20})$$

with a structure factor

$$\frac{1}{S_T^{coll}(q)} = \frac{q^2a^2}{12\phi(1-\phi)} \quad (\text{I.21})$$

I.3 Common tangent construction

If $\mu_i^0(T, p)$ denotes the molar chemical potential of the pure species i and ΔG_m the mixing Gibbs energy is³

$$G = \sum_{i=1}^2 n_i \mu_i^0 + \Delta G_m \quad (\text{I.22})$$

Setting $x = n_1 / n$, $(1-x) = n_2 / n$, with $n = n_1 + n_2$ and $g = G / n$ one finds

$$g = \mu_2^0 + x(\mu_1^0 - \mu_2^0) + \Delta g_m \quad (\text{I.23})$$

In the common tangent construction (figure I.1) one looks for concentrations $x = X$ and $x = Y$ such that

$$g'(X) - g'(Y) = 0 \quad (\text{I.24})$$

and that

$$g(Y) - g(X) = (Y - X)g'(X) \quad (\text{I.25})$$

Differentiating g gives

$$g'(X) - g'(Y) = \Delta g'_m(X) - \Delta g'_m(Y) \quad (\text{I.26})$$

so that equation (I.24) is equivalent to

$$\Delta g'_m(X) - \Delta g'_m(Y) = 0 \quad (\text{I.27})$$

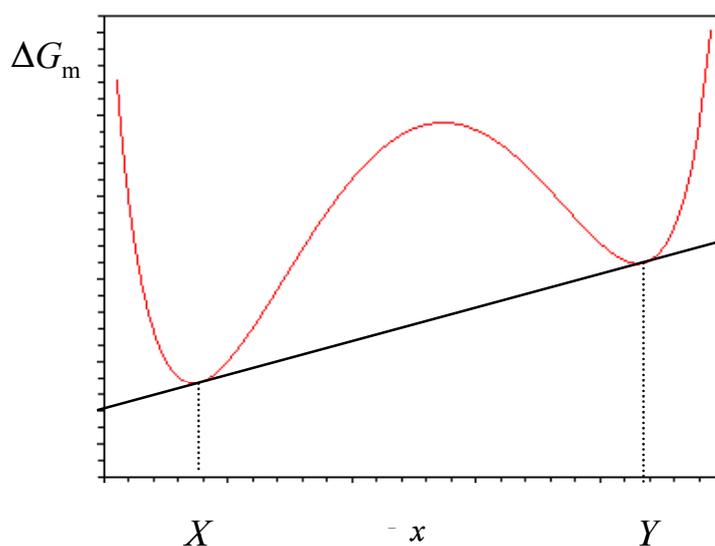


Figure I.1 Gibbs free energy and common tangent construction.

From the definition for g one finds at first

$$g(Y) - g(X) = (Y - X)(\mu_1^0 - \mu_2^0) + (\Delta g_m(Y) - \Delta g_m(X)) \quad (\text{I.28})$$

For every concentration one has

$$g'(x) - \Delta g'_m(x) = \mu_1^0 - \mu_2^0 \quad (\text{I.29})$$

Taking $x = X$ in particular, then gives

$$g'(X) - \Delta g'_m(X) = \mu_1^0 - \mu_2^0 \quad (\text{I.30})$$

Finally, using equation (I.29) to eliminate $(\mu_1^0 - \mu_2^0)$ from equation (I.28) leads to

$$g(Y) - g(X) - (Y - X)g'(X) = \Delta g_m(Y) - \Delta g_m(X) - (Y - X)\Delta g'_m(X) \quad (\text{I.31})$$

Therefore, if equation (I.25) is met it follows that also

$$\Delta g_m(Y) = \Delta g_m(X) + (Y - X)\Delta g_m'(X) \quad (\text{I.32})$$

It can be concluded that the common tangent construction applied to the total Gibbs energy leads to the same result as the common tangent construction applied to a plot of the Gibbs energy of mixing. Moreover, because $g'' = \Delta g_m''$ we see that the spinodal points and the critical point can also be determined by using the Gibbs energy of mixing instead of the total Gibbs energy.

I.4 Conservation law³

Let the volume density f of the Helmholtz energy F depend on the concentration ϕ and its gradient $\nabla\phi$. The first variation of the total Helmholtz energy

$$F = \int_V f(\phi, \nabla\phi) dV \quad (\text{I.33})$$

is given by

$$\delta F = \int_V [f(\phi, \nabla\phi) - f(\phi + \delta\phi, \nabla(\phi + \delta\phi))] dV \quad (\text{I.34})$$

Expanding (I.34) and using the Gauss theorem gives

$$\delta F = \int_V \left(\frac{\partial f}{\partial \phi} - \nabla \cdot \frac{\partial f}{\partial \nabla \phi} \right) \delta\phi dV + \int_S \left(\mathbf{n} \cdot \frac{\partial f}{\partial \nabla \phi} \right) \delta\phi dS + \dots \quad (\text{I.35})$$

where S indicates the surface of V and \mathbf{n} the outwardly directed normal on S . The first variation of F vanishes if

$$\mu = \frac{\delta F}{\delta \phi} = \frac{\partial f}{\partial \phi} - \nabla \cdot \frac{\partial f}{\partial \nabla \phi} = 0 \text{ everywhere in } V \quad (\text{I.36})$$

and if the surface term is also zero for arbitrary variations $\delta\phi$. When the concentration is prescribed on the surface S the variation is zero and the surface term vanishes. Alternatively, the surface term can be made to disappear if on the surface

$$\mathbf{n} \cdot \frac{\partial f}{\partial \nabla \phi} = 0 \quad (\text{I.37})$$

I.4.1 Conserved quantities in the one-dimensional case

Consider equation (I.36) for the one-dimensional case:

$$\frac{\partial f}{\partial \phi} - \frac{d}{dy} \cdot \frac{\partial f}{\partial \phi'} = 0 \quad (\text{I.38})$$

where $\phi' = d\phi / dy$. Multiplying both sides of this equation by ϕ' leads to

$$\frac{d}{dy} (f - \phi' \frac{\partial f}{\partial \phi'}) = 0 \quad (\text{I.39})$$

Integrating this equation over y leads to

$$f - \phi' \frac{\partial f}{\partial \phi'} = k_0 = \text{constant} \quad (\text{I.40})$$

Since the right-hand side of this equation is constant, we say that $f - \phi' (df / d\phi')$ is a conserved quantity. Note that:

- The conservation law given by equation (I.40) is true provided one takes for the concentration ϕ any solution of the equilibrium equation $\mu = 0$.
- The value for k_0 is determined by the values for ϕ and ϕ' at the boundary.

A special but practically important case is when

$$f = f_0(\phi) - \omega(\phi)(\phi')^2 \quad (\text{I.41})$$

in this case we find for the conservation law

$$f_0(\phi) - \omega(\phi)(\phi')^2 = k_0 \quad (\text{I.42})$$

or

$$\left(\frac{d\phi}{dy}\right)^2 = \frac{f_0(\phi) - k_0}{\omega(\phi)} \quad (\text{I.43})$$

If we next consider y as a function of ϕ instead of the other way around, we can use this equation to find a solution for $y(\phi)$ using

$$\frac{dy}{d\phi} = \pm \sqrt{\frac{\omega(\phi)}{f_0(\phi) - k_0}} \quad (\text{I.44})$$

I.4.2 Calculation of k_0 for an asymmetric system

For symmetric systems the calculation of the constant k_0 that shifts the energy given by equation (3.25) to $\mu = 0$ is straightforward. However, for asymmetric systems the shifting of the Gibbs energy to $\mu = 0$ requires of two different values for k_0 (k_1 and k_2) one at each minimum, as illustrated in figure I.2.

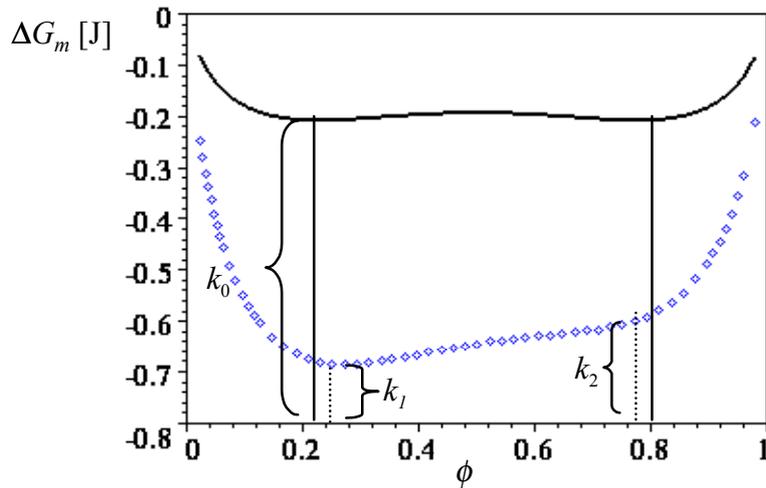


Figure I.2 Gibbs energy of mixing, k_0 , k_1 and k_2 are constants shifting the Gibbs energy to $\mu = 0$.
—Symmetric system, $\diamond\diamond$ asymmetric system.

To shift both minima of the energy to $\mu = 0$ in the case of an asymmetric system we do the following mathematical transformation that keeps unmodified the physics of the system and lead to a unique value of k_0 . The evaluation of the set of equations (3.31) for $\Delta\mu_1$ and $\Delta\mu_2$ at the equilibrium concentration of the phase α or the β , respectively, gives a couple of “artificially” symmetric chemical potentials $\Delta\mu_1^c$ and $\Delta\mu_2^c$.

$$\begin{aligned}\Delta\mu_1^c &= \frac{1}{N_1}(\Delta\mu_1 - \Delta\mu_1|_{\phi=\phi^\alpha}) \\ \Delta\mu_2^c &= \frac{1}{N_2}(\Delta\mu_2 - \Delta\mu_2|_{\phi=\phi^\beta})\end{aligned}\tag{I.45}$$

By integrating $\Delta\mu_1^c$ and $\Delta\mu_2^c$ with respect to ϕ , followed by addition of the integrals results (equation I.45) one obtains an “artificially” symmetric mixing energy from where it is possible to derive the unique value of k_0 we were looking for.

$$\Delta g_m^c = N_1 \int \Delta\mu_1^c d\phi + N_2 \int \Delta\mu_2^c d\phi\tag{I.46}$$

I.4.3 Maximum slope method

For systems where it is not allowed to use the Taylor expansion for the free energy, we follow the method of the maximum slope sketched in figure I.3 to calculate the interfacial thickness of the profile starting at $\phi = \phi^\alpha$ at $y = -\infty$ and changing to $\phi = \phi^\beta$ at $y = +\infty$. This profile is governed by equation (I.44).

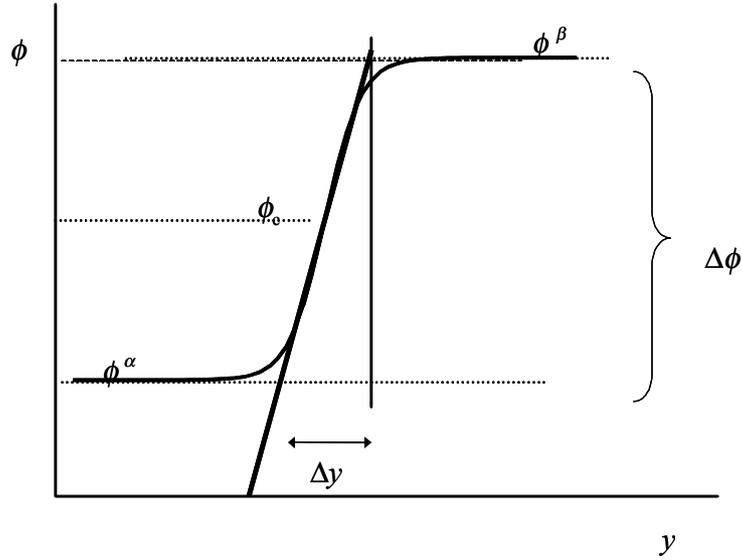


Figure I.3 Method of the maximum slope,
 Δy corresponds to twice the interfacial thickness.

This method requires the evaluation of the inverse of (I.23) in the point ϕ_c where the slope is a maximum, giving

$$\left. \frac{d\phi}{dy} \right|_{\max} = \sqrt{\left. \frac{f_0(\phi) - k_0}{\omega(\phi)} \right|_{\phi_c}} = m \quad (\text{I.47})$$

In the right-hand side of equation (I.24), k_0 as before is a constant determined by the values for ϕ and $d\phi/dy$ at the boundary, f_0 is given by equation (3.26) for symmetric systems, for non-symmetric systems we calculate k_0 as explained in the previous section, $\omega(\phi)$ equals $\frac{1}{2} \kappa(\phi)$ with $\kappa(\phi)$ calculated with equation (3.41). The concentration ϕ_c corresponds to the critical point concentration. Considering the boundary conditions we obtain that the interfacial thickness is given by:

$$2\xi = \Delta y = \frac{1}{m} \Delta\phi, \quad \text{with } \Delta\phi = \phi^\beta - \phi^\alpha \quad (\text{I.48})$$

I.5 Interaction parameter of a binary polymer blend in contact with a rigid wall

As a wall acts as an adsorbing boundary, it is important to consider adsorption. In a polymer blend, when the chain segments of one of the polymers have no affinity for the surface, depletion takes place. On the other hand if the polymer chain has affinity for the surface adsorption occurs. The way of predicting adsorption is by means of the adsorption interaction parameter χ_s , which is defined by⁴:

$$\chi_s = \frac{u_1^a - u_2^a}{kT} \quad (\text{I.49})$$

where u_i^a is the adsorption energy of each component. When χ_s is positive, the component labeled as two is adsorbed at the interface, if χ_s is negative, component one is adsorbed and when χ_s equals zero, preferential adsorption doesn't take place.

The adsorption energy of a component taking only into account nearest neighbors interactions in a lattice is expressed as $u_i^a = z' \chi_{iw}$, where z' is the coordination number of the surface and χ_{iw} is the interaction parameter of component i with the wall, given by $\chi_{iw} = \epsilon_{iw} - \frac{1}{2} \epsilon_{ii}$, the difference in energy contact interaction of pairs $i-w$ and $i-i$. Considering these last definitions one obtains for the adsorption energy

$$\begin{aligned} u_1^a &= z' \left(\epsilon_{1w} - \frac{1}{2} \epsilon_{11} \right) \\ u_2^a &= z' \left(\epsilon_{2w} - \frac{1}{2} \epsilon_{22} \right) \end{aligned} \quad (\text{I.50})$$

Substitution of (I.50) into (I.49) yields for the interaction parameter χ_s

$$\chi_s = \frac{z'}{kT} \left[\left(\epsilon_{1w} - \frac{1}{2} \epsilon_{11} \right) - \left(\epsilon_{2w} - \frac{1}{2} \epsilon_{22} \right) \right] \quad (\text{I.51})$$

It is possible and convenient to find a relationship between the interaction parameter χ_s and a property of easy experimental access. This property turns out to be the surface energy or interfacial tension, which is present at every interface. According to Jones,⁵ the interfacial energy for a component i in contact with a wall is given by

$$\gamma_{iw} = -\frac{z'(\epsilon_{ii} - 2\epsilon_{iw})}{2a^2} \quad (\text{I.52})$$

here a is the lattice spacing and the number two in the denominator avoids double counting of interactions. With equation (I.52) we can re-write χ_s as:

$$\chi_s = -\frac{a^2}{kT} (\gamma_{2w} - \gamma_{1w}) = -\frac{a^2}{kT} \Delta\gamma_i \quad (\text{I.53})$$

I.5.1 Calculation of $\Delta\gamma$ for $\theta \neq 0$

As an example in this section is used silicon as a rigid wall. To calculate γ_{1w} , the interfacial tension between the wall and component one is used⁶

$$\gamma_{1w} = \gamma_w + \gamma_1 - 2\sqrt{\gamma_1^d \gamma_w^d} \quad (\text{I.54})$$

The disperse contribution to the surface energy of the wall γ_w^d , is obtained with

$$\gamma_w^d = -\frac{w(r)}{2A} \quad (\text{I.55})$$

where $A = \pi r^2$ is the area and $w(r)$ is the dispersion interaction potential

$$w(r) = -\frac{C_{disp}}{r^6} = -\frac{a_0^3 I e}{r^6} \quad (\text{I.56})$$

$a_0 = 0.53$ nm is the Bohr radius, $I = 14$ J/C is the first ionization potential for the silicon atom,⁷ $r = 0.084$ nm is the interatomic distance for Si^{4+} and $e = 1.602 \times 10^{-19}$ C is the electron charge. The surface tension of semi-conductor silicon is known to be⁸ 1100 mJ/m².

The dispersion contribution to the interfacial tension of component one γ_1^d , can be estimated with

$$\begin{aligned} \gamma_1^d &= \gamma_1 - \gamma_1^p \\ \text{and } \gamma_1^d &= x^p \gamma_1 \end{aligned} \quad (\text{I.57})$$

when the polarity x^p is known⁹. When there is not information available for x^p , a longer way¹⁰ must be taken to calculate γ_1^d . Further, the surface tension of the pure component one γ_1 , at a temperature at which the system is quenched can be estimated using¹¹

$$\begin{aligned} \gamma_1 &= \gamma_0 \left(1 - \frac{T}{T_{cr}}\right)^{11/9}, \quad \text{with} \\ \gamma_0 &= -\frac{9T_c}{11} \left(\frac{d\gamma}{dT}\right) \left(1 - \frac{T}{T_{cr}}\right)^{-2/9} \end{aligned} \quad (\text{I.58})$$

γ_0 is the surface tension at $T = 0$ K, $(d\gamma/dT)$ is known for some polymer systems from tables,⁹ T_{cr} is the imaginary critical temperature (do not confuse with the critical solution temperature T_c) that has a value around 1000 K for most of polymers according to Wu.¹² With the surface tension of the pure component 1 and the bulk interfacial tension at a temperature T , is possible to calculate the interfacial tension of the second component in the blend with⁶

$$\gamma_2 = \gamma_1 - \gamma_{12} \quad (\text{I.59})$$

I.6 References

- ¹ De Gennes, P.G. *Scaling concepts in polymer physics* Cornell University Press, USA (1979)
- ² Flory, P.J. *Principles of polymer chemistry* Cornell University Press, USA (1953)
- ³ Notes by Paul van der Varst after discussions on the subject
- ⁴ Fleer, G.J.; Cohen Stuart, M.A. and Scheutjens, J.M.H.M. *Polymers at interfaces* Chapman & Hall, London (1993)
- ⁵ Jones, R.A.L.; Kramer, E.J.; Rafailovich, M.H. et al. *Mat. Res. Soc. Symp. Proc.* **153** (1989) 133
- ⁶ Israelachvili, J. *Intermolecular and surface forces* 2nd ed. Academic Press limited, London (1992)
- ⁷ Weast, R.C. and Selby, S.M. *CRC Handbook of chemistry and physics* 48th ed. The chemical rubber Co. (1967)
- ⁸ Wawra, H. *Z. Metallkde.* **66** (1975) 395, 492
- ⁹ Brandrup, J.; Immergrut, E.H.; and Grulke, E.A. *Polymer handbook* 4th ed. John Wiley & Sons, Inc. Chapter VI, p. 521
- ¹⁰ Van Krevelen, D.W. *Properties of polymers* 3rd ed. Elsevier, the Netherlands (1997)
- ¹¹ Guggenheim, E.A. *J. Chem. Phys.* **13**, no. 7 (1945) 253
- ¹² Wu, S. *Polymer interface and adhesion*, Marcel Dekker, New York (1982)

APPENDIX II

SOLUBILITY REGION OF THE BINARY SYSTEM BISPHENOL-A-DIGLYCIDYLEETHER / COPOLYMER POLY [CF₃(CF₂)₆SO₂NCH₂CH₃BA-CO-MMA]

II.1 Introduction

In this appendix we propose an alternative method to make homogeneous solutions of any binary or multicomponent polymer blend. The polymers used are a thermosetting epoxy resin and a thermoplastic hybrid fluorinated copolymer. To get a homogeneous solution of the polymers mentioned, which have a different miscibility behavior, we make use of two different approaches; the one of Nelson, Hemwall and Edwards¹ and that of Hansen.^{2,3,4} With the approach of Nelson and colleagues, the miscibility region of each polymer in solution is obtained; once locating the line limiting the two miscibility regions, we apply partially the method of Hansen to define the miscibility of a binary polymer blend in a common solvent, at constant temperature (similar to a polymer map). The advantage of the combined approach proposed in this appendix is that with a far lower amount of solubility tests we are able to predict correctly the solubility region of two polymers in one solvent. We focus on the solubility behavior of the blended polymers at diluted concentrations ranging from 0.04 to 0.24 in volume fraction. This range covers the concentration values used typically in coating formulations.⁵ Details about the method followed are explained in the theoretical part of this appendix.

A possible practical application of the polymer solutions studied is the preparation of coatings that would stratify due to the difference in surface tension of the two mixed polymers. To check whether this is possible, solutions of the polymer blend are applied on a metallic substrate and brought to the inhomogeneous region by evaporating the solvent, with subsequently cross-linking of the thermosetting polymer. The stratification achieved is investigated with microscopic techniques such as scanning electron microscopy with energy dispersive X-ray analysis.

II.2 Theory

The Hildebrand and Scott solubility parameter theory⁶ has been widely used to determine solubility regions at a constant temperature for a huge amount of polymer solutions. This theory has two main limitations it cannot be applied directly to polymers, because experimentally the determination of latent heats of vaporization of a polymer is difficult and

the solubility parameter was designed for hydrocarbon solvents, where only dispersion forces play a major role. At this point the work of Nelson, Hemwall and Edwards is relevant.¹ These authors state that the solubility of a polymer in a solvent or solvent mixture can be extrapolated if two parameters: the Hildebrand solubility parameter and the hydrogen bonding accepting ability (also known as hydrogen bonding index) of the solvent in which the polymer is dissolved are known. Fortunately, these parameters can be obtained easily; first the Hildebrand solubility parameter of a solvent or solvent mixture in the presence of a polymer is calculated from:⁷

$$\delta_m = \sum_{i=1} \phi_i^* \delta_i \quad (\text{II.1})$$

where ϕ_i^* is the volume fraction of the component i at the cloud-point and δ_i is the correspondent solubility parameter or square root of the cohesion energy⁸ ($\delta_i = [\Delta E_{\text{evap}}/V_m]^{1/2}$). These values were taken from an available database.⁹ The sub-index m refers to the mixture of solvents.

Further, the hydrogen bonding accepting ability θ_A of the solvent mixture^{1,10} indicates the ability of a solvent or solvent mixture to form hydrogen bonds. Systems with large, positive values are better solvents for polymers. This parameter is given by

$$\theta_A = \sum_i \kappa_i \phi_i^* \gamma_i \quad (\text{II.2})$$

where γ_i is the hydrogen bonding parameter, obtained from IR experiments^{11,12} and κ_i is a weighting factor taken as -1 for simple alcohols, 0 for ether-alcohols, and $+1$ for all other compounds. The values of θ_A were calculated by introducing the volume fraction of the components present in the solvent mixture using an available program.¹³

By plotting θ_A as a function of δ_m for a polymer in a solution mixture of variable composition, a solubility envelope for that polymer is obtained, giving the location of the solubility and non-solubility regions of the polymer in a solvent or a solvent mixture. However, to find the region where a polymer blend is soluble in a common solvent or solvent mixture, we found it convenient to make partially use of Hansen's partial solubility parameter approximation.³

In Hansen's method the Hildebrand solubility parameter is divided in its three contributions: polarisation, hydrogen bonding and dispersion, the addition of these three components give back the total Hildebrand solubility parameter

$$\delta_t^2 = \delta_d^2 + \delta_p^2 + \delta_h^2 \quad (\text{II.3})$$

with δ_t , the total Hildebrand parameter, δ_d , the dispersion component, δ_p , the polar component and δ_h the hydrogen bonding component.

For a mixture of solvents the partial solubility parameters are defined by:

$$\delta_{k,m} = \sum_i \phi_i^* \delta_{k,i} \quad (\text{II.4})$$

where ϕ_i^* is the volume fraction of the i^{th} component in the solvent mixture at the cloud-point and $\delta_{k,i}$ is the dispersion ($k = d$), polarization ($k = p$), or hydrogen bonding ($k = h$) partial solubility parameter of the pure i^{th} component. The partial solubility parameters of the solvents used are known from literature¹⁰ and electronic databases.¹³

In our approach to find the solubility and non-solubility regions, we make use of the curve limiting the solubility and non-solubility regions in a traditional Hildebrand polymer map, then the partial polarisation and hydrogen bonding Hansen solubility parameters for the solvent volume fractions corresponding to this curve are calculated, and plotted versus the volume fraction of the polymer. The projection of the points obtained on the x - y plane corresponding to the partial solubility parameters gives a very good definition of the solubility and non-solubility regions of interest.

II.3 Experimental

A polymer epoxy resin (diglycidylether of bisphenol A, Epikote 1001) was acquired from Shell chemicals (Amsterdam, the Netherlands). The copolymer poly [CF₃(CF₂)₆SO₂NCH₂CH₃BA-co-MMA], with a molar mass of 32 kg/mol and a molar composition 90% MMA to 10% of CF₃(CF₂)₆SO₂NCH₂CH₃BA, abbreviated as PMMA:FX14, was synthesized in our laboratory.¹⁴ Polyoxypropylenediamine (Jeffamine D-230) from Huntsman (Everberg, Belgium) was used as cross-linking agent. For each polymer separately, a 30% w/w solution in methyl isobutyl ketone was prepared. Titrations of 10 g of such a solution were carried out at 298.15 K until cloudiness, using different volume fractions of cyclohexane and isopropanol. This solvent mixture $\phi_{\text{C}_6\text{H}_{12}}:(1-\phi)_{\text{IPA}}$ with variable volume fraction ϕ , has the advantage of covering a wide range in the solubility parameter δ_m and hydrogen bonding accepting ability θ_A , here are the necessary parameters to determine the solubility and insolubility regions of the polymers in study (solubility map). The volume fractions ϕ_i^* for each component at the cloud-point were obtained according to:

$$\phi_i^* = \frac{m_i / \rho_i}{\sum_i m_i / \rho_i} \quad (\text{II.5})$$

where m_i and ρ_i are the mass and the density, respectively, of the i^{th} component in the solvent mixture.

Calculations of the solubility parameter for a mixture of a specific polymer and a solvent mixture at the cloud point, δ_m , were done using equation II.1. The way of getting the polymer solubility map was explained in section II.2.

II.4 Results

In figure II.1 the miscibility map of the Epikote 1001 is shown. This map is in good agreement with the one reported in the literature.⁷ It can be concluded from these results that this polymer is dissolved more easily in solvents with high hydrogen bonding accepting

ability θ_A . The abbreviations $\phi_{\text{Cyc6}}:\phi_{\text{IPA}}$ correspond to solvent mixtures of cyclohexane and isopropyl alcohol containing variable volume fraction.

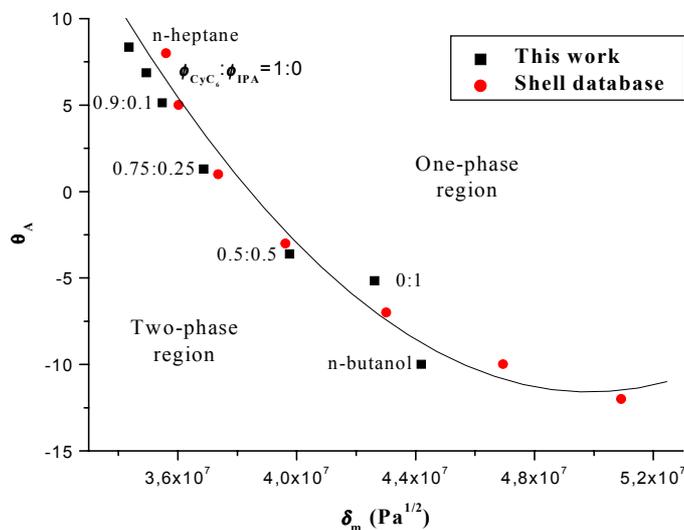


Figure II.1. Solubility map of the Epikote 1001, 30% w/w solids at $T = 298.15$ K. (Line drawn to guide the eye)

The solubility map for the fluorinated copolymer MMA:FX14 is shown in figure II.2, this copolymer was completely soluble in mixtures of $\phi_{\text{Cyc6}}:\phi_{\text{IPA}}$, when ϕ_{IPA} is above 0.4. This fact indicates that this polymer is rather soluble in solvents with a low θ_A .

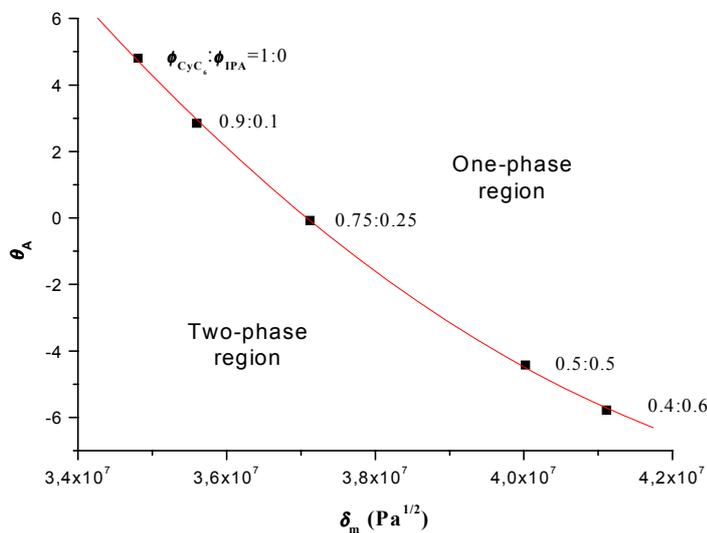


Figure II.2 Solubility map for MMA:FX14; 30% w/w solids at $T = 298.15$ K.

From figures II.1 and II.2, it can be concluded that both the epoxy resin and the fluorinated copolymer can be dissolved in a solvent or solvent blend with high θ_A .

To have a better outline of the solubility region of both polymers in solution, we calculated first with equation II.4 the partial solubility parameters corresponding to the cloud-point line

or line separating the solubility and non-solubility regions. A plot of these parameters and the total Hildebrand parameter (equation (II.3)) versus the volume fraction of the polymer allows us to visualise which parameters could contribute to a large extent to the solubility of the polymer; these plots are shown below in figure II.3 for each polymer.

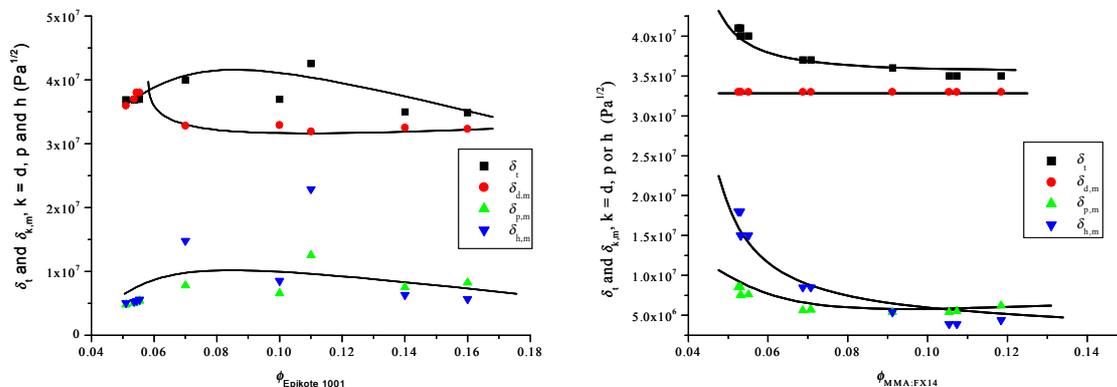


Figure II.3 Total Hildebrand solubility parameter and partial Hansen solubility parameters.
Left plot: Epikote 1001, right plot: MMA:FX14 at $T = 298.15$ K.
(Lines drawn to guide the eye).

It is clear from figure II.3 that, although the dispersion contribution to the total Hildebrand solubility parameter gives the highest contribution to the total value of this property, it doesn't change drastically with the modification of the volume fraction of the polymer. This fact made us think that the solubility region is defined mainly by the polarisation and the hydrogen bonding contributions, together with the variation of the concentration of the polymer. When these three variables are plotted a quite interesting result is obtained, shown in figures II.4 and II.5.

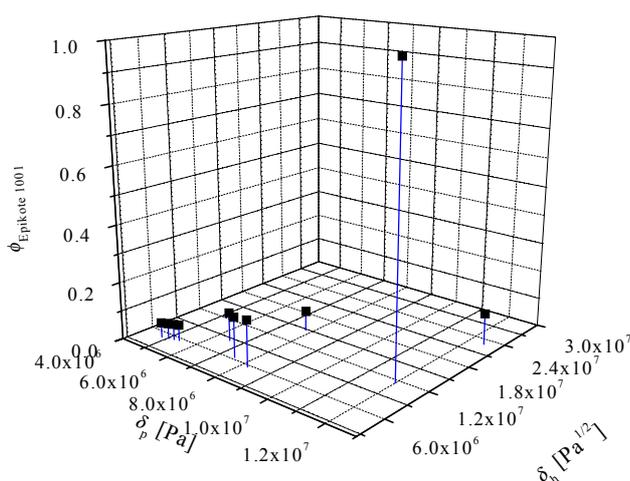


Figure II.4 Polarization and hydrogen bonding Hansen solubility parameters, Epikote 1001.

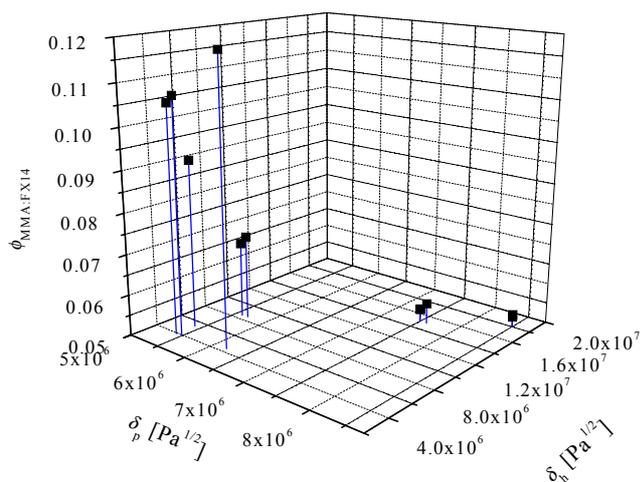


Figure II.5 Polarization and hydrogen bonding Hansen solubility parameter, copolymer MMA:FX14.

In first sight, it looks like the points define an enclosed solubility region. To make this picture simpler and to check our assumption, the projection on the δ_p and δ_h axis of the previous figures II.4 and II.5 were plotted together (figure II.6). Additionally tests were done with 30% of solids of the two different polymers in pure solvents. The results of these tests are included and indicated in open symbols in figure II.6.

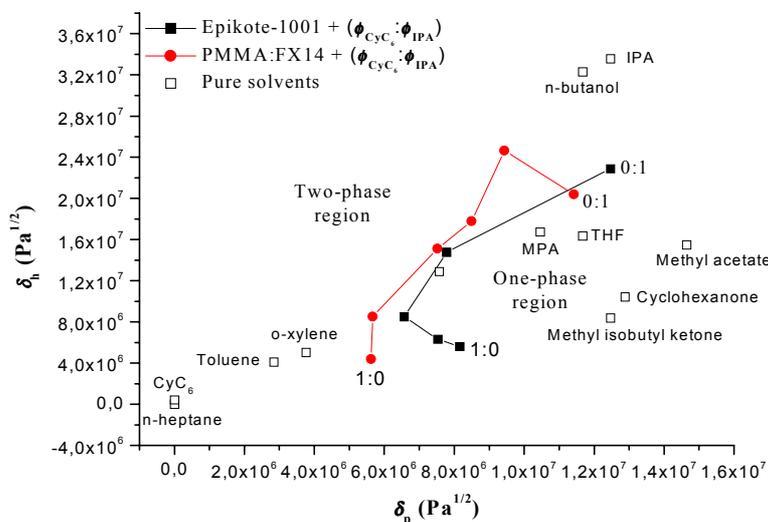


Figure II.6 Solubility region for Epikote 1001 and for MMA:FX14, polymer/copolymer ratio: 1/1, 30 % w/w solids at $T = 298.15$ K.

This picture illustrates clearly that our assumption was correct and that following this procedure it is possible to formulate and predict which solvent or solvent mixture will dissolve the polymer blend Epikote 1001 / MMA:FX14 without performing so many solubility tests. Another advantage of this way of finding the solubility region is that it is not necessary to know the exact value of the Hildebrand or Hansen parameters of the polymers, which requires also a huge amount of experimental work.

It is clear that the method outlined is a quite useful tool to formulate solutions of polymers with a different chemical and physical nature. This seems interesting in any application requiring a mixture of polymers in a homogeneous phase.

II.5 A possible application

It is our interest to achieve stratification in a coating prepared from an initially homogeneous solution of the system studied that is formed by two polymers with a remarkably difference in surface tension. Once the solvent is evaporated, the blend undergoes phase separation. Therefore, we expect to obtain a stratified system where the driving forces are both the phase separation and the difference in surface tension between the two polymers. We investigated by using X-ray photoelectron spectroscopy (XPS) and scanning electron microscopy with energy dispersive X-ray analysis (SEM-EDX) whether stratification is achieved.

II.5.1 Coating preparation

For the coating preparation, the amount of solids was gradually increased to 40% w/w, keeping the ratio Epikote 1001/PMMA:FX14 1/1. Methoxy propyl acetate (MPA) was used as a solvent because of its high boiling point, which allows having a low viscous medium for a longer time, that would favor the diffusion of the components during the chemical reaction. To this polymer solution an amount of cross-linking agent was added, according to:

$$y = \frac{xH}{E} \quad (\text{II.6})$$

where y is the amount in grams of cross-linking agent, x is the amount in grams of epoxy resin, H is the ratio between molar mass of cross-linking agent and the total number of active hydrogen atoms in it and E is the ratio between the molar mass of epoxy resin and the amount of epoxy groups present in this molecule. These values are 57.3 and 473.9 for the Epikote 1001 and the Jeffamine D-230, respectively. This final solution was applied on a clean aluminium surface at 298.15 K using a roller applicator. The resulting film was cured in an oven at 373.15 K for one hour; the thickness of the dried coating was 75 μm . This film was released from the panel and characterized by SEM-EDX and XPS. The former technique permits to have not only a topological analysis, but also allows the determination of chemical composition on a scale of about 5 to 10 nm, by analyzing the emitted X-rays which are characteristic for each element.¹⁵ The latter analysis technique gives also information on the elemental composition within a depth of 1.5 to 6 nm.

II.5.2 Results

Figure II.7 illustrates the elemental composition of the coating surface; the higher proportion of fluorine compared to the other elements present in the sample, suggests surface enrichment with the fluorinated copolymer.

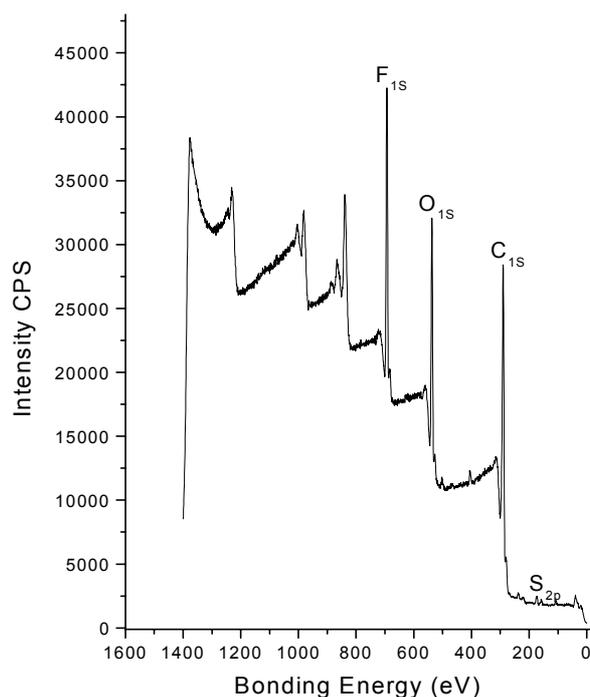


Figure II.7. XPS spectrum for a coating made of Epikote 1001/0.9MMA:0.1FX14 (50/50) showing the composition of the coating surface.

This surface enrichment of the coating/air interface and coating/substrate interface with one of the polymers contained in the polymer blend is observed quite nicely in the normalised spectrum shown in figure II.8, where a comparison of the spectrum of the pure components Epikote 1001 and 0.9MMA / 0.1FX14 and those from both interfaces are shown. As can be observed, the spectrum corresponding to the interface coating/air matches quite good with that of the pure fluoro-acrylate compound, and the spectrum corresponding to the interface coating/substrate is quite similar to that of the pure Epikote 1001, presenting also a small shoulder at the $-CF_2-$ and $-CF_3$ bonding energy region, indicating also traces of fluoro-acrylate in this interface.

When a scan on the cross-section of the coating was carried out by SEM-EDX (figure II.9), it was observed that the concentration profile of fluorine in the films exhibited a gradient, with a clear enrichment of this element on the interface coating/air.

Solubility region of the binary system bisphenol-A-diglycidylether / copolymer poly [CF₃(CF₂)₆SO₂NCH₂CH₃BA-co-MMA]

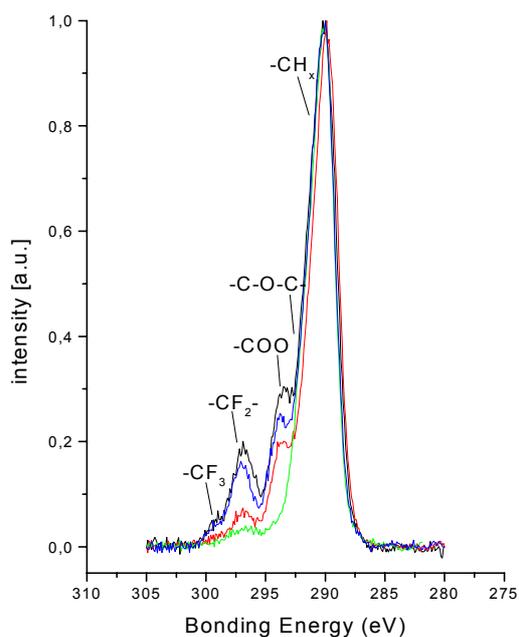


Figure II.8 Normalized XPS spectrum of C₁S for DGEBA trimer (—), PMMA:FX14 (—), interface coating/air (—), interface coating/substrate (—).

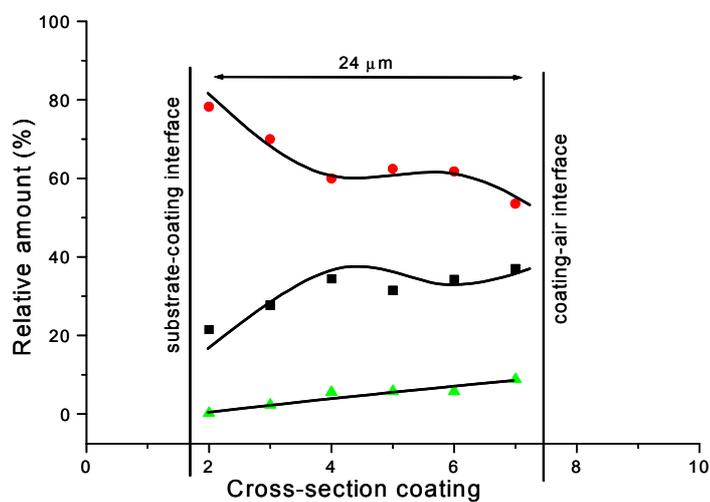


Figure II.9 Chemical composition of the coating cross-section, measured by SEM-EDX. Fluorine (■), oxygen (●) and sulfur (▲) are shown. (Lines drawn to guide the eye).

II.6 Conclusions

It was possible to determine the solubility region at 298.15 K for the binary polymer blend Epikote 1001 and the copolymer poly [CF₃(CF₂)₆C₇F₁₅SO₂NCH₂CH₃BA-co-MMA] following an alternative method.

The coating characterization done by SEM-EDX and XPS shows that self-stratification takes place partially in the system.

To understand how the stratification process would occur under isothermal conditions read this thesis.

II.7 References

- ¹ Nelson, R.C.; Hemwall, R.W. and Edwards, G.D. *J. Paint Techn.* **42**, no. 550 (1970) 636
- ² Hansen, C. *J. Paint Techn.* **39**, no. 505 (1967) 104
- ³ Hansen, C. *J. Paint Techn.* **39**, no. 511 (1967) 505
- ⁴ Hansen, C. and Skaarup, K. *J. Paint Techn.* **39**, no. 511 (1967) 511
- ⁵ Carr, C. and Wallstöm, E. *Prog. Org. Coat.* **28** (1996) 161
- ⁶ Hildebrand, J. and Scott, R. *The solubility of Non-electrolytes* 3rd ed. Reinhold Publishing Corp., New York (1949)
- ⁷ Paul, S. *Surface coatings. Science and technology* 2nd ed., John Wiley & Sons, England (1985)
- ⁸ Hansen, M. *J. Paint Technology* **39**, no. 505 (1967) 104
- ⁹ Shellblendpro database
- ¹⁰ Barton, A. *CRC Handbook of solubility parameters and other cohesion parameters* CRC Press. Inc. Florida (1985)
- ¹¹ ASTM, ANSI/ASTM D3132-72, American society for testing and materials, Philadelphia, American Standards Institute, New York (1976)
- ¹² Cosaert, E. *Chim. Peint.*, **34** (1971) 169
- ¹³ BPsolve database
- ¹⁴ van de Grampel, R.D.; van Geldrop, J.; Laven, J. and van der Linde, R.. *J. Appl. Polm. Sci.* **79** (2001) 159
- ¹⁵ Niemansverdriet, J.W. *Spectroscopy in catalysis* VCH Verlagsgesellschaft, Germany (1995)

SUMMARY

Polymers are widely used because they offer many advantages: they are relatively cheap, it is possible to tailor their chemical structure, the processing temperatures are accessible and they can be deposited easily on different substrates. Most polymer blends phase separate at room temperature when the components interact via dispersion forces or at higher temperatures when specific interactions such as hydrogen bonds are present. Phase separation induces formation of structure(s) on a mesoscopic scale, which determines the final performance of a material. Therefore, the prediction of morphology development at this scale is of great importance because it allows to bridge and to understand the relationship between microscopic parameters and macroscopic properties, consequently it is possible to control and to optimize the desired properties in a material.

Experimentally, it is possible to study, to determine and to characterize the morphology developed in a polymer blend; nevertheless, it is necessary to have a theoretical model to rationalize experimental evidence and to have a tool to predict the morphology behavior of an unknown and/or a complicated system. The prediction of morphology development implies the coupling of hydrodynamics and thermodynamics via the chemical potential; this task has been done in phenomenological models where the chemical potential used is derived from a Helmholtz energy functional expanded and truncated to a fourth order, and only contributions of concentration gradients to enthalpy are considered. Nevertheless, for polymer systems at interfaces, there is a loss of conformational entropy and therefore concentration gradient contributions to entropy must be considered as well.

As here is our interest to study the morphology development in thin films made of binary polymer blends, the modification of an available numerical model to predict structure development for regular solutions was necessary. The extensions done are: the use of a chemical potential derived from the exact form of the Flory-Huggins lattice model, the consideration of concentration gradients to entropy (de Gennes), the formulation and introduction of a wall-polymer interaction potential, based on short and long-range interactions. The implementation of the modified model into a finite element numerical method required re-scaling of the balance equations that avoids numerical instabilities.

The extended square-gradient model is applied to the study of the early-stage of the spinodal decomposition. The selection of this early-stage was not only because of the controversy found in experimental and theoretical work reported on the literature, but also because of the processes developing such as wetting and coarsening that define the final morphology and therefore the properties. The effect on morphology development of number of segments, quench (upwards or downwards) in temperature within the miscibility gap of the phase diagram, and initial concentration at which the system is quenched is studied. Additionally, for systems where a co-continuous structure in bulk is observed, the wall effect is switched on and investigated as a function of quench in temperature and magnitude of the wall-polymer interaction potential.

Summary

The results obtained show that the connectivity of the morphology depends on the symmetry or ratio of segments conforming the chain polymers present in the blend. Symmetric systems present a more interconnected co-continuous structure. Subsequently, the introduction of the wall-polymer interaction potential influences the development of the spinodal decomposition, resulting in a morphology with different growth rates of the concentration fluctuations close and far away from the wall. The net change of the morphology due to the wall depends on two factors: the magnitude and extension into the bulk of the wall-polymer interaction potential and the magnitude of the chemical potential. The results presented in this thesis clarify the early-stage of the spinodal decomposition.

Additionally, the model proposed was also applied to experimental results obtained in this thesis; the simulation results gave an appropriate answer to questions raised from the experiments and allowed a better understanding of the relationship between phase behavior and morphology development in the system.

SAMENVATTING

Polymere materialen worden op grote schaal gebruikt omdat ze vele voordelen kennen: ze zijn relatief goedkoop, het is mogelijk de chemische structuur te beïnvloeden, de procestemperaturen zijn goed toegankelijk en ze kunnen gemakkelijk worden aangebracht op verschillende substraten. De meeste polymere blends ondergaan fasescheiding bij kamertemperatuur wanneer de componenten interactie ondervinden via dispersie-krachten, of bij hogere temperaturen wanneer specifieke interacties zoals waterstofbrugvorming aanwezig zijn. Fasescheiding induceert de vorming van een structuur op een mesoscopische schaal, die de uiteindelijke eigenschappen van het materiaal mede bepalen. Daarom is het belangrijk de meso-structuurontwikkeling te kunnen voorspellen. Het stelt de gebruiker in staat de relatie tussen microscopische parameters en macroscopische eigenschappen beter te begrijpen. Vervolgens is het dan mogelijk de eigenschappen van het materiaal te sturen en te optimaliseren.

Het is experimenteel mogelijk gebleken de meso-structuurontwikkeling, ook wel morfologieontwikkeling genoemd, in polymere blends te volgen en te karakteriseren. Echter, het is noodzakelijk een theoretisch model te ontwikkelen om de experimentele resultaten mee te vergelijken en de structuurontwikkeling van complexe en onbekende systemen te kunnen voorspellen. Het voorspellen van morfologie ontwikkeling wordt mogelijk door de hydrodynamica te koppelen aan de thermodynamica via de chemische potentiaal. Dit is reeds gedaan in fenomenologische modellen waarbij de chemische potentiaal is afgeleid van een energiefunctie, die ontwikkeld is rond een kritisch punt, waarbij slechts de termen tot en met de vierde orde worden gebruikt. Alleen de bijdragen van de concentratiegradient aan de enthalpie worden hierbij in beschouwing genomen. Echter, voor polymere systemen in de buurt van grensvlakken of substraten treedt verlies van entropie op, en dus moeten ook bijdragen van de concentratiegradient aan de entropie meegenomen worden.

Om de morfologieontwikkeling in dunne films van polymere blends te kunnen bestuderen, was het nodig een beschikbaar numeriek model, dat de structuurontwikkeling van gewone oplossingen beschrijft, te veranderen. De aangebrachte veranderingen bestaan uit een chemische potentiaal, afgeleid van de exacte vorm van de Flory-Huggins vergelijking. Verder is de entropie bijdrage aan de concentratiegradient term meegenomen (de Gennes) en tenslotte is een substraat-interactie-potentiaal geïntroduceerd, voor zowel korte- als lange-afstands interacties. De implementatie van het aangepaste model in een eindige elementen context vereist een herschaling van de evenwichtsvergelijkingen en wordt eveneens beschreven in dit proefschrift.

Het uitgebreide, zo genaamde kwadratische gradient-model is toegepast om het vroege stadium van spinodale decompositie te bestuderen. De keuze voor dit vroege stadium was niet alleen vanwege de controverse in de experimentele en theoretische literatuur, maar ook vanwege processen zoals 'wetting' en groei, die de uiteindelijke morfologie van een materiaal en dus de eigenschappen mede bepalen. Het effect op de morfologie ontwikkeling van het aantal segmenten, de grootte van de temperatuursprong in het inhomogeen gebied van het

Samenvatting

fasediagram (zowel omhoog als omlaag) alsmede de initiële concentratie op de morfologieontwikkeling zijn bestudeerd.

De verkregen resultaten laten zien dat de co-continuïteit van de morfologie sterk afhankelijk is van de symmetrie of verhouding van de segmenten in de polymere keten. Symmetrische systemen vertonen een meer verbonden of co-continue structuur. De introductie van een substraat-potentiaal beïnvloedt de ontwikkeling van de spinodale decompositie met als gevolg dat de morfologie verschillende groeisnelheden dichtbij en ver van het substraat vertoont. De netto verandering van de morfologie als gevolg van de substraat-potentieel hangt af van twee factoren. Het bereik van de potentiaal in de bulk en de grootte relatief ten opzichte van de chemische potentiaal. De resultaten in dit proefschrift verduidelijken de processen die plaats vinden in het vroege stadium van spinodale decompositie.

Tenslotte, het model is ook getoetst aan uitgevoerde experimenten die zijn beschreven in dit proefschrift. De simulatieresultaten gaven een duidelijk antwoord op diverse vragen die ontstonden bij de experimenten en verhoogden het inzicht in de relatie tussen fasegedrag en morfologieontwikkeling in het systeem.



RESUMEN

Los polímeros son materiales ampliamente utilizados debido a que ofrecen muchas ventajas: son relativamente baratos, es posible diseñar su estructura químicamente, se procesan a temperaturas accesibles y pueden ser fácilmente depositados sobre diferentes sustratos. La mayor parte de mezclas de polímeros se separan en diferentes fases, a temperatura ambiente cuando sus componentes interactúan vía fuerzas de dispersión ó a temperaturas más elevadas en la presencia de interacciones específicas, tales como puentes de hidrógeno. La separación de fases induce la formación de estructura(s) a escala mesoscópica, la cual determina el desempeño final de un material. Por lo tanto, la predicción de la morfología a esta escala es de gran importancia, porque permite unir y entender la relación entre parámetros microscópicos y propiedades macroscópicas, consecuentemente es posible controlar y optimizar las propiedades deseadas en un material.

Experimentalmente, es posible estudiar, determinar y caracterizar la morfología desarrollada en una mezcla de polímeros; sin embargo, es necesario tener un modelo teórico tanto para racionalizar la evidencia experimental, como para tener una herramienta que permita predecir la morfología en un sistema no explorado ó en uno complicado. La predicción temporal de morfología implica el acoplamiento de la hidrodinámica y la termodinámica vía el potencial químico; esta tarea ha sido realizada en modelos fenomenológicos donde el potencial químico usado es derivado de un funcional de energía de Helmholtz expandido y truncado en el cuarto orden y donde sólo contribuciones de gradientes de concentración en entalpía son consideradas. Sin embargo, para sistemas poliméricos en presencia de interfaces, hay una pérdida de entropía conformacional y por lo tanto la contribución de gradientes de concentración en entropía debe también ser considerada.

Como es de nuestro interés estudiar el desarrollo de la morfología de películas finas, hechas de mezclas binarias de polímeros; la modificación de un modelo numérico existente que predice el desarrollo de estructura en soluciones regulares fue necesaria. Las extensiones hechas son: el uso de un potencial químico derivado de la forma exacta del modelo de malla de Flory-Huggins, la consideración de gradientes de concentración en la entropía (de Gennes), la formulación e introducción del potencial de interacción de la pared, basado en interacciones de corto y largo alcance. La implementación del modelo modificado en un método numérico requiere el re-escalamiento de las ecuaciones que definen el equilibrio del sistema, para evitar inestabilidades numéricas.

El modelo extendido del gradiente al cuadrado se aplica al estudio de la etapa temprana de descomposición espinodal - intervalo escogido no sólo por la controversia encontrada en trabajo experimental y teórico en la literatura, sino también porque procesos como el mojado y la iniciación de la separación de fases que definen la morfología final de un material, se desarrollan en esta etapa -. El efecto sobre el desarrollo de la morfología, del número de segmentos, el abatimiento ó la elevación de la temperatura dentro del domo de inmiscibilidad del diagrama de fases y la concentración inicial a la cual el sistema es introducido a la región de dos fases, es estudiado. Adicionalmente, para sistemas donde se observa una estructura de

Resumen

bulto bi-continua, el efecto de la pared es activado e investigado como función del abatimiento ó elevación de la temperatura y la magnitud del potencial de interacción de la pared.

Los resultados obtenidos muestran que la conectividad de la morfología depende de la simetría o relación del tamaño de las cadenas de los polímeros presentes en la mezcla. Los sistemas simétricos presentan una estructura bi-continua más interconectada que los sistemas asimétricos. Subsecuentemente, la introducción del potencial de la pared influencia el desarrollo de la descomposición espinodal, resultando en una morfología con fluctuaciones en concentración que crecen a diferentes velocidades cerca y lejos de la pared. El cambio neto de la morfología debido a la pared depende de dos factores: la magnitud y extensión del potencial de la pared hacia el bulto y la magnitud del potencial químico. Los resultados presentados en esta tesis clarifican la etapa temprana de la descomposición espinodal.

Adicionalmente, el modelo propuesto fue aplicado también a resultados experimentales obtenidos en esta tesis; los resultados de las simulaciones dieron una respuesta apropiada a preguntas planteadas durante los experimentos y permitieron un mejor entendimiento de la relación entre el comportamiento del diagrama de fases y la morfología del sistema.

ACKNOWLEDGMENTS

I want to thank to the Nederlandse Organisatie voor Wetenschappelijk Onderzoek for the sponsoring given to my research project, and to the Technische Universiteit Eindhoven for the extra sponsoring granted and for all the facilities provided along my studies. Thanks to dr. Anderson, prof. de With, prof. Meijer, dr. Nies, prof. ten Brinke and prof. van de Vosse, for the time all of you spent in reading my thesis, and for your suggestions to improve it. I also thank prof. Fraaie, prof. van Herk, prof. Koning, and the chairman, prof. Niemansverdriet to come to my promotion as members of the committee. Thanks Erik for the year of coaching, and Frans thanks again for the initial motivating discussions that opened the door to have collaboration with the Mechanical Engineering Department. Graag zou ik Patrick Anderson en Bert Kestra willen bedanken voor hun enorm steun en motivatie. Paul van der Varst bedankt voor de goede discussies over mijn project, ook veel dank aan prof. Han Meijer voor uw steun en vertrouwen, en prof. Bert de With bedankt voor de kans om dit onderzoek tot een succesvol einde te brengen. Niek Lousberg, Marco Hendrix, Hans Heijligers, Sasha Kondentsov, Pauline Schmidt, Han Goosens, Hans Wilderbeek, Joachim Loos, Hartmut Fischer, Joost van Dongen, Mike Schellekens, Michel Pepers, Robert van de Grampel and Wieb Kingma bedankt voor jullie hulp in alle verschillende experimentele technieken. Bert en Luc Habets bedankt voor jullie hulp met Matlab. Jos Laven, bedankt voor het lezen en verbeteren van het concept “solubility parameters”. En tevens zou ik prof. van der Linde bedanken voor uw vriendelijkheid.

Agradezco a todas las personas que han motivado mi interés por el conocimiento, sobre todo gracias a la UNAM y sus buenos elementos académicos de quienes aprendí lo suficiente para poder llegar a esta defensa doctoral.

I want to thank all my colleagues in the SVM and in the former Coating group for the nice working atmosphere. Specially thanks to Slobodan for your hospitality at my arrival in the Netherlands, and to Joost for all your orientation and help. Linda, Pascal and Huub thanks for the time you spent in organizing different social activities in the group. Sasha thanks for your help on searching the meaning of difficult scientific terms. Jaap(ito), Francis(co), Joyce, Hans, o. a. bedankt voor de kans om jullie taal te oefenen, want dat is niet altijd mogelijk bij de TU/e. Thanks Niels, Emilio and Robert, the creators of my last 20’s present and of course thanks to the rest of the *sexy boys* (Mark, Marshall, Chouaib, Alope, Dennis, Pascal and Victor) to be on that funny picture.

STO 2.41 was a kind of “International Affairs Bureau”, having inhabitants from different parts of the world, even the Netherlands. I thank to all my roommates for the nice working atmosphere, especially to Shukiko, Julianne and Kamuran. This international environment was also present at home along my two years of living in the Fellowtel. It was a very nice time and a good chance to share and to learn a bit of Italian, Venezuelan-Cuban, Spanish, Russian, French, German and even Dutch cuisines. So, I start by thanking Giuseppina and Eva for the delicious Italian dinners and the nice time. Joost en Robert, bedankt voor het goede koken, misschien niet echt Nederlandse eten, maar wel echte Nederlandse koken!

Agradecimientos

Rusmely gracias por las ricas cenas junto con Ramiro y las niñas, las partidas de Rumiekub y por seguirme haciendo reír tanto con tus mensajes cargados de tan buen humor. A Emilio y Mariana gracias por los ricos gazpachos, las paellas y por su hospitalidad aquí y en España. Aan papa Marco, Els en kinderen heel hartelijk bedankt voor jullie affectie en gezelligheid. Niek en Irina bedankt voor de heerlijke diners met jullie in “het buitenland”. In the next two years living on my own I continuous enjoying my international friends and their culinary culture, then I tasted Moroccan and Japanese dishes. Merci Chouaib et Assia pour le délicieux cous-cous, les tartes, les alles au cinema, et votre hospitalité ici et à Mulhouse. Shukiko *doumo arigatou* for the nice dinners, the enjoyable long chats and for your great sense of humor. All these delicious dinners needed a load of sports; luckily I met Alina and Mayela, my constant sporting team, *spasibo* and *gracias* for your very nice company and for cheering me up in the difficult times. Also thanks Cornelia for joining the long and late excursions to swim. Marcel y Robèr gracias por su hospitalidad y las agradables conversaciones políglotas. También gracias *Lucky* Luc por los cumplidos.

Eindhoven is the light city of the Netherlands, but it is not the most *gezellig* urban spot in this country, as the Dutch people from outside affirm. Nevertheless it is a place with very friendly Brabant people and is definitely a city to sport. I enjoyed very much the sport Centrum facilities of the TU/e and the kindness of the people working there. Vandaar wil ik Ignace danken voor zijn geduld en voor zijn hulp bij het overwinnen van mijn angst voor diepte bij zwemmen en ook aan Fritz voor zijn vriendelijkheid.

En mis viajes a México, me dio muchísimo gusto reunirme con mis buenos amigos, aunque fuera por breves momentos, a todos ustedes Yuri, Gina, Kira, Dara, Fer, Memo, Mariana, César, Silvia, Gastón, Merit, Diego, Ivonne, Graciela, Andrea, Rubí, Gabriel, Mary Carmen y Rafa, muchas gracias por seguir tan cerca aún estando tan lejos. Y de este lado del charco, agradezco a la familia Greusing, por su hospitalidad, en especial gracias a Meike e Inka por su amistad. Monserrat y Eugenia, ha sido grato el tenerlas cerca. Alma, gracias por esta larga y continua amistad. Vanesaa, el que nuestra estancia de este lado del mundo haya coincidido por un tiempo fue super importante y alentador para mi, mil gracias por todo a ti y a Mariano. Kira, gracias por unirme a la vagancia y por revisar mi resumen. Maarten, nog bedankt voor de mooie reizen samen en jouw bijzondere vriendschap. Marieke, Joke, Wim en de rest van de familie Verhoeven bedankt voor jullie vriendelijkheid en genegenheid.

A Mony, a la sra. Carmelita y al resto de la familia Rico Ayala, les agradezco de corazón por tantos años de amistad y por el gran apoyo y respeto que ha existido entre su familia y la mía. Agradezco a mi amiga y hermana Paty, a mis hermanos Alejandro, Miguel, Jorge y Roberto, por los buenos tiempos que compartimos en casa con nuestros padres y por los buenos momentos que seguimos compartiendo junto con sus respectivas familias. A Eduardo, Luz María, Lupita, Laura y Rosaura, gracias por su afecto y hospitalidad. A mis sobrinos, Alexis, Ricardo, Alejandra y Lalito, gracias por tenerme presente y por sus cartitas. Víctor, David, Marisela, Andrea y Luis, ya tendré tiempo suficiente para estar con ustedes y para conocernos más. A mi super tío Juan, gracias por toda la alegría que nos transmitiste y en fin, a mi extensa familia gracias por todo. Por último quiero agradecerles a ustedes mamá y papá por la educación, la confianza y los valores que me enseñaron, gracias a ellos he podido vivir y disfrutar mi vida de la forma que lo he hecho.

Maru
Eindhoven, Octubre 12 del 2002



CURRICULUM VITAE

María Eugenia Velázquez Sánchez was born in Mexico City on the 21st of February in 1972; she finished her studies in Chemistry in 1994 at the Department of Chemistry of the Universidad Nacional Autónoma de México, presenting in 1995 her bachelor's thesis. In the same year, she continued her Master's degree courses in Physical Chemistry at the same Department, to obtain at the end of 1997 her degree with the thesis entitled *Thermodynamic study of the addition of alcohols to microemulsions*. In 1998, she moved to the Netherlands, and started her Ph. D. research in the laboratory of Solid State and Materials Chemistry of the Eindhoven University of Technology; which resulted in this thesis.